Novel Roles of Glial Precursors in Early Neurogenesis

Yunlu Zhu
Charlottesville, Virginia

B.S., University of Science and Technology of China, Hefei, 2013

A Dissertation presented to the Graduate Faculty
of the University of Virginia in Candidacy for the Degree of
Doctor of Philosophy

Department of Biology

University of Virginia
August, 2019

_____

_____

_____

_____

_____

_____

ABSTRACT

During vertebrate embryonic development, the ectoderm-derived neural plate along and anterior-posterior axis rises and folds into the neural tube. Neuroepithelial cells inside the neural tube proliferate and ultimately differentiate into neurons and glia in the central nervous system (CNS). Neural crest cells (NCC) specified at the border of the neural plate undergo an epithelial to mesenchymal transition and delaminate from the neural epithelium upon the folding of the neural tube. Subsequently, NCCs migrate through the periphery and give rise to most neurons and glia in the peripheral nervous system (PNS). However, as an exception, perineurial glia associated with PNS nerves derive from the floorplate in the spinal cord. Their CNS precursors migrate to the periphery through motor exit point transition zones, where spinal motor neuron send axons to the PNS. Over the past decades, the specification and differentiation of neurons and glia from precursor cells during embryogenesis have been studied extensively as a fundamental question in neurogenesis. However, how these cells coordinate with each other during neural development to ensure the correct patterning of the nervous system is poorly understood.

In this dissertation, using zebrafish embryos as a model organism, I demonstrate novel roles of two types of glial precursors, perineurial glial precursors and neural crest cells, in directing motor axon pathfinding out of the spinal cord and phagocytosing cellular debris in the CNS and PNS, respectively. This work not only fills gaps in our knowledge about nervous system assembly, but also sheds light on the under-appreciated but essential roles of precursors cells besides giving rise to their derivatives.

To Mom and Dad,

who installed a love for nature in my childhood.

Also to my wife, Isabelle,

for marrying me.

Couldn’t have done it without your support.

ACKNOWLEDGEMENT

First and foremost, I would like to express my sincere gratitude to my tremendous supervisor, Dr. Sarah Kucenas, who have supported and guided me throughout my PhD for the past six years. Thanks for allowing me to chase my curiosity. I will definitely miss your pumpkin cookies!

This dissertation would not have been possible without the help and support from family, friends and fellow scientists. I'm extremely grateful to the members of my dissertation committee, Dr. Dorothy Schafer, Dr. Christopher Deppmann, Dr. David Parichy, Dr. Sarah Siegrist, and Dr. Xiaowei Lu, for their valuable comments and suggestions. I would like to thank all the past and present members in the Kucenas lab for teaching me techniques, criticizing my work, and making delicious bakeries. Many thanks to Lori for taking good care of our fish. Special thanks to my brilliant undergraduate research assistant, Samantha Crowley, for her helpful contributions to this study. I'd like to recognize the assistance that I received from members of the Ravichandran lab. Thank you for valuable suggestions and discussions. I also wish to thank my friends and colleges at the University of Virginia, particularly Xin, Ryan, Jen and Qijun, for bringing me positive energy and joy.

I cannot leave Charlottesville without mentioning Mudhouse Coffee Roasters, who produce "thoughtfully sourced & carefully roasted" coffee beans that have kept me caffeinated throughout my PhD.

TABLE OF CONTENTS

FIGURES AND TABLES

CHAPTER I

Introduction: The Assembly of Spinal Motor Nerves

During early development of the vertebrate embryo, the ectoderm-derived neural plate arises from a thick epithelium of cells, cavitates to form a hollow neural tube, and differentiates into the central nervous system (CNS), which consists of the brain and the spinal cord (Nikolopoulou *et al.*, 2017). During or after neural tube closure, neural crest cells (NCC) delaminate from the dorsal neural tube, migrate ventrally in the periphery and give rise to the peripheral nervous system (PNS), which is responsible for transmitting sensory and motor signals between the CNS and other tissues and organs (Bronner and Simões-Costa, 2016). Motor neurons in the spinal cord project axons to the PNS and play critical roles in the output pathway for sending control signals from the interneuronal network in the neural tube to muscles and glands in the periphery. The normal function of motor neurons requires precise assembly and proper coordination of multiple types of glial cells, including oligodendrocytes (OL), Schwann cells (SC), motor exit point glia (MEP glia) and perineurial glia (PG) (Davis-Dusenbery *et al.*, 2014; Kucenas, 2015). However, the coordinated specification, migration and assembly of motor nerves and glia during embryonic development are not fully understood. Importantly, many studies have shown that dysfunction of glial cells leads to a variety of neurodegenerative diseases, such as multiple sclerosis, amyotrophic lateral sclerosis and spinal muscular atrophy. In order to better dissect the cellular and molecular mechanisms of neural developmental and neurodegenerative diseases, we need a comprehensive

understanding of how these neurons and glia coordinate their development during embryogenesis.

In this introduction, I will review what is known about the development of spinal motor nerves and glial cells. In the following chapters, I will demonstrate novel roles of glial precursors during early neurogenesis in zebrafish and discuss how that fills gaps in our knowledge regarding motor nerve assembly.

Motor neuron development

Specification of spinal motor neurons

After folding of the neural plate, the cells of the neural tube are specified along both the rostral-caudal and the dorsal-ventral axes. The major signal that contributes to the neural tube specification along the rostral-caudal axis is retinoic acid. Retinoic acid released from the caudal paraxial mesoderm is crucial for the formation and distinction of major components of the CNS, including the brain, midbrain, hindbrain and spinal cord (Maden, 2007). In the dorsal-ventral axis of the neural tube, progenitor cells are divided into five ventral domains: p0, p1, p2, pMN and p3. The specification and formation of ventral domains requires a precise gradient of *Sonic hedgehog (Shh)* signals provided by notochord cells and floorplate (FP) cells and Wnt/BMP signaling released from the roof plate (Figure 1-1A) (Odenthal *et al.*, 2000; Briscoe and Ericson, 2001; Avilés, Wilson and Stoeckli, 2013; Davis-Dusenbery *et al.*, 2014). Transcription factors downstream of Shh can be divided into two classes: class II proteins that are activated by Shh, such as NKX2.2, OLIG2 and NKX6.1, and class I proteins that can be repressed by Shh, including IRX3, PAX6, DBX1 and DBX2 (Briscoe *et al.*, 2000; Jessell, 2000; Alaynick,

Jessell and Pfaff, 2011; Davis-Dusenbery *et al.*, 2014). It is believed that the combination of these cross-repressive transcription factors generates robust separation and consolidation of progenitor identity among these domains.

Spinal cord motor neurons derive from ventral progenitor cells expressing transcription factors *Olig2* in the pMN domain (Figure 1-1A). *Olig2* primes motor neuron progenitors to differentiate by both promoting the expression of *Ngn2* and *Lhx3* and antagonizing pre-mature expression of these genes (Scardigli *et al.*, 2001; Lu *et al.*, 2002a; Lee *et al.*, 2005). This antagonistic relationship between *Olig2* and *Ngn2* serve as a gate for the proper timing of motor neuron specification.

During early neurogenesis, motor neuron cell bodies migrate dorsal-laterally from the pMN domain following various guidance cues and go through cell divisions to form segmentally clustered motor neuron pools (Kania, 2014; Ravanelli and Appel, 2015; Dewitz *et al.*, 2018; Kim, Bjorke and Mastick, 2019). Motor neurons within each pool can be further classified into subgroups by their anatomical and functional properties. Motor neuron classification has been studied extensively in zebrafish, because its embryonic transparency allows the observation of the development of motor neurons at all stages *in vivo*. In zebrafish embryos, 3 primary motor neurons are first specified in each hemisegment at approximately 16 hours post fertilization (hpf): the Caudal Primary (CaP), the Rostral Primary (RoP), and the Middle Primary (MiP) (Figure 1-1B) (J. S. Eisen, 1991). In addition to these 3 primary motor neurons, about half of the hemisegments contain a fourth one, named Variable Primary (VaP) (J S Eisen, 1991). The primary motor neurons can be distinguished by the localization of their cell bodies along the anterior-posterior axis in the pMN domain and the muscle regions they

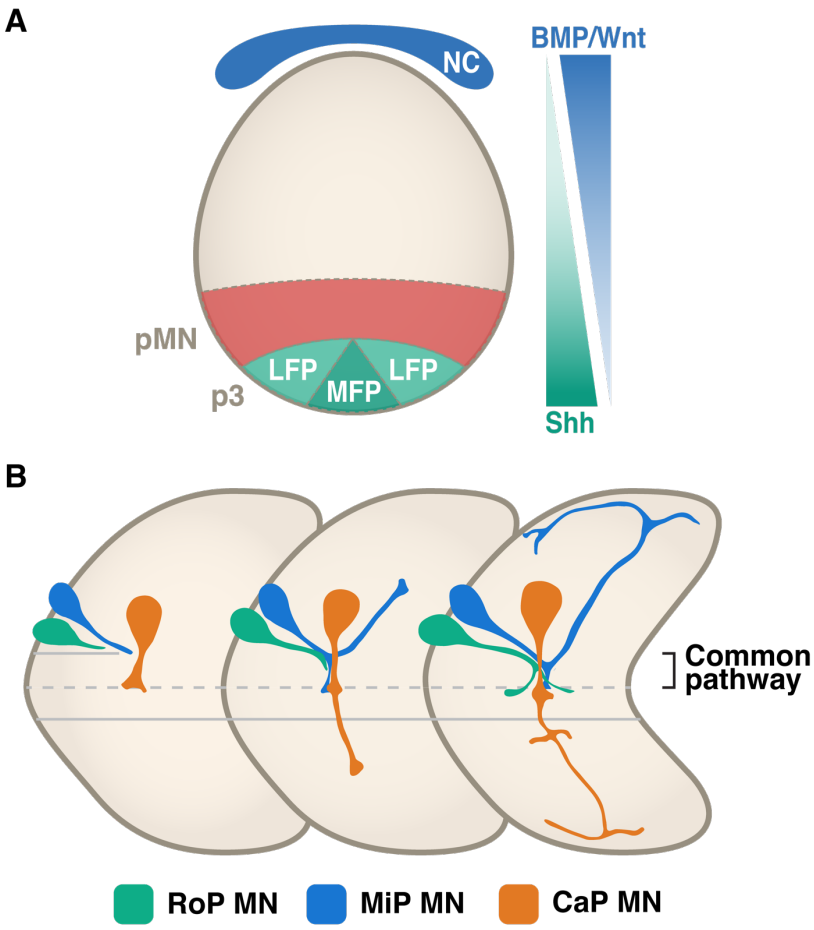

Figure 1-1. Motor neuron specification and motor axon pathfinding in zebrafish. **(A)** A cross section of the neural tube showing the patterning of the ventral spinal cord requires a precise gradient of *Shh* signals provided by the notochord and the p3 domain and Wnt/BMP signaling released from the roof plate. Motor neurons are specified in the pMN domain. **(B)** Lateral view of the zebrafish trunk showing motor axon pathfinding in zebrafish. Primary motor neurons extend their axons to the periphery through specialized MEP TZs in the middle of each segments. Abbreviations: LFP, lateral floorplate; MFP, medial floorplate; NC, neural crest; Shh, Sonic hedgehog; MN, motor neurons; RoP, rostral primary; MiP, middle primary; CaP, caudal primary.

innervate in the periphery. After specification of primary motor neurons, secondary motor neurons are differentiated and send their axons to the periphery, following primary motor axons.

Motor axon pathfinding

Because motor neurons are located in the CNS while the muscle fibers they innervate are in the periphery, all of their axons have to exit the spinal cord in order to reach their targets. Intriguingly, although axons from different motor neurons innervate muscle fibers at distinct regions, at the beginning of their pathfinding, they all exit the spinal cord through the same specialized location in every hemisegment, named the motor exit point (MEP) transition zone (TZ) (Figure 1-1B). For instance, zebrafish CaP axons exit CNS through MEP TZs located in the middle of each hemisegment at 16 hpf. Immediately after that, RoP and MiP axons leave the spinal cord through the same MEP TZs (Figure 1-1B) (P. Z. Myers, Eisen and Westerfield, 1986; Pike and Eisen, 1990).

A few molecules have been identified that lead to ventral motor axon exit and/or are localized to MEPs, including *nkx6*, *zfh1* in *Drosophila*, *lh3* and *npn1a* in Zebrafish, and *Lhx3/Lhx4* and *Npn2* in Mouse (Dillon *et al.*, 2005; Bravo-Ambrosio, Mastick and Kaprielian, 2012). However, most of these studies didn't indicate the cellular mechanism during the axon exit stage, and only focused on the attractive and repulsive guidance cues that direct the pathfinding process once axons were in the periphery. Recently, mice spinal accessory motor neurons (SACMNs) have been used as a model system to study motor axon exit (Bravo-Ambrosio, Mastick and Kaprielian, 2012). SACMNs are a homogeneous population of spinal motor neurons with axons that leave the CNS through

a discrete lateral exit point (LEP). A homeodomain transcription factor *Nkx2.9* controls SACMN exit by regulating *Robo2* expression in SACMN. ROBO2 binds its ligands SLIT1/2 expressed by LEP associated cells, which facilitates SACMN exit (Bravo-Ambrosio, Mastick and Kaprielian, 2012). However, compared with the SACMNs, ventral motor neurons (vMNs) derive from a different population of cells and they do not rely on *Nkx2.9* to exit the spinal cord (Pabst *et al.*, 2003; Dillon *et al.*, 2005; Bravo-Ambrosio, Mastick and Kaprielian, 2012). Interestingly, results from several studies suggest that motor axons exit from ectopic ventral roots in zebrafishmutants with axon branching and/or pathfinding defects, such as *plexin A3* and *turnout* (Palaisa and Granato, 2007; Sainath and Granato, 2013). However, the specification of MEP TZs and the cellular and molecular mechanisms that facilitate motor axon exit remain largely unknown.

Motor axon pathfinding after crossing the CNS-PNS TZ has been extensively studied. In mouse, the G protein-coupled receptor CXCR4 transiently expressed by vMN is enticed by its cytokine ligand CXCL12 in mesenchymal cells (Lieberam *et al.*, 2005), which forms an attractive signaling for motor axon pathfinding. Meanwhile, a set of NCCs called boundary cap cells help prevent motor neuron cell body from exiting the spinal cord by expressing repulsive cues, such as SEMA6A (Hjerling-Leffler *et al.*, 2005; Mauti *et al.*, 2007). The convergence of motor axons into ventral roots shows a characteristic repetitive rostro-caudal growth pattern. Many other repulsive signaling molecules localized in the posterior-half of the somites have been found, including SEMA3A/3F, EFNB1 and F-Spondin, to confining axons to the specific part of somites (Bonanomi and Samuel L Pfaff, 2010). Ultimately, under the selection of various

signaling molecules, motor axons make their choices to follow different pathways and innervate muscle fibers in various locations in the organism.

Gliogenesis

Neural crest cell migration and Schwann cells in PNS myelination

A major event happening during the earliest stages of nervous system development is the migration of neural crest cells (NCC). NCCs are a conserved cell lineage in vertebrate embryos that differentiates into a variety of cell types, including skeletal tissues, pigment cells and neurons and glia in the PNS (Roberto Mayor and Theveneau, 2013). NCCs are generated along the entire length of the anterior-posterior axis of the developing embryo and are separated into four populations: cranial, cardiac, vagal and trunk. For the sake of simplicity, I will only focus on the development of trunk NCCs in the introduction.

During or after folding of the neural tube, NCCs expressing transcription factor *sox10*, are specified at the border of the neural plate, undergo an epithelial to mesenchymal transition, and delaminate from the neural epithelium upon the folding of the neural tube (Figure 1-1A; Figure 1-2, blue) (Theveneau and Mayor, 2012). When CNS motor neurons send their axons out of the spinal cord, the first wave of trunk NCCs migrate ventral-medially around the outside boundary of the neural tube as segmentally-restricted streams towards MEP TZs, which happens between 16 to 20 hpf in zebrafish (Figure 1-2B) (Roberto Mayor and Theveneau, 2013). These NCCs then migrate along with outgrowing motor axons and differentiate into dorsal root ganglion neurons, satellite glia, and SCs (Figure 1-2C & D). Following the first wave of NCC streaming, a second wave of NCCs delaminate from the dorsal neural tube, migrate ventral-laterally and give

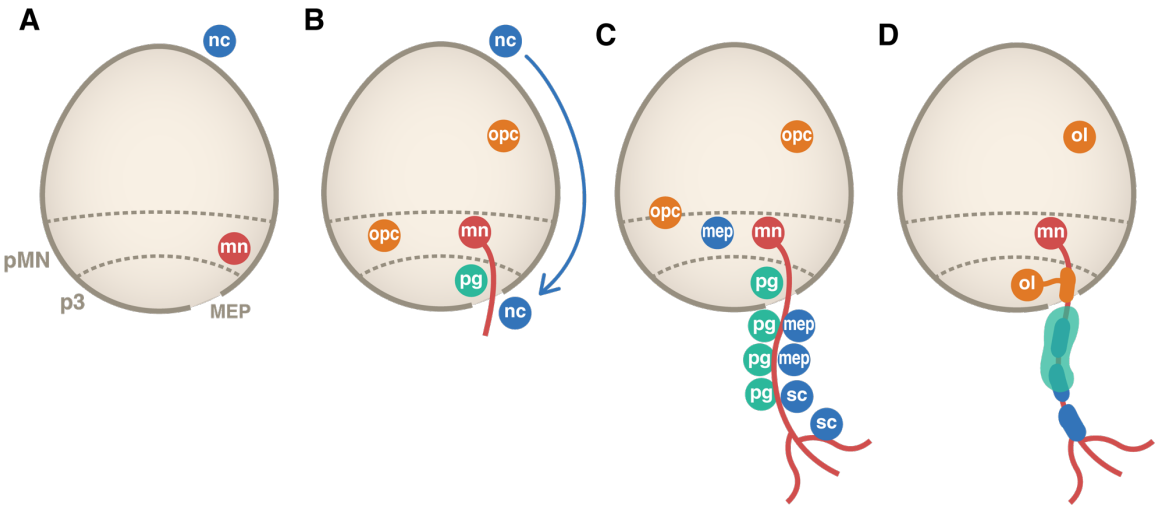

Figure 1-2. Summary of zebrafish spinal motor nerve assembly. (A) Motor neurons are specified in the pMN domain in the spinal cord. NCCs delaminate from the dorsal spinal cord. **(B)** Motor neurons project axons to the periphery through specialized MEP TZs. NCCs migrate along the outside margin of the spinal cord. OPCs are specified in the pMN domain. **(C)** PG and MEP glia migrate to the periphery through MEP TZs. **(D)** OLs differentiated from OPCs and SCs derived from NCCs myelinate motor axons in the CNS and PNS, respectively. PG form the perineurium around myelin sheath. Abbreviations: nc, neural crest cells; mn, motor neurons; pg, perineurial glia; opc, oligodendrocyte progenitor cells; mep, MEP glia;

rise to pigment cells of the skin.

Most of the PNS axons are myelinated by SCs derived from NCCs. During development, NCCs that have associated with axons first differentiate into immature Schwann cells (ISCs), which then begin radial sorting and finally ensheath individual axons and become mature SCs (Jessen and Mirsky, 2005). Previous studies demonstrate that changes of the expression of a variety transcription factors, such as *sox2, Oct6, Krox20*, is crucial to the SC lineage progression (Le *et al.*, 2005; Ghislain and Charnay, 2006). SC differentiation is driven by various intrinsic and extrinsic factors, including Notch signaling pathway, Neuregulin 1 signals from the axons and interactions between SCs and the extra cellular matrix through G protein coupled receptors (Lyons *et al.*, 2005; Monk *et al.*, 2009; Woodhoo *et al.*, 2009).

Oligodendrocytes in CNS myelination

While NCCs generating neurons and glia in the PNS, motor neurons are specified in the neural tube and, subsequently, oligodendrocyte progenitor cells (OPC) in the pMN domain start their proliferation and migration (Figure 1-2A). Ultimately, OPCs become widely disperse in the CNS and differentiate into OLs, the myelinating glial cell type in the CNS (Figure 1-2) (Mitew *et al.*, 2014).

Because motor neurons and OLs both derive from the pMN domain, significant effort has been made to understand the mechanisms that regulate the differentiation of motor neurons and OLs. Previous studies demonstrate that the timing of OPC specification and differentiation are strictly regulated by various transcription factors and extracellular signaling molecules, such as *Pdgf*, *Fgf*, *Nkx2.2*, *Sox10* and *Olig1* (Noble *et*

al., 1988; Barres, Lazar and Raff, 1994; Qi *et al.*, 2001; Soula *et al.*, 2001; Lu *et al.*, 2002b). Additionally, signaling between these neural cells, such as the Notch signaling pathway, also contributes to the specification of motor neurons and OLs. Previous studies demonstrate that elevated Notch activity can block neurogenesis and promote gliogenesis (Gaiano, Nye and Fishell, 2000; B Appel, Givan and Eisen, 2001; Chambers, 2001; Shin *et al.*, 2003).

Motor exit point glia bridge CNS and PNS myelin

SCs and OLs have traditionally been thought to be the only two types of myelinating glial cells in the entire nervous system. However, intriguingly, recent work in zebrafish describes the presence of an additional type of glia, named MEP glia, sitting at the ventral MEP TZs, myelinating motor nerve roots outside the spinal cord (Figure 1-2) (Smith *et al.*, 2014). Although MEP glia eventually reside in the PNS, they derive from precursors in the spinal cord pMN domain which also give rise to motor neurons and OLs. Before the onset of OPC migration at around 50 hpf in zebrafish, MEP glia precursors migrate through MEP TZs and divide to populate motor nerve roots (Figure 1-2) (Smith *et al.*, 2014). By 3 days post fertilization (dpf), MEP glia differentiate into myelinating glia and ensheath the proximal portion motor nerve roots (Smith *et al.*, 2014). Although significant evidence supports the hypothesis that MEP glia derive from the *olig2*$^{+}$ pMN domain in the neural tube, how MEP glial precursors are specified during early spinal cord patterning remains unknown.

Although MEP glia share a common ancestor with OLs, expressing characteristic transcription factors for CNS myelinating cells, such as *sox10* and *olig2* (Smith *et al.*,

2014), they are also positive for *foxd3*, a transcription factor found in NCCs and SCs in the PNS (Smith *et al.*, 2014). However, MEP glia do not express *krox20*, which is required for PNS SCs to initiate myelination. Taken together, MEP glia originate in the CNS, function in the PNS and express a subset of both central and peripheral glial markers. MEP glia are classify as a type of hybrid glial cell bridging the myelin sheath between CNS and PNS (Fontenas and Kucenas, 2018).

The development of perineurial glia

Following the association of SCs with motor axons in the PNS, myelinated axon bundles become further ensheathed by the perineurium. Intriguingly, recent studies in zebrafish and mice demonstrate that the perineurium consists of perineurial glia (PG) derive from precursors in the *Nkx2.2*$^{+}$ p3 domain of the spinal cord (Figure 1-2B) (Kucenas *et al.*, 2008; Clark *et al.*, 2014). Similar to MEP glia, PG precursors migrate ventrally away from the p3 domain to the periphery through MEP TZs at around E12.5 in mice and 50 hpf in zebrafish (Figure 1-2) (Kucenas *et al.*, 2008; Clark *et al.*, 2014). After their exit, PG proliferate and migrate to populate axonal bundles and ensheath myelinated axons (Kucenas *et al.*, 2008; Clark *et al.*, 2014). Previous studies show that adjacent PG form tight junctions which serve as a component of the blood-nerve barrier to protect PNS axons (Figure 1-2) (Burkel, 1967; Kristensson and Olsson, 1971; K. Akert *et al.*, 1976; Kucenas *et al.*, 2008).

Unlike well-studied SCs and OLs, the development of PG is poorly understood, mainly because of the fairly recent discovery and the lack of specific markers. As stated above, PG derive from the *Nkx2.2*$^{+}$ p3 domain, which is also called the lateral floorplate

(LFP) (Kucenas *et al.*, 2008). Because PG do not turn off the transcription factor *Nkx2.2* (or *nkx2.2a* in zebrafish), it has been used as the marker for PG in previous studies (Kucenas *et al.*, 2008; Clark *et al.*, 2014; Lewis and Kucenas, 2014). However, because *Nkx2.2* also labels other cells in the LFP, it becomes extremely challenging to study the development of PG. Therefore, the location of PG precursors in the spinal cord and their behavior during the exit remain unknown.

Using zebrafish as a model to study vertebrate neural development

Rodents (especially *Mus musculus* and *Rattus norvegicus*) have been the most widely used models in vertebrate neuroscience research for many years. These studies have made significant progress in our understanding of how the nervous system assembles. However, researchers using rodent models to study neural development have inevitably faced limitations raised by the *in utero* development of rodent embryos, such as the inability to visualize cell migration and interactions in real-time in intact embryos. Given the dynamic and complicated cellular behavior during neural development, these limitations of rodent models have significantly impeded further studies in the field. Other invertebrate model organisms, such as *Drosophila* and *C. elegans*, have also made outstanding contribution to our understanding of the nervous system assembly. Although invertebrate models are more tractable, certain research questions cannot be addressed in these models because of their fundamental differences in neural development and types of cells composing the nervous system.

Over the past 30 years, zebrafish has become a popular and powerful model organism (Meyers, 2018). The power of zebrafish as a vertebrate developing rapidly and

externally with a relatively short generation time makes it very attractive for studying neural development. The true beauty of zebrafish as a model vertebrate comes down to the incredible imaging capability enabled by its embryonic transparency. Using transgenic zebrafish embryos expressing fluorescent protein under the control of cell-specific promoters, we can visualize real-time behavior of cells of interest inside intact animals. Moreover, combining *in vivo* imaging with genetically encoded calcium sensors allows measurement of neuronal and glial activity during neural development, which has provided valuable contribution to our understanding of the formation of neural network and how that generates behaviors (Leung, Wang and Mourrain, 2013).

Although zebrafish was initially known as a powerful vertebrate forward genetic system because of their small size and ease of manipulation, recent evolution of the CRISPR/Cas9 system facilitates the ability to perform gene knock-outs in zebrafish (Hwang *et al.*, 2013). In addition, taking advantage of the DNA double-strand break repair caused by CRISPR/Cas9, genes of interest can be precisely inserted into the zebrafish genome, providing a feasible method to generate knock-in animals (Kawahara, 2017).

In this dissertation, I demonstrate novel roles of PG precursors and NCCs during early development of the nervous system using zebrafish as a model organism. In Chapter III, I provide a detailed description of the origin of PG precursors in the p3 domain of the spinal cord using *in vivo* fluorescent confocal microscopy. I also show that PG precursors send dynamic actin-based protrusions to the periphery at MEP TZs before the outgrowth of motor axons. These data lead me to hypothesize that PG precursors are likely specified

at the earliest stages during spinal cord patterning and direct motor axons to exit through MEP TZs.

Neural tube closure and subsequent neural development generate significant cellular debris. Because neurogenesis happens prior to the maturation of professional phagocytes, how these dead cells removed from the developing nervous system remains unknown. However, it is extremely difficult to study this question in mice because of the *in utero* development of mouse embryos and the dynamic cellular behavior during debris clearance. In Chapter IV, taking advantage of the imaging capability of zebrafish embryos, I tackle this question by demonstrating a novel role of NCCs in engulfing dead cells during early developmental stages. I show that NCCs can migrate away from their previously-described segmentally-restricted pathway, towards dead cells around the spinal cord and engulf them. Occasionally, NCCs even enter the spinal cord through MEP TZs to clear CNS debris. The mechanisms of NCC clearance behavior closely resembles phagocytosis in professional phagocytes.

Taken together, studies presented in this dissertation demonstrate unexpected but essential roles of glial precursors in motor nerve pathfinding and debris clearance during neural development besides giving rise to their derivatives.

CHAPTER II

Material and Methods

Experimental model and method details

Descriptions and abbreviations of transgenic lines used in this study

Transgene Name	Abbreviation	Cells Labeled	Transgene action
Tg(sox10(4.9):nls-Eos)	*Tg(sox10:nls-Eos)*	NCCs, Schwann cells	Nuclear-localized Eos expression in *sox10*$^{+}$ cells
Tg(sox10(4.9):Eos)	*Tg(sox10:Eos)*	NCCs, Schwann cells	Cytoplasmic Eos expression in *sox10*$^{+}$ cells
Tg(sox10(4.9):TagRFP)	*Tg(sox10:TagRFP)*	NCCs, Schwann cells	RFP expression in *sox10*$^{+}$ cells
Tg(sox10(7.2):mEGFP)	*Tg(sox10:mEGFP)*	NCCs, Schwann cells	Membrane GFP expression in *sox10*$^{+}$ cells
Gt(foxd3:mCherry)	*Gt(foxd3:mCherry)*	NCCs, Schwann cells	mCherry expression in *foxd3*$^{+}$ cells
Tg(sox10(4.9):lamp1-GFP, cmlc2:EGFP)	*Tg(sox10:lamp1-GFP)*	NCCs, Schwann cells	Lamp1-GFP expression in *sox10*$^{+}$ cells
Tg(sox10:Gal4-VP16,cmlc2:EGFP)	*Tg(sox10:Gal4)*	NCCs, Schwann cells	Gal4 expression in *sox10*$^{+}$ cells
Tg(bactin2:Gal4-VP16,cmlc2:EGFP)	*Tg(bactin2:Gal4)*	Ubiquitously expressed	Ubiquitous Gal4 expression
Tg(pBH-UAS:secA5-YFP)	*Tg(UAS:secA5-YFP)*	Cells expressing Gal4	Labels apoptotic cells under the regulation of Gal4
Tg(4xUAS:EGFP-2xFYVE)	*Tg(UAS:GFP-FYVE)*	Cells expressing Gal4	Labels PI(3)P activity under the regulation of Gal4
Tg(olig2:DsRed2)	*Tg(olig2:DsRed)*	Motor neurons and OPCs	DsRed2 expression in *olig2*$^{+}$ cells
Tg(mnx1:mCerulean3)	*Tg(mnx1:mCerulean)*	Motor neurons	mCerulean3 expression in *mnx1*$^{+}$ cells

Tg(hb9:mGFP)	*Tg(hb9:mGFP)*	Motor neurons	Membrane-tethered GFP expressed in $hb9^+$ cells
Tg(UAS:Lifeact-GFP)	*Tg(UAS:Lifeact-GFP)*	Cells expressing Gal4	Labels filamentous actin under the regulation of Gal4
Tg(nkx2.2a(3.5):nls-EGFP)	*Tg(nkx2.2a:nls-EGFP)*	Floorplate cells, OPCs	Nuclear-localized EGFP expression in $nkx2.2a^+$ cells
Tg(nkx2.2a(3.5):nls-mCherry)	*Tg(nkx2.2a:nls-mCherry)*	Floorplate cells, OPCs	Nuclear-localized mCherry expression in $nkx2.2a^+$ cells
Tg(nkx2.2a(3.5):Gal4-VP16,cmlc2:EGFP)	*Tg(nkx2.2a:Gal4)*	Floorplate cells, OPCs	Gal4 expression in $nkx2.2a^+$ cells
Tg(gfap:NTR-mCherry)	*Tg(gfap:NTR-mCherry)*	Radial glia	NTR-mCherry expression in $gfap^+$ cells
Tg(mpeg1:EGFP)	*Tg(mpeg1:GFP)*	Macrophages, microglia	EGFP expression in $mpeg1^+$ cells

Fish Husbandry

All animal studies were approved by The University of Virginia Institutional Animal Care and Use Committee (Protocol No. 3782). Adult zebrafish were raised in group at 28.5ºC at a density of 8-10 fish/L. Zebrafish embryos were produced by pairwise mating, group raised at 28.5ºC in 10 cm petri dishes filled with egg water (6 g Instant Ocean/20 L RO water), and staged by hours post fertilization (hpf) (Kimmel *et al.*, 1995). Embryos used for live imaging after 24 hpf were treated with 0.004% phenylthiourea (PTU) in egg water to reduce pigmentation. Embryos and larvae were anesthetized using Tricaine. Euthanasia used an overdose of Tricaine. Because zebrafish sex cannot be determined until 25 days post-fertilization (TAKAHASHI, 1977), the sex of animals used for experiments was unknown.

The following published zebrafish strains were used in this study: AB*, *Tg(sox10(4.9):Eos)*^{w9}, *Tg(sox10(4.9):nls-Eos)*^{w18} (McGraw *et al.*, 2012), *Tg(sox10(7.2):mEGFP)*^{sl3} (Kirby *et al.*, 2006), *Tg(olig2:DsRed)*^{vu19} (Shin *et al.*, 2003), *Gt(foxd3:mCherry)*^{ct110R} (Hochgreb-Hägele and Bronner, 2013), *Tg(gfap:NTR-mCherry)*^{sc129} (Johnson *et al.*, 2016a; Smith *et al.*, 2016), *Tg(4xUAS:EGFP-2xFYVE)*^{la214} (Rasmussen *et al.*, 2015), *Tg(pBH-UAS:secA5-YFP)* (van Ham *et al.*, 2010), *Tg(sox10:Gal4-VP16,cmlc2:EGFP)*^{sq9} (Lee *et al.*, 2013), *Tg(hb9:mGFP)*^{ml2} (Flanagan-Steet *et al.*, 2005), *Tg(UAS:Lifeact-GFP)*^{mu271} (Helker *et al.*, 2013) and *Tg(mpeg1:EGFP)*^{gl22} (Felix Ellett *et al.*, 2011). The following lines are created in this study: *Tg(nkx2.2a(3.5):nls-EGFP)*^{uva1}, *Tg(nkx2.2a(3.5):nls-mCherry)*^{uva2}, *Tg(mnx1:mCerulean3)*^{uva3}, *Tg(nkx2.2a(3.5):Gal4-VP16, cmlc2:EGFP)*^{uva4}, *Tg(sox10(4.9):TagRFP)*^{uva5}, *Tg(sox10(4.9):lamp1-GFP, cmlc2:EGFP)*^{uva8} and *Tg(bactin2:Gal4-VP16,cmlc2:EGFP)*^{uva33}. See methods for details. Table 2 denotes abbreviations used for each strain and summarizes what each transgene labels. All the strains above are used as stable, germline transgenic lines in this study. Mosaic transgenesis of *il1b:GFP-FTASE* was generated by injection of reporter construct *il1b:GFP-FTASE* into zebrafish embryos at one-cell stage (Nguyen-Chi *et al.*, 2014).

Generation of transgenic lines

All constructs were generated using the Tol2kit Gateway-based cloning system (Kristen M Kwan *et al.*, 2007). Vectors used for making the expression constructs were p5E-bactin2, pME-nls-mCherry, pME-Gal4-VP16 and p3E-polyA (Kristen M. Kwan *et al.*, 2007), pME-mCerulean3, pME-TagRFP (Don *et al.*, 2017), p5E-nkx2.2a(-3.5) (Pauls *et*

al., 2007), p5E-sox10(-4.9) (Carney *et al.*, 2006), p5E-mnx1 (Jao, Appel and Wente, 2012) and pME-lamp1-GFP (Rasmussen *et al.*, 2015), as well as pDestTol2pA2 and pDesTol2CG2 destination vectors (Kristen M. Kwan *et al.*, 2007). Corresponding p5E, pME vectors and p3E-polyA were inserted into destination vectors through LR reactions (Kristen M Kwan *et al.*, 2007). Final constructs were amplified and sequenced to confirm the insertions. To generate stable transgenic lines, plasmid DNAs were microinjected at a concentration of 24 ng/µL in combination with 36 ng/µL *Tol2* transposase mRNA at the one cell stage and screened for founders (Kawakami, 2004).

In vivo imaging

For imaging, embryos were manually dechorionated, anesthetized with 3-aminobenzoic acid ester (Tricaine), immersed in 0.8% low-melting point agarose and mounted laterally in 35 mm glass bottom petri dishes (Fisher, Greiner Bio-One). After mounting, petri dishes were filled with egg water containing Tricaine. PTU was used to reduce pigmentation when larvae were older than 24 hpf when mounted. A 25X multi-immersion objective (NA = 0.8), 40X water objective (NA = 1.1) or a 63X water objective (NA = 1.2) mounted on a motorized Zeiss AxioObserver Z1 microscope equipped with a Quorum WaveFX-XI (Quorum Technologies Inc.) or Andor CSU-W (Andor Oxford Instruments plc.) spinning disc confocal system was used to capture all images except for orthogonal views of Lamp1-GFP+ vesicles. Time intervals for time-lapse imaging were set at 2 min, 5 min or 10 min depending on the experiment. Image processing was performed with MetaMorph and Fiji (ImageJ) to enhance brightness and

contrast. Movies in the supporting information were annotated using Fiji plugin Manual Tracking.

Live imaging of embryos younger than 19 hpf was performed after yolk shrinkage. Embryos were dechorionated and put on petri dishes coated with 2% agarose. An injection needle linked to a 50-ml syringe was used to poke into the yolk of embryos. Once an opening was created, the yolk was carefully squeezed without damaging the embryo. Embryos were then mounted immediately on the lateral side for imaging.

Images of Lamp1-GFP+ vesicles in NCCs (Figure 4F; Figure S3B) were taken using a Zeiss (Jena, Germany) LSM880 scanning laser confocal microscopes equipped with a 63x water objective and Airyscan detectors.

Eos photoconversion and lineage tracing

For whole-embryos photoconversion, *Tg(sox10:Eos)* embryos were mounted for imaging as described above and then exposed to UV light using a DAPI filter for 20 s with a Zeiss Axiozoom microscope at 20 hpf. Single-cell photoconversion and lineage tracing were performed using a nitrogen-pulsed MicroPoint laser (Andor) attached to the spinning disk confocal systems mentioned above, a dye (wavelength 404 nm) and a 40x water immersion objective. A region of interest (ROI) was created inside cells of interest to ensure precise photo-conversion. MicroPoint laser power was set between 3 to 8 depending on the location of cells. Successful photoconversion was confirmed immediately by imaging with both red and green filter sets. For lineage tracing, individual NCCs in *Tg(sox10:Eos)* embryos with engulfment vesicles larger than 4 μm were photoconverted at 20 hpf and time-lapse imaged immediately afterwards.

Cell ablation

For radial glial ablation, Tg(sox10:nls-Eos);Tg(gfap:NTR-mCherry) embryos were immersed in 15 mM Metronidazole (MTZ) solution in egg water with 1% DMSO starting at 10 h prior to imaging (at 10 hpf or 30 hpf) (Johnson et al., 2016; Smith et al., 2016). Fresh MTZ solution with Tricaine was applied when embryos were mounted for imaging (at 20 or 40 hpf). Control embryos were immersed in 1% DMSO in egg water. Single-cell laser ablation was performed using a nitrogen-pulsed MicroPoint laser (Andor) attached to the spinning disk confocal system mentioned above, a coumarin dye (wavelength 435 nm) and a 40x water immersion objective. To ablate individual cells, a ROI was first created inside the cell of interest to ensure precise ablation. MicroPoint laser was then fired within the ROI using a laser power between 20 to 40 depending on the location of the cell to ablate. Successful laser ablation was confirmed by the disappearing of the fluorescence of the cell (Lewis and Kucenas, 2014). Immediately after the ablation, conditions of cells and tissue around the ablation site were carefully examined. Embryos with unspecific damage caused by excessive laser power were excluded from experiments and/or quantification.

Vital dye staining

LysoTracker Red DND-99 (Thermo Fisher Scientific) and LysoTracker Deep Red (Thermo Fisher Scientific) were diluted to final concentrations of 10 μM with egg water. Embryos were manually dechorionated at 18 hpf and immersed in LysoTracker solution for 1 h in the dark at 25°C. Embryos were then rinsed for 3 times with fresh egg water

and immediately mounted for imaging. For neutral red staining, embryos were manually dechorionated at 16 hpf and incubated in 2.5 μg/ml neutral red (Sigma-Aldrich) dissolved in egg water at 25°C in the dark for 4 h. After incubation, embryos were rinsed for 3 times with fresh egg water and immediately mounted for imaging.

Immunohistochemistry

Dechorionated embryos were fixed with 4% PFA at 20 hpf, permeabilized in 1mg/ml collagenase for 8 min, followed by a 5 min wash with PBSTx (1% TritonX-100, 1x PBS). Embryos were then pre-blocked in 5% goat serum/PBSTx for 1 hour, incubated in primary antibody with 5% goat serum/PBSTx for 1 hour at 24 °C and overnight at 4 °C. Embryos were washed extensively with 1x PBSTx at 24 °C and incubated in secondary antibody for 1 hour at 24 °C and overnight at 4 °C. After antibody incubation, embryos were washed extensively with 1x PBSTx and stored in 50% glycerol/PBS at 4 °C until imaging. Antibodies used were: rabbit anti-Il-1β (1:200, Proteintech) (Tsarouchas *et al.*, 2018) and Alexa 488 goat anti-rabbit (1:600, ThermoFisher).

Chemical treatments

Ac-YVAD-cmk (YVAD) (Sigma) was dissolved in DMSO to a stock concentration of 10 mM. For treatment, the stock solution was diluted with egg water to a working concentration of 75 μM with 1% DMSO (Chan and Yager, 2002; Tsarouchas *et al.*, 2018). At 10 hpf, embryos were manually dechorionated, immersed in the YVAD solution and incubated at 25°C for 12 hours. Embryos were then mounted for imaging and cell ablation in fresh YVAD solution (with Tricaine) from 20 to 40 hpf. Control

groups were treated with 1% DMSO. For IL-1Ra experiments, embryos were manually dechorionated at 16 hpf and treated with 10 μM IL-1Ra (Sigma) in egg water (or egg water only as a control) at 25°C (Mesureur *et al.*, 2017). Embryos were then mounted for imaging and cell ablation from 20 to 36 hpf. Similarly, for Suramin treatment, embryos were dechorionated at 16 hpf and treated with 5 mM Suramin (Sigma) in egg water with 1% DMSO at 25°C (Casano, Albert and Peri, 2016). Embryos were then mounted for imaging and cell ablation from 20 to 36 hpf.

GM6001 (abcam) were diluted in egg water at a stock concentration of 10 mM. For treatment, embryos were manually dechorionated at 36 hpf and treated with 15 μM GM6001 in egg water with 1.5% DMSO. Embryos were mounted for imaging between 48 to 50 hpf.

Cell dissociation for flow cytometry

For NCC dissociation, 36 hpf and 72 hpf *Gt(foxd3:mCherry);Tg(sox10:mEGFP)* embryos were chilled in egg water on ice and the anterior halves of the embryos were removed using a scalpel. Trunk pieces were placed in calcium-free Ringer's solution with 2.5mM EDTA and rocked for 15 minutes at 4°C. The trunk pieces were washed three times with chilled Dulbecco's PBS (D-PBS) and then transferred to microcentrifuge tubes along with 100ul D-PBS. A pellet pestle was used to break up the trunk pieces and then 30ul Liberase TM was added. The samples were incubated for 15 minutes at 28.5°C, 1ml 1x Trypsin with 5% EDTA solution was added, and the samples were incubated for 15 more minutes at 28.5 °C. The samples were pipetted into 5ml D-PBS with 1% BSA and then passed through a 40um cell strainer and a syringe plunger was used to gently

mash the samples into a petri dish. The contents of the petri dish were passed through a new cell strainer and the samples were then transferred to a microcentrifuge tube and were washed 2x with D-PBS+BSA. Three samples of cells (1750 ± 750) at each stage were used for RNA-sequencing. Total RNA was extracted using the RNeasy Micro Kit (QIANGEN) followed by cDNA preparation using Smart-Seq v4 Ultra Low Input RNA Kit for Sequencing (Takara). For library preparation, I used NEBNext Ultra II DNA Library Prep Kit for Illumina (NEB).

RNA-seq analysis

Abundance of transcripts from RNA-seq datasets were first imported into "DESeq2" pipeline using the R package "tximport" (Love, Huber and Anders, 2014; Soneson, Love and Robinson, 2016). R package "AnnotationDbi" was used to acquire ENTREZ IDs and Gene Symbols (Pagès H, Carlson M, Falcon S, 2019). Normalized FPKM counts were generated using the "fpkm()" function in the "DESeq2" package and were used for making Figure S1E & F (Love, Huber and Anders, 2014). Differentially expressed genes were analyzed using the "DESeq2" package (abs(log2FoldChange) > 1 & padj < 0.1) (Love, Huber and Anders, 2014). Lists of differentially expressed genes were then used to perform functional analysis using the "clusterProfiler" package (Yu et al., 2012). Genes with padj == NA were removed to exclude genes with low counts. Gene set enrichment analysis (GSEA) for Gene Ontology and KEGG pathway were then performed using functions "gseGO()" and "gseKEGG()", respectively (Figure S1C & D) (Kanehisa and Goto, 2000; Yu et al., 2012; Hancock, Zvelebil and Stevens, 2014). Functions "enrichGO()" and "enrichKEGG()" were used to perform over-representation

tests (Figure S1A & B) (Yu et al., 2012). Raw sequencing data is available on GEO. Transcript abundance files are available on Mendeley Data: http://dx.doi.org/10.17632/htdnfjb22c.3.

Key resources table

Antibodies		
Rabbit anti-IL1β	Proteintech	CAT#16806-1-AP; RRID:AB_10646432
Goat anti-Rabbit IgG (H+L) Cross-Adsorbed Secondary Antibody, Alexa Fluor 488	ThermoFisher	CAT#A-11008; RRID:AB_2536607
Chemicals, Peptides, and Recombinant Proteins		
Dimethyl sulfoxide (DMSO)	Sigma	Cat#D2650; CAS#67-68-5
Metronidazole (MTZ)	Sigma	Cat#M1547; CAS#443-48-1
Ac-YVAD-cmk	InvivoGen	Cat#inh-yvad; CAS#178603-78-6
Interleukin 1 receptor antagonist (IL-1Ra)	Sigma	Cat#SRP3327
1-Phenyl-2-thiourea (PTU)	Sigma	Cat#P7629; CAS#103-85-5
Deposited Data		
Neural crest cell RNA-Sequencing abundance files	Mendeley Data	http://dx.doi.org/10.17632/htdnfjb22c.3
Neural crest cell RNA-Sequencing raw data	GEO	https://www.ncbi.nlm.nih.gov/geo/query/acc.cgi?acc=GSE135237
Experimental Models: Organisms/Strains		
Zebrafish: *Tg(sox10(4.9):Eos)*^{w9}	(McGraw *et al.*, 2012)	ZDB-ALT-110721-1
Zebrafish: *Tg(sox10(4.9):nls-Eos)*^{w18}	(McGraw *et al.*, 2012)	ZDB-ALT-110721-2

Zebrafish: *Tg(sox10(7.2):mEGFP)^{sl3}*	(Kirby *et al.*, 2006)	ZDB-ALT-150113-6
Zebrafish: *Tg(olig2:DsRed)^{vu19}*	(Shin *et al.*, 2003)	ZDB-ALT-080321-2
Zebrafish: Gt(foxd3:mCherry)	(Hochgreb-Hägele and Bronner, 2013)	ZDB-ALT-130314-2
Zebrafish: *Tg(gfap:NTR-mCherry)^{sc129}*	(Johnson *et al.*, 2016b)	ZDB-ALT-160630-3
Zebrafish: *Tg(4xUAS:EGFP-2xFYVE)^{la214}*	(Rasmussen *et al.*, 2015)	ZDB-ALT-150424-5
Zebrafish: *Tg(pBH-UAS:secA5-YFP)*	(van Ham *et al.*, 2010)	ZDB-FIG-150323-2
Zebrafish: *Tg(sox10:Gal4-VP16,cmlc2:EGFP)^{sq9}*	(Lee *et al.*, 2013)	ZDB-ALT-130826-2
Zebrafish: *Tg(mpeg1:EGFP)^{gl22}*	(F. Ellett *et al.*, 2011)	ZDB-ALT-120117-1
Zebrafish: *Tg(nkx2.2a(3.5):nls-mCherry)^{uva2}*	This paper	N/A
Zebrafish: *Tg(mnx1:mCerulean3)^{uva3}*	This paper	N/A
Zebrafish: *Tg(sox10(4.9):TagRFP)^{uva5}*	This paper	N/A
Zebrafish: *Tg(sox10(4.9):lamp1-GFP, cmlc2:EGFP)^{uva8}*	This paper	N/A
Zebrafish: *Tg(bactin2:Gal4-VP16,cmlc2:EGFP)^{uva33}*	This paper	N/A

Oligonucleotides

pDestTol2 expression construct FWD	This paper	N/A
pDestTol2 expression construct REV	This paper	N/A

Recombinant DNA

p5E-*bactin2*	(Kristen M. Kwan *et al.*, 2007)	N/A

p5E-*sox10(-4.9)*	(Carney *et al.*, 2006)	N/A
p5E-*nkx2.2a(-3.5)*	(Pauls *et al.*, 2007)	N/A
p5E-*mnx1*	(Jao, Appel and Wente, 2012)	N/A
pME-*nls-mCherry*	(Kristen M. Kwan *et al.*, 2007)	N/A
pME-*Gal4-VP16*	(Kristen M. Kwan *et al.*, 2007)	N/A
pME-*mCerulean3*	(Don *et al.*, 2017)	N/A
pME-*TagRFP-CAAX*	(Don *et al.*, 2017)	N/A
pME-*EGFP-CAAX*	(Don *et al.*, 2017)	N/A
pME-*TagRFP*	(Don *et al.*, 2017)	N/A
pME-*lamp1-GFP*	(Rasmussen *et al.*, 2015)	N/A
p3E-*polyA*	(Kristen M. Kwan *et al.*, 2007)	N/A
pDestTol2pA2	(Kristen M. Kwan *et al.*, 2007)	N/A
pDestTol2CG2	(Kristen M. Kwan *et al.*, 2007)	N/A
il1b:GFP-FTASE	(Nguyen-Chi *et al.*, 2014)	ZDB-TGCONSTRCT-151008-4

Software and Algorithms

MetaMorph	Molecular Devices	http://moleculardevices.com/
ImageJ	NIH	https://imagej.net/
Prism6	GraphPad	http://Graphpad.com
R(v3.5)	R-project	http://www.r-project.org/
RStudio	R Studio	http://Rstudio.com/
DESeq2	(Love, Huber and Anders, 2014)	http://bioconductor.org/packages/DESeq2/
tximport	(Soneson, Love and Robinson, 2016)	http://bioconductor.org/packages/tximport/

clusterProfiler	(Yu *et al.*, 2012)	http://bioconductor.org/packages/clusterProfiler/
AnnotationDbi	(Pagès H, Carlson M, Falcon S, 2019)	https://bioconductor.org/packages/AnnotationDbi

Quantification and statistical analysis

Quantification of NCC numbers and behavior

For quantification of CNS located NCCs, z-stack images from 20 h time-lapse movies taken with a 25X multi-immersion objective were used to detect NCC entrance into the spinal cord. Distortion of the nucleus indicated passage through MEP TZs (Smith *et al.*, 2016). The number of NCCs with CNS experience divided by total NCC number in the field of view (185 µm x 185 µm) was used to calculate the percentage of NCCs that have entered the CNS. For the number of NCCs entering the CNS per hemisegment, the number of entering events were counted and divided by the number of hemisegments in the field of view. Quantification of NCC recruitment after cell ablation was done with composite z image stacks compiled using Metamorph software. Individual z images were sequentially observed and cells were counted within the entire z stack.

Quantification of the formation of PI(3)P$^+$ vesicles and neutral red intensity

Individual z images were sequentially observed to determine time point 0 as when GFP-FYVE fluorescence on NCC vesicles became the brightest. For quantification of the roundness of GFP-FYVE vesicles and neutral red intensity over time, square ROIs were created around individual NCC vesicles in Fiji. *Circularity* (*4π*area/perimeter^2*) and *Aspect Ratio* of GFP-FYVE signals in the ROIs were first calculated using the measurement function in Fiji. *Roundness* values, defined as *Circularity*/*Aspect Ratio*,

were used to distinguish between large, ring-like, vesicle signals and small, granule-like, endosome signals. Neutral red intensity was calculated within the same ROI using *Mean Gray Value* measurement and then normalized to [0,1] using min-max scaling.

Statistical analysis

GraphPad Prism was used for all statistical analyses. Two-way ANOVA followed by Tukey's multiple comparison test was used for quantification of NCC recruitment. Unpaired student's t-test or, for multiple comparisons, one-way ANOVA followed by Tukey's multiple comparison test were used for all other quantifications. A confidence interval of 95% was used to determine the level of significance. Other statistical details, such as sample size, p-value and dispersion, are labeled on the figures or can be found in the legends.

CHAPTER III

The Origin of Perineurial Glia and their Roles in Motor Axon Pathfinding

Abstract

Motor nerves play critical roles in transmitting information out of the central nervous system (CNS). During spinal motor nerve formation, motor neurons (MN) project axons out of the CNS to their targets in peripheral nervous system (PNS) by navigating through specialized CNS/PNS locations known as motor exit point (MEP) transition zones (TZ) (Figure 1-1) (Kucenas *et al.*, 2009; Bonanomi and Samuel L Pfaff, 2010). However, little is known about the cellular mechanisms of motor axon exit through MEP TZs. Besides correct pathfinding of motor axons, efficient motor function also depends on the proper assembly of spinal motor nerves which requires interactions of several distinct cell types, including Schwann cells, MEP glia, perineurial glia (PG) and motor axons (Figure 1-2). Despite of being a type of PNS glia, PG derive from the CNS and migrate out of the spinal cord through MEP TZs to form the motor nerve perineurium (Figure 1-2) (Kucenas *et al.*, 2008; Clark *et al.*, 2014). However, how PG precursors are specified in the spinal cord and how they coordinate with other cells during motor nerve assembly remain unknown. Here, using *in vivo*, time-lapse imaging in zebrafish, I provide a detailed description of the origin of PG precursors in the p3 domain of the spinal cord. Moreover, I found that PG precursors send dynamic protrusions to the periphery at MEP TZs during the initial outgrowth of motor axons, leading me to hypothesize that they contribute to MEP TZ specification at the earliest stages during spinal cord patterning and are likely involved in motor axon pathfinding through MEP TZs.

Introduction

Vertebrate motor neurons in the neural tube extend axons out of the CNS to innervate peripheral targets. The precision of these projections is crucial for motor axons to reach their intended targets and thus, has a profound impact on proper motor functions (Bonanomi and Samuel L Pfaff, 2010). Although various subtypes of motor neurons within each segment of vertebrate animals exhibit divergent axon pathways towards their assigned targets, they all exit the spinal cord through the same specialized locations known as MEP TZs (Figure 1-1B; Figure 1-2A) (Mauti *et al.*, 2007; Kucenas *et al.*, 2009; Bonanomi and Samuel L. Pfaff, 2010). During neural development, the first set of motor neurons specified in the pMN domain of the spinal cord project their axons through ventral TZs located in the rostral part of each somite in mice and the middle of each hemisegment in zebrafish at around E9.5 and 16 hpf, respectively (Paul Z Myers, Eisen and Westerfield, 1986; Bonanomi and Samuel L Pfaff, 2010). Although a large number of guidance cues involved in motor axon pathfinding in the periphery have been identified (Dillon *et al.*, 2005; Paulus and Halloran, 2006; Bonanomi and Samuel L Pfaff, 2010; Bravo-Ambrosio, Mastick and Kaprielian, 2012), little is known about the cellular and molecular mechanisms that direct their initial exit through MEP TZs.

After motor axon exit, PG originating from the *nkx2.2*$^{+}$ lateral floorplate (LFP) in the neural tube migrate out of the CNS through MEP TZs at around E12.5 and 16 hpf in mice and zebrafish, respectively (Figure 1-2) (Kucenas *et al.*, 2008; Clark *et al.*, 2014). Once in the PNS, PG proliferate and migrate along motor axons (Kucenas *et al.*, 2008; Clark *et al.*, 2014; Kucenas, 2015). Ultimately, they wrap around myelinated motor axons

and differentiate into the perineurium which serves as a component of blood-nerve-barrier in the PNS (Figure 1-2) (Burkel, 1967; Kristensson and Olsson, 1971; K Akert *et al.*, 1976; Kucenas *et al.*, 2008). Previous studies show that *Nkx2.2* is required for PG specification in mice and fish (Kucenas *et al.*, 2008; Clark *et al.*, 2014), and their exit from the spinal cord require Notch signaling (Binari, Lewis and Kucenas, 2013). Nevertheless, the location of PG precursors in the spinal cord and mechanisms of their exit through MEP TZs remain largely unknown due to the fairly recent discovery and the lack of specific markers.

Interestingly, in *Nkx2.2* knock-out mice and zebrafish embryos injected with *nkx2.2a* morpholino where PG specification was blocked, motor neurons project axons out of the spinal cord at ectopic locations and, occasionally, their cell bodies exit the spinal cord (Kucenas *et al.*, 2008; Clark *et al.*, 2014), suggesting that early development of *nkx2.2*$^{+}$ LFP precursors is crucial to both proper motor axon exit and PG specification. Therefore, I hypothesize that PG precursors located in the LFP are involved in the specification of MEP TZs at early developmental stages.

Here, using time-lapse imaging in zebrafish embryos, I demonstrate that, in each hemisegment, PG derive from two precursors specified in the LFP next to MEP TZs. Ablation of these two precursors leads to the absence of PG with no replacement up to 70 hpf. Moreover, specialized *nkx2.2a*$^{+}$ cells in the LFP around MEP TZs project dynamic actin-based filopodia into the periphery when motor axons first exit the spinal cord, leading me to hypothesize that PG precursors may facilitate the formation of MEP TZs. These data provide detailed descriptions of the origin and migration of PG and suggest a novel mechanism governing motor axon exit through MEP TZs.

Results

PG derive exclusively from two precursors in the LFP close to the MEP TZ in each hemisegment

Although previous studies demonstrate that PG are derived from the *nkx2.2a*$^{+}$ LFP precursors at approximately 50 hpf in zebrafish (Kucenas *et al.*, 2008; Binari, Lewis and Kucenas, 2013), the number of PG precursors that exit the spinal cord remains unknown. To answer this question, I used *Tg(nkx2.2a:nls-EGFP)* transgenic fish, where *nkx2.2a* regulatory sequences drive nuclear-localized EGFP expression in lateral floorplate cells. Compared with the *Tg(nkx2.2a:mEGFP)* line used in previous studies (Kucenas *et al.*, 2008; Binari, Lewis and Kucenas, 2013), the *Tg(nkx2.2a:nls-EGFP)* line labels nuclei of LFP cells, which makes it possible to distinguish individual cells and allows precise quantification of the number of PG precursors that migrate out of the spinal cord. In time-lapse movies of *Tg(nkx2.2a:nls-EGFP)* embryos starting at 48 hpf, I always observed two *nkx2.2a*+ cells migrate ventrally towards the inner boundary of the neural tube and leave the spinal cord one after another at approximately 50 hpf (Figure 3-1A). Once in the PNS, they divide multiple times and migrate along motor axons as previously described (data not shown) (Kucenas *et al.*, 2008). Occasionally, cell division of the first cell leaving the neural tube occurs before the exit of the second cell (Figure 3-1B). These data demonstrate that, in each hemisegment, two PG precursors located dorsal to the MEP TZ migrate out of the spinal cord at approximately 50 hpf.

Next, I asked whether other LFP cells other than the two located near MEP TZs could differentiate into PG. To investigate this question, I laser ablated these two

precursors and tested whether other *nkx2.2a*$^{+}$ cells were able to leave the neural tube and compensate for the loss of the original PG. To do this, I crossed *Tg(nkx2.2a:nls-EGFP)* fish to *Tg(olig2:DsRed)* transgenic fish, where olig2 regulatory sequences label spinal cord motor neurons, and ablated the two *nkx2.2a*$^{+}$ PG precursors in the periphery (Figure 3-1C, asterisks) at 52 hpf using a pulsed nitrogen dye laser. After ablation, I performed time-lapse imaging of these embryos to investigate the behavior of other *nkx2.2a*$^{+}$ LFP cells. In these embryos, I did not observe any other *nkx2.2a*$^{+}$ cells in the LFP migrate out of the spinal cord up to 70 hpf (Figure 3-1C). Similarly, ablation of PG precursors during or before their migration out of the spinal cord leads to the absence of *nkx2.2a*$^{+}$ PG in the periphery (Figure 3-1D & E). Taken together, these findings led me to conclude that the two *nkx2.2a*$^{+}$ cells dorsal to the MEP TZ are the exclusive PG precursors.

PG precursors are determined during early spinal cord development

The data I describe above show that ablation of the two nkx2.2a^{+} cells at 48 hpf while they are in the LFP, results in the absence of PG, which is consistent with the hypothesis that PG precursors in the LFP are specified at early developmental stages. Therefore, I wanted to examine the origin of PG precursors during early development of the spinal cord. To do this, I performed time-lapse imaging of *Tg(nkx2.2a:nls-EGFP)* embryos from 28 to 50 hpf and traced the location of two PG precursors near MEP TZs. In these movies, I found that PG precursors derive from two mother cells (Figure 3-2A, arrows) located dorsal to the potential MEP TZ in the middle of each hemisegment. At around 30 to 40 hpf, each of these two cells (Figure 3-2A, arrows) divides once and one of the daughter cells (filled arrowheads) from each mother cell migrate away from the LFP,

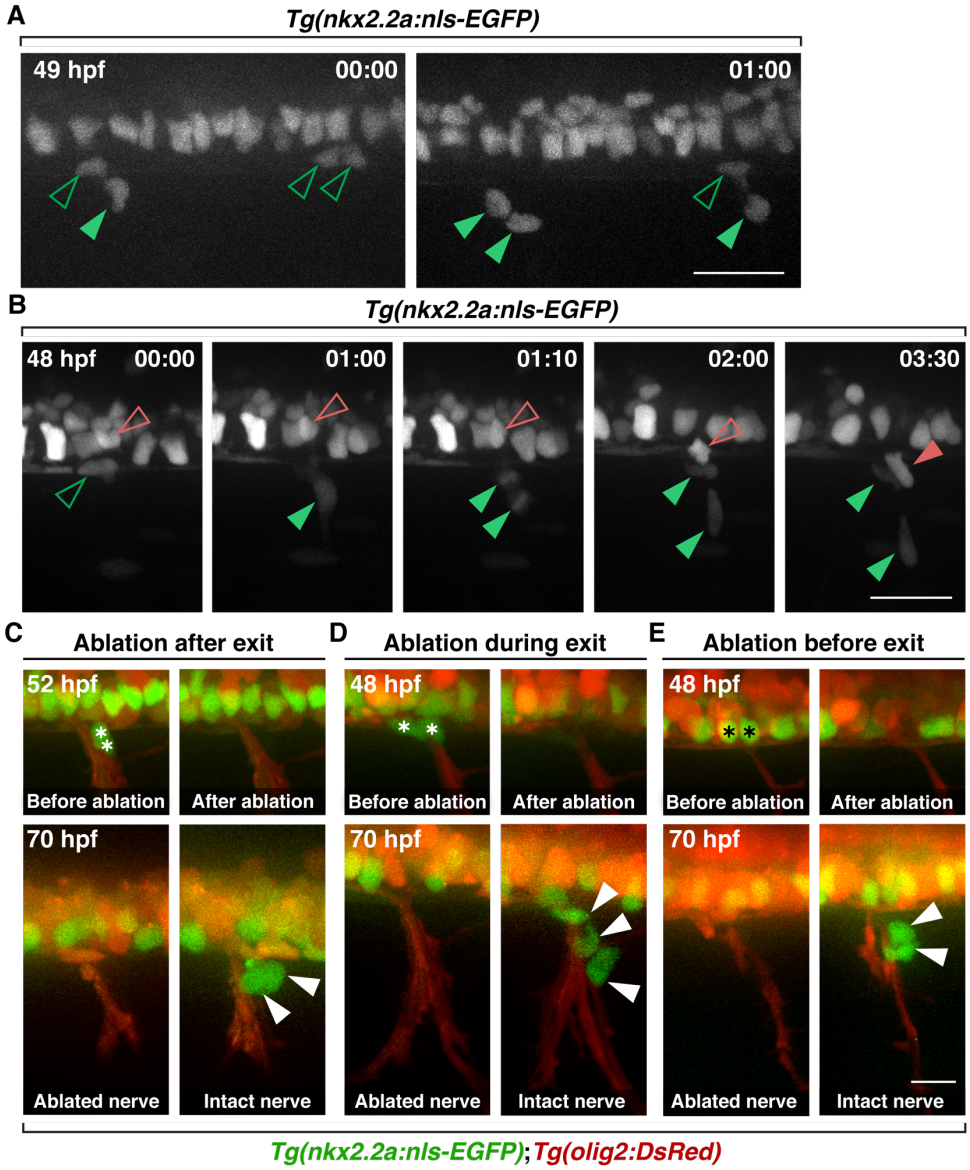

Figure 3-1. PG derive exclusively from two precursors at the MEP TZ in each hemisegment. (A) Images from a time-lapse movie of *Tg(nkx2.2a:nls-EGFP)* embryo showing PG precursors (arrowheads) migrate out of the spinal cord. Open arrowheads denote precursors in the CNS; filled arrowheads denote precursors in the PNS. **(B)** Images from a time-lapse movie of *Tg(nkx2.2a:nls-EGFP)* embryo showing cell division of PG precursors (arrowheads). **(C-E)** Ablation of PG precursors (asterisks) after, during or before their exit lead to an absence of PG at 70 hpf. PG (arrowheads) development on neighboring nerves remain intact. Scale bars: 20 µm.

while the other one remains in the spinal cord till the end of the imaging session (Figure 3-2A, open arrows). Therefore, I name the two mother cells "primary precursors" and the two daughter cells giving rise to PG "secondary precursors" (Figure 3-2B). These results indicate that the cell fate of primary PG precursors in the LFP are determined during early spinal cord patterning.

PG precursors require MMP to exit

To better visualize the cellular behavior of PG precursors during their exit, I wanted to generate a transgenic line labeling the cytoplasm of LFP cells. Because previous studies show that *nkx2.2b* is expressed in the LFP (Schäfer *et al.*, 2005), I generated a *nkx2.2b:TagRFP* construct and tested whether PG and their precursors were *nkx2.2b*$^{+}$. To do this, I injected *nkx2.2b:TagRFP* construct into *Tg(nkx2.2a:mEGFP)* embryos at the one-cell stage, screened for embryos with PG precursors labeled by both mEGFP and TagRFP at MEP TZs, and performed time-lapse imaging of these embryos starting at 40hpf. In these movies, I observed mEGFP^{+}/TagRFP^{+} PG precursors migrate out of the spinal cord at around 53 hpf (Figure 3-3A, arrowheads), indicating that *nkx2.2b* can be used to label PG and their precursors.

To understand how PG precursors migrate out of the spinal cord, I careful examined the migratory behavior of individual PG precursors. I noticed that the position of the first PG precursor that fully migrate out of the spinal cord is always relatively lateral to the other precursor (Figure 3-3C). However, there seems to be no correlation between the anterior-posterior (A-P) position of precursors in the LFP and the sequence of their exit (Figure 3-3C).

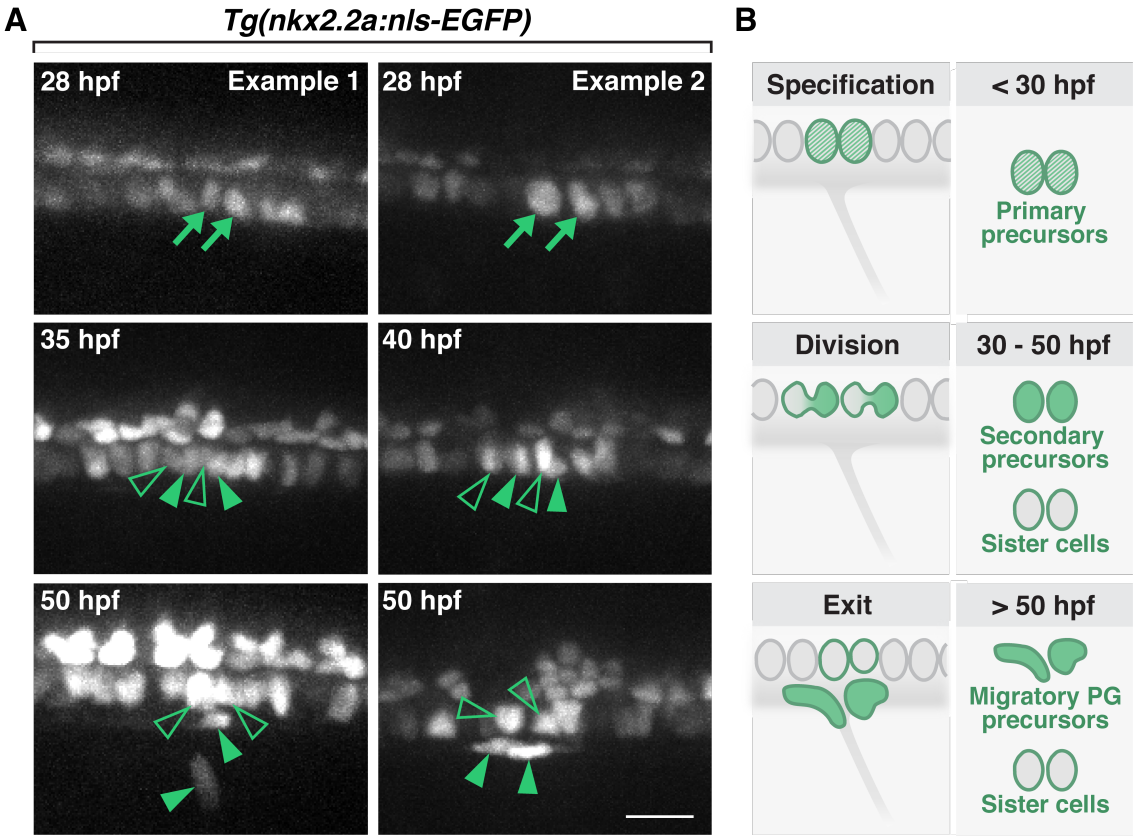

Figure 3-2. PG drive from precursors located at MEP TZs. (A) Images from two time-lapse movies of *Tg(nkx2.2a:nls-EGFP)* embryo starting at 28 hpf. Arrows denote primary PG precursors. Filled and open arrowheads denote secondary PG precursors and their sister cells, respectively. **(B)** Schematic diagrams of the specification, division, and exit of PG precursors. Scale bars: 20 μm.

Interestingly, I observed PG precursors (Figure 3-3B, asterisks) project dynamic protrusions (arrowheads) out of the spinal cord at MEP TZs before leaving the LFP in all of these movies (Figure 3-3B; See also Figure 3-3C). Compared with PG precursors, other LFP cells do not have such protrusions but only form static end-feet (Figure 3-3B open arrowheads; See also Figure 3-3C) along the ventral edge of the spinal cord. The dynamic protrusions of PG precursors and their migratory behavior notably resemble the invasive behavior of cancer cells and *C.elegans* anchor cells when they migrate through the basement membrane (Murphy and Courtneidge, 2011; Morrissey, Hagedorn and Sherwood, 2013). Because previous studies demonstrate that cancer cells and *C.elegans* anchor cells send dynamic protrusions named invadopodia through the basement membrane and secrete matrix metalloproteases (MMP), a family of secreted endopeptidases that degrade extracellular matrix (ECM) components (Hagedorn and Sherwood, 2011; Murphy and Courtneidge, 2011; Morrissey, Hagedorn and Sherwood, 2013), I wanted to examine whether PG precursors require MMP to exit the spinal cord. To block MMP, I treated *Tg(nkx2.2a:mEGFP);Tg(nkx2.2a:nls-mCherry)* embryos with 15 μM of GM6001, a MMP inhibitor, starting at 36 hpf and performed time-lapse imaging. Quantification of the number of PG in the periphery at 65 hpf showed that GM6001 treated embryos had fewer PG in the periphery compared with DMSO-treated controls (Figure 3-3E, n = 3/6 fish for control/GM6001, 20-27 nerves per fish were quantified). In GM6001-treated embryos, some PG precursors still migrated ventrally towards the MEP TZ and sent protrusions to the periphery (Figure 3-3D, open arrowheads). However, unlike control precursors that cross the CNS/PNS boundary immediately after leaving the LFP, these cells stay inside the spinal cord for more than 15

hours after their migration from the LFP (Figure 3-3D). This data indicates that the reduced number of PG in the periphery at 65 hpf after MMP inhibition is mainly caused by migratory defects of PG precursors. Based on these results, I conclude that PG precursors send dynamic protrusions out of the spinal cord at MEP TZs and require MMP to migrate through the CNS/PNS boundary.

PG precursors send dynamic actin-based protrusions to the periphery at MEP TZs during motor axon outgrowth

Because I demonstrate that PG precursors are specified as early as 28 hpf (Figure 3-2), I then asked whether PG precursors also send protrusions to the periphery at earlier developmental stages. To answer this question, I performed time-lapse imaging in *Tg(nkx2.2a:mEGFP);Tg(olig2:DsRed)* embryos from 18 hpf and observed dynamic *nkx2.2a*$^{+}$ protrusions at every ventral TZ during motor axon outgrowth starting from the beginning of the imaging window (Figure 3-4A). Excitingly, these protrusions cluster around the middle of each hemisegment but are not present at other locations along the A-P axis (Figure 3-4B). Unlike axonal growth cones which extend further into the periphery, *nkx2.2a*$^{+}$ protrusions do not grow longer but stay at MEP TZs and remain dynamic until the exit of *nkx2.2a*$^{+}$ PG (Figure 3-4A).

To verify that the *nkx2.2a*$^{+}$ protrusions around MEP TZs at early stages derive from PG precursors, I sparsely labeled the membrane of LFP cells by injecting *nkx2.2b:EGFP-CAAX* or *nkx2.2b:TagRFP-CAAX* into embryos at the one-cell stage. Between 20 and 30 hpf, embryos were screened for LFP protrusions labeled by

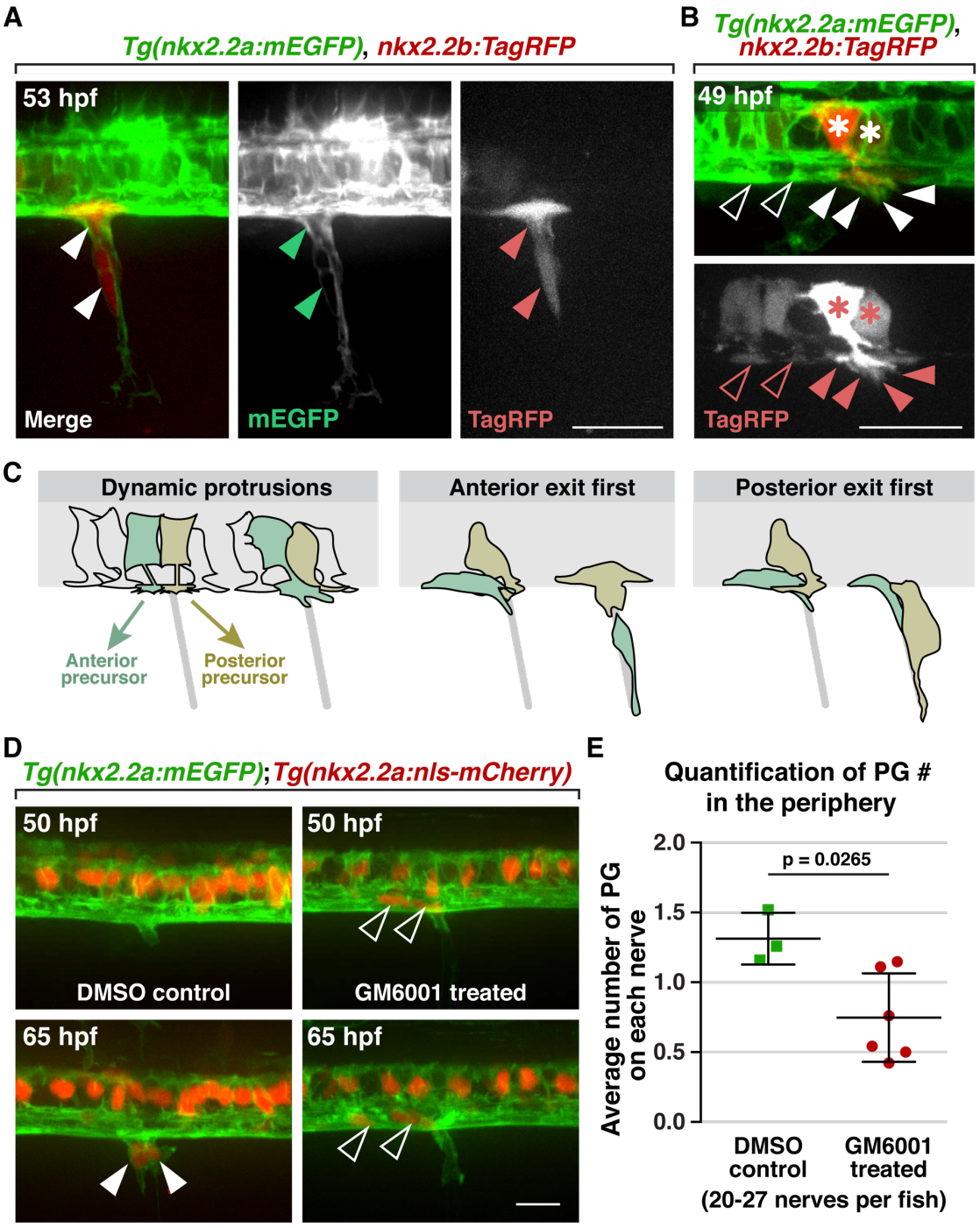

Figure 3-3. PG precursors send dynamic protrusions to the periphery and require MMP to exit. (A) Images from a 53 hpf *Tg(nkx2.2a:mEGFP)* embryo injected with *nkx2.2b:TagRFP*. Arrowheads denote *nkx2.2a*$^{+}$/*nkx2.2b*$^{+}$ PG precursor. **(B)** PG precursors (asterisks) send protrusions to the periphery while other LFP cells do not. **(C)** Schematic diagrams showing the position of PG precursors and their two

ways of exit. **(D)** In embryos treated with GM6001, PG precursors (open arrowheads) struggle to exit the spinal cord and pause at MEP TZs while PG precursors (arrowheads) in DMSO treated embryos exit normally. **(E)** Quantification of the number of PG in the periphery at 65 hpf in DMSO (n = 3 fish) and GM6001 (n = 6 fish) treated embryos. The number of PG on 20-27 nerves were quantified for each fish. Scale bars: 20 µm.

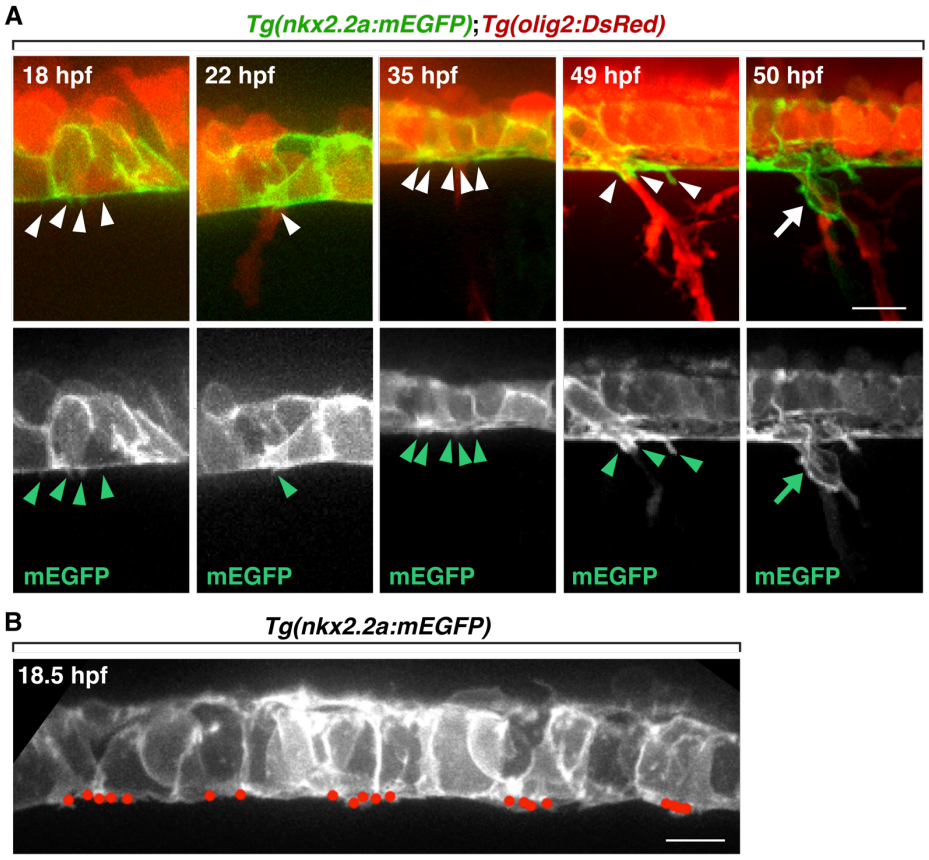

Figure 3-4. *nkx2.2a*$^+$ protrusions at MEP TZs during motor axon outgrowth. (A) Images of MEP TZs in *Tg(nkx2.2a:mEGFP);Tg(olig2:DsRed)* embryos at different stages showing *nkx2.2a*$^+$ protrusions (arrowheads) and PG migration (arrows). **(B)** *nkx2.2a*$^+$ protrusions are clustered at segmentally organized MEP TZs in *Tg(nkx2.2a:mEGFP)* at 18.5 hpf. Scale bars: 10 µm.

membrane-tethered EGFP or TagRFP (Figure 3-5A & B). Nerves with labeled protrusions were time-lapse imaged starting at 48 hpf to trace the behavior of these cells. In these movies, I found that PG precursors labeled by EGFP or TagRFP migrate out of the spinal cord at around 50 hpf (Figure 3-5A & B). These results support the hypothesis that PG precursors located at MEP TZs project dynamic protrusions during motor axon outgrowth.

Because the formation of filopodia and invadopodia in invasive cells is dependent on actin filaments (Yamaguchi and Condeelis, 2007; Olson and Sahai, 2009; Hagedorn and Sherwood, 2011), I wanted to examine whether PG protrusions were also actin-based structures. To do this, I generated *Tg(nkx2.2a:Gal4)* transgenic fish, which express Gal4 transcription factor in LFP cells, and crossed it with *Tg(UAS:Lifeact-GFP)* zebrafish to label filamentous actin with GFP (Riedl *et al.*, 2008; Helker *et al.*, 2013). *Tg(nkx2.2a:Gal4);Tg(UAS:Lifeact-GFP)* double transgenic zebrafish were further crossed to *Tg(mnx1:mCerulean3)* where mCerulean3 is expressed in primary motor neurons. Time-lapse imaging of *Tg(nkx2.2a:Gal4);Tg(UAS:Lifeact-GFP)*;*Tg(mnx1:mCerulean3)* embryos starting at 22 hpf showed that LFP cells at MEP TZs project dynamic GFP^+ protrusions out of the spinal cord (Figure 3-6A, arrowheads), indicating that actin filaments are enriched in these protrusions. In addition, these actin-rich protrusions do not extend further into the periphery and are only present at MEP TZs in the middle of each somite (Figure 3-6A & B), indicating that they belong to PG precursors located at MEP TZs.

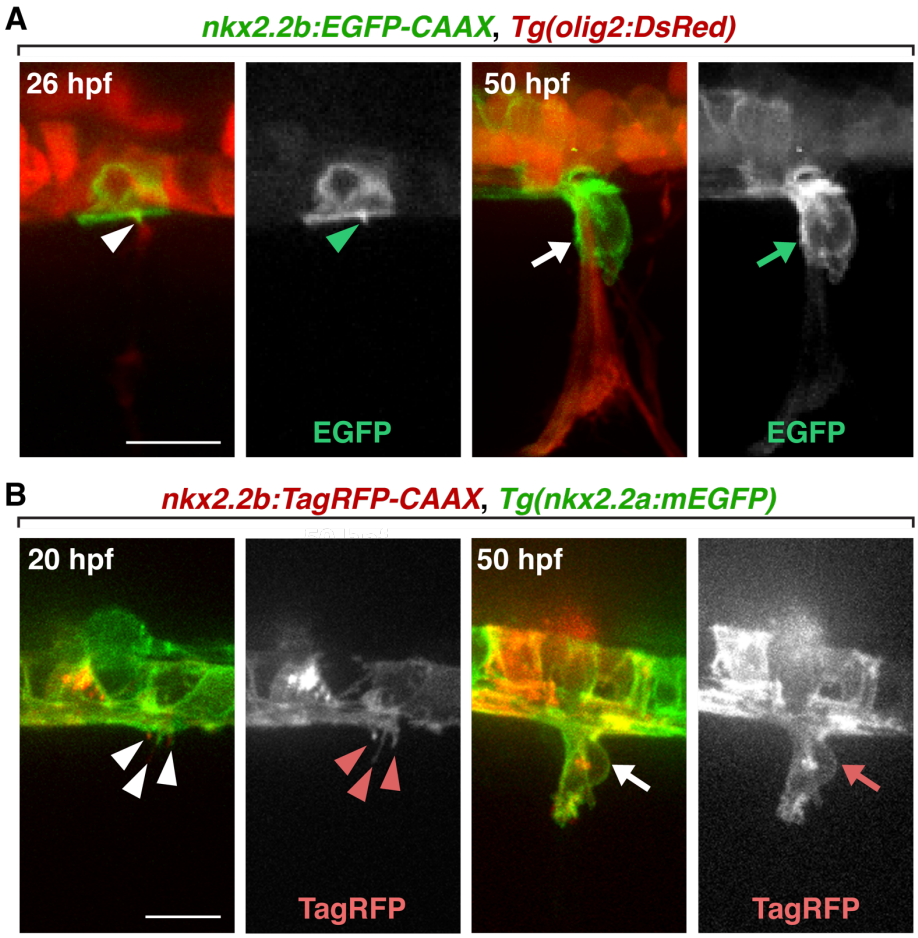

Figure 3-5. LFP cells with *nkx2.2a*$^{+}$ protrusions give rise to PG. (A) Images from a *Tg(olig2:DsRed)* embryo injected with *nkx2.2b:EGFP-CAAX.* Arrowheads denote LFP cells with protrusions labeled by EGFP at 26 hpf. Arrows denote PG labeled by EGFP at 50 hpf on the same nerve. **(B)** Images from a *Tg(nkx2.2a:mEGFP)* embryo injected with *nkx2.2b:TagRFP-CAAX.* Arrowheads denote LFP cells with protrusions labeled by TagRFP at 20 hpf. Arrows denote PG labeled by TagRFP at 50 hpf on the same nerve. Scale bars: 10 µm.

Interestingly, time-lapse imaging of *Tg(nkx2.2a:Gal4);Tg(UAS:Lifeact-GFP)* embryos revealed extremely bright and dynamic Lifeact-GFP labeling on the ventral side of the LFP around MEP TZs (Figure 3-6A & B, arrows). These structures with highly concentrated actin were only present at the root of protrusions projected by PG precursors, resembling the actin-rich core in the middle of invadopodia (Murphy and Courtneidge, 2011; Morrissey, Hagedorn and Sherwood, 2013).

Based on these results, I conclude that PG precursors form dynamic invadopodia-like protrusions at MEP TZs during the initial outgrowth of motor axons.

LFP cells project protrusions at ectopic MEP TZs in sidetracked mutants

My findings demonstrate that PG precursors project dynamic protrusions at MEP TZs during motor axon pathfinding through the CNS/PNS boundary. These protrusions resemble invadopodia and may secrete MMP to degrade the basement membrane (Murphy and Courtneidge, 2011). Given the spatiotemporal correlation between these invasive protrusions and motor axon outgrowth from the spinal cord, I hypothesized that PG precursors are involved in the determination of MEP TZs on the ventral spinal cord and motor axon exit from the CNS.

If this hypothesis is true, *nkx2.2a*$^{+}$ protrusions should be present at all MEP TZs even in embryos with motor axons exit from ectopic locations. To test this, I used the zebrafish *sidetracked* mutant where motor axons exit from non-segmental, ectopic positions (Palaisa and Granato, 2007), and performed time-lapse imaging starting at 22 hpf. Excitingly, in *Tg(nkx2.2a:mEGFP);Tg(olig2:DsRed)*, sidetracked embryos, I observed dynamic *nkx2.2a*$^{+}$ protrusions (Figure 3-7A, arrowheads) at all MEP TZs

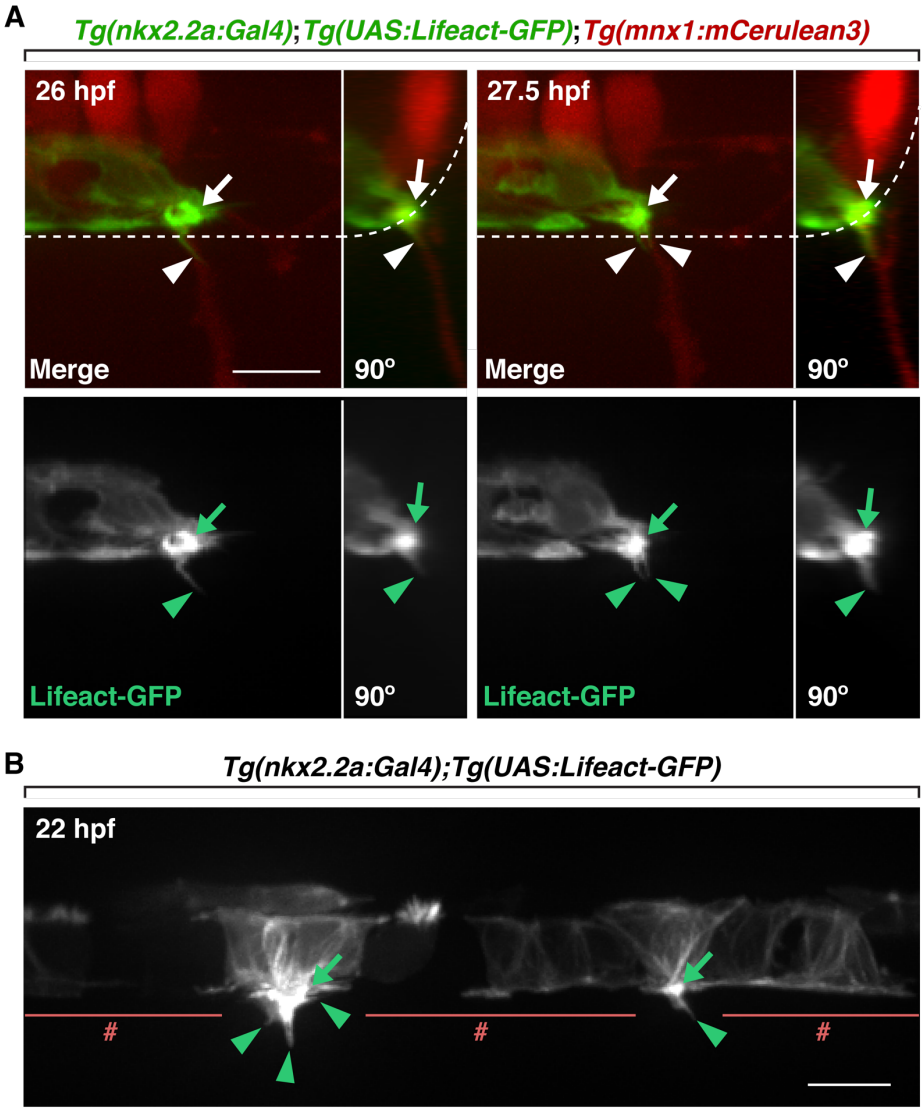

Figure 3-6. Protrusions of PG precursors are actin-based structures. (A) Images from a time-lapse movie of a *Tg(nkx2.2a:Gal4);Tg(UAS:Lifeact-GFP);Tg(mnx1:mCerulean3)* embryo showing dynamic GFP^{+} protrusions (arrows) at MEP TZs. Arrows denote a region with concentrated GFP signal at the root of protrusions. **(B)** Images from a *Tg(nkx2.2a:Gal4);Tg(UAS:Lifeact-GFP)* embryo at 22 hpf showing actin-based protrusions (arrowheads) are clustered at MEP TZs but not other positions along the LFP (red lines). Arrows denote a region with concentrated GFP signal at the root of protrusions. Scale bars: 10 μm.

starting from the beginning of the imaging window, favoring the hypothesis that LFP protrusions at MEP TZs facilitate motor axon exit from the spinal cord. At 52 hpf when PG precursors (Figure 3-7B, open arrowhead) start to migrate out of the spinal cord, *nkx2.2a*$^{+}$ protrusions (filled arrowheads) remain present on ectopic nerves (arrows). However, selective labeling of PG precursors and extended time-lapse imaging are required to determine whether these *nkx2.2a*$^{+}$ protrusions belong to ectopic PG precursors or other LFP cells such as interneurons.

Primary motor neurons migrate towards potential MEP TZs before axonogenesis

Although I demonstrate that *nkx2.2a*$^{+}$ protrusions correlate spatiotemporally with the motor axon exit, it is possible that these protrusions are not involved in axon guidance, instead, primary motor axons may locate the exit positions prior to the formation of LFP protrusions.

To investigate whether LFP protrusions are present before the outgrowth of motor axons, I wanted to perform time-lapse imaging of *Tg(nkx2.2a:mEGFP);Tg(olig2:DsRed)* embryos at 17 hpf before motor axon outgrowth. However, due to some technical difficulties which will be discussed in Chapter V, I modified my experimental design and imaged *Tg(nkx2.2a:nls-mCherry);Tg(hb9:mEGFP)*, where the *hb9* promoter drives the expression of membrane tethered EGFP in primary motor neurons, starting at 17 hpf. In these movies, I found that cell bodies of *hb9*$^{+}$ primary motor neurons (Figure 3-8A, arrows) are elongated and located away from the potential MEP TZs. They migrate in relative to *nkx2.2a*$^{+}$ LFP cells (Figure 3-8A, arrowheads) towards MEP TZs and send their axons out of the spinal cord (Figure 3-8A). These results indicate that primary motor

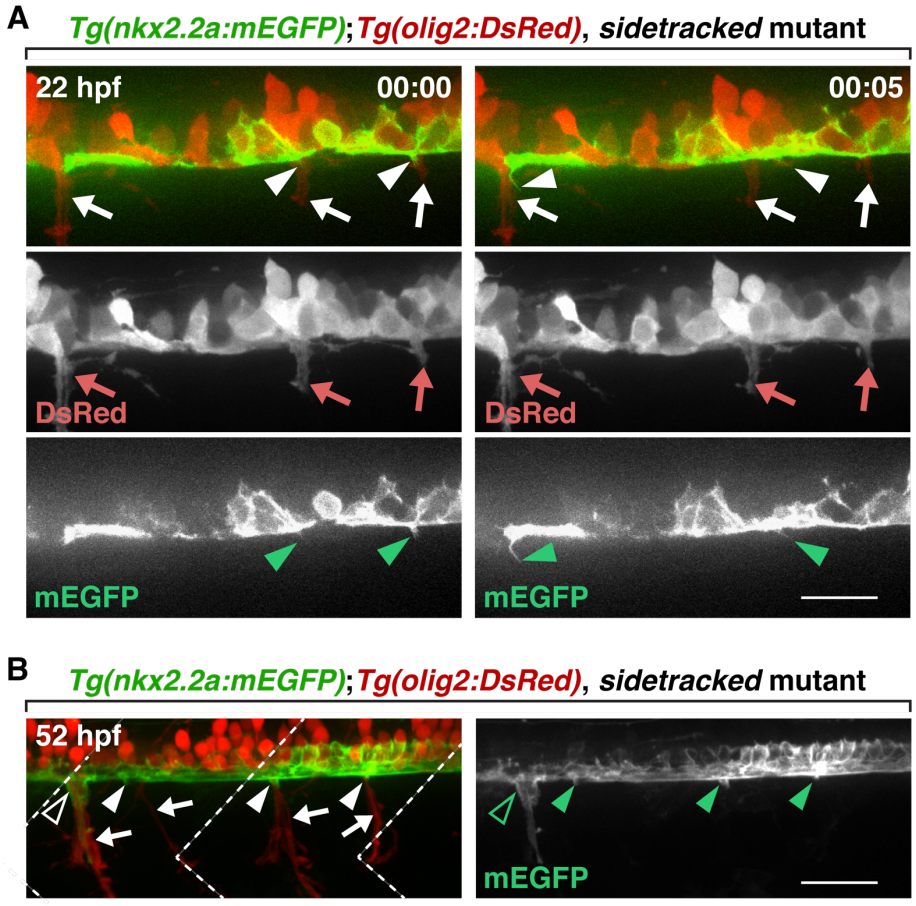

Figure 3-6. *nkx2.2a*$^{+}$ protrusions are present at extopic MEP TZs in *sidetracked* mutants. (A) Images from a time-lapse movie of *Tg(nkx2.2a:mEGFP);Tg(olig2:DsRed), sidetracked* mutant embryos showing dynamic GFP^{+} protrusions (arrowheads) along ectopic motor nerves (arrows). **(B)** Images of a *Tg(nkx2.2a:mEGFP);Tg(olig2:DsRed), sidetracked* mutant embryos at 52 hpf. Filled arrowheads denote GFP^{+} protrusions along ectopic motor nerves (arrows). Open arrowheads denote a PG migrating out of the spinal cord. Scale bars: 20 µm.

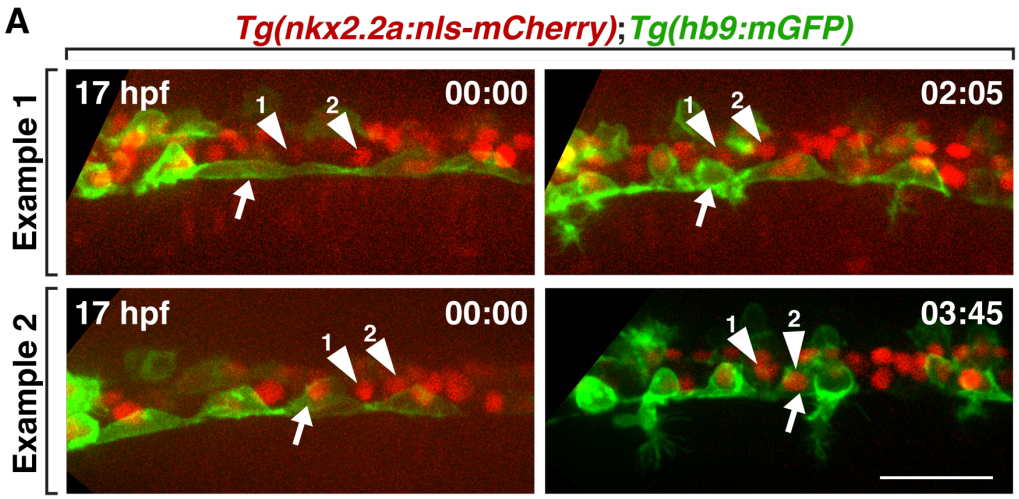

Figure 3-8. Primary motor neurons migrate towards MEP TZs in relative to LFP cells. (A) Images from time-lapse movies of two *Tg(nkx2.2a:nls-mCherry); Tg(hb9:mGFP)* embryos showing that GFP^{+} primary motor neurons (arrows) migrate along the A-P axis towards potential MEP TZs in relative to LFP cells (arrowheads) before axonal outgrowth. Scale bar: 20 µm.

neurons initially spread along the A-P axis need to migrate towards each other, in order to form motor neuron pools (Stifani, 2014). Hence, it is unlikely that future MEP TZs are specified by these pre-mitotic neurons. Moreover, my imaging data show that LFP cells are relatively static compared to pMN motor neuron progenitors, indication that LFP cells in the middle of each hemisegment may specify MEP TZs.

Taken together, my results support the hypothesis that *nkx2.2a*$^{+}$ PG precursors project invadopodia-like protrusions which facilitate the formation of MEP TZs and direct motor axon exit from the spinal cord.

Discussion

Relate segmentation to spinal cord patterning

Live imaging results of *Tg(nkx2.2a:nls-EGFP)* embryos showed that primary PG precursors are already specified at MEP TZs at 28 hpf (Figure 3-2). Transient expression of fluorescent protein driven by *nkx2.2b* promoter demonstrated that LFP cells with dynamic protrusions ultimately give rise to PG (Figure 3-5). Moreover, early imaging of *Tg(nkx2.2a:mEGFP)* embryos revealed the presence of segmental *nkx2.2a*$^{+}$ protrusions at 18 hpf (Figure 3-4B). These data indicate that primary PG precursors are likely specified in the LFP as early as 18 hpf. Because, PG precursors are specified precisely in the middle of each hemisegment along the A-P axis, a possible explanation is that PG precursors receive segmental signaling during early segmentation. If this is true, these LFP cells in the center of each hemisegment may differentially express genes related to segmental signaling. Excitingly, a recent study from the Huang lab demonstrate that some LFP cells may express *pax9*, a transcription required for sclerotome development, in a

segmentally organized pattern, supporting the hypothesis suggested above. In Chapter V, I will further discuss how segmental signaling may contribute to early patterning of the spinal cord.

Previous studies also demonstrate that Hedgehog (Hh) and Notch signaling play critical roles in LFP patterning and contribute to the differentiation of distinct LFP cell populations along the A-P axis, including early-born Kolmer-Agduhr" (KA") interneurons, V3 interneurons, and LFP progenitors (Bruce Appel, Givan and Eisen, 2001; Schäfer, Kinzel and Winkler, 2007; Huang *et al.*, 2012). However, they did not relate the spatial patterning of different LFP cell types to their relative positions in each segment. Here, my data demonstrate that PG precursors in the LFP are located at in the middle of each hemisegment. Unfortunately, using current transgenic lines and markers, PG precursors cannot be separated from other LFP progenitors, which impedes our understanding of their specification and cellular behavior. An alternative approach is to examine the segmental organization of other LFP cells and PG precursors. For example, *Tg(nkx2.2a:nls-EGFP)* embryos fixed at different stages can be stained for *tal2*$^{+}$ KA" cells and *sim1*$^{+}$ v3 interneuron progenitors using high-resolution *in situ* hybridization (Schäfer, Kinzel and Winkler, 2007; Yang, Rastegar and Strähle, 2010; Huang *et al.*, 2012). Relative positions of PG precursors and other LFP cells can thus be investigated at the cellular level. These experiments may help us apply our knowledge of LFP patterning to the specification of PG precursors. In Chapter V, I will review what is known about spinal cord patterning and further discuss how segmental signals signaling may play a role in the specification of PG precursors.

Because PG precursors form dynamic actin-based protrusions while other LFP cells do not, one potential method to differentially visualize PG precursors is to use reporters to actin network regulators, such as Rho and Src biosensors (Wang *et al.*, 2005; Clay and Halloran, 2014; Johnsson *et al.*, 2014). These reporter lines may also provide new approaches to understand cytoskeleton dynamic in PG precursors during their migration out of the spinal cord.

Characterization of PG precursor protrusions

My data demonstrate that PG precursors send dynamic actin-based protrusions to the periphery (Figure 3-3 & 3-6) and MMP is required for migration of PG precursors to the PNS (Figure 3-3). During their migration, PG precursors change their morphology from cuboid epithelial-like cells to polarized migratory cells (Figure 3-3). Even though all of these data indicate that the dynamic protrusions of PG precursors are likely invadopodia, which are known to secret MMP and play critical roles in cell invasion (Murphy and Courtneidge, 2011; Morrissey, Hagedorn and Sherwood, 2013), future studies are required to better characterize protrusions of PG precursors.

Although markers specific to invadopodia have not been discovered to date, one may examine whether invadopodia-related components, such as adaptor protein Tks4, Tks5 and cortactin (Buschman *et al.*, 2009; Murphy and Courtneidge, 2011; Lam *et al.*, 2015), are colocalized with PG precursor protrusions using immunohistochemistry.

Although the results of my GM6001 treatment indicate that MMP is involved in PG exit, further validations using specific MMP inhibitors are necessary. One possible MMP used by PG precursors is Mmp14a because previous studies demonstrate that

MT1MMP (or MMP14) is required for invadopodia-mediated cell invasion (Gawden-Bone *et al.*, 2010). A potential method to test whether Mmp14 (or Mmp14a in zebrafish) is involved in PG migration is to express established Mmp14a-mCherry fusion protein in LFP cells using *nkx2.2a* promoter (Seiler *et al.*, 2012), and perform time-lapse imaging starting at 46 hpf to capture the exit of PG precursors. Additionally, PtdIns(3,4)P_2 and PtdIns(3)P are involved in the exocytic pathway required for the secretion of MMP in filopodia (Oikawa, Itoh and Takenawa, 2008). Established reporter lines for PtdIns(3,4)P_2 and PtdIns(3)P can be used to examine their activities in PG precursors (Furutani *et al.*, 2006; Rasmussen *et al.*, 2015).

Moreover, because invadopodia secret MMPs to degrade ECM components (Murphy and Courtneidge, 2011), a characteristic of invadopodia is its colocalization with matrix degradation. Therefore, immunohistochemistry against Laminin in *Tg(nkx2.2a:Gal4);Tg(UAS:Lifeact-GFP)* embryos can be used to detect the degradation of the basement membrane. However, one caveat of this experiment is that motor nerves may appear as dark regions on the Laminin staining, making it difficult to assess matrix degradation generated by invadopodia.

Functional analyses of PG precursor protrusions

Because my results suggest that protrusions of PG precursors are likely invadopodia, these protrusions can be crucial to the invasion of PG precursors through the CNS/PNS boundary. Moreover, given the spatiotemporal correlation between these protrusions and motor axon outgrowth from the spinal cord, I hypothesize that these protrusions may play a role in the formation of MEP TZs and motor axon exit from the spinal cord. Therefore,

inhibition of the formation of PG precursor protrusions may lead to two possible phenotypes: (1) delayed or failed exit of PG precursors from the LFP, and (2) delayed or ectopic exit of motor axons from the spinal cord.

Because I show that protrusions of PG precursors are actin-rich structures (Figure 3-6), a direct approach to test their functions is to arrest actin dynamics by expressing dominant negative small G proteins (Clark *et al.*, 2011; Seiler *et al.*, 2012; Morrissey, Hagedorn and Sherwood, 2013). For example, expression of established mCherry-Rab5c-S34N or mCherry-Rab7-T22N in LFP cells may inhibit the formation of PG precursor protrusions and thus be used to investigate functions of these protrusions (Clark *et al.*, 2011). However, one caveat of these experiments is that blocking Rab5c or Rab7 may directly inhibit the migration of PG precursors (Margiotta, 2019).

A more specific approach is to target components only required for the formation of invadopodia. Tks5 may be a good candidate because its expression can be evaluated using an available antibody (Lam *et al.*, 2015). An easy experiment to knock down Tks5 is to inject established *sh3pxd2a* morpholino oligonucleotide into transgenic embryos (Seiler *et al.*, 2012). To further investigate the function of Tks5 and block the formation of PG precursor protrusions, *sh3pxd2a* knock-out animals can be generated using the CRISPR-Cas9 technique (Cong *et al.*, 2013; Hwang *et al.*, 2013).

Another approach is to induce the formation of invadopodia using constitutively active Src (caSrc). To do this, I can express established caSrc, Src-Y528F (Seiler *et al.*, 2012), in LFP cells using *nkx2.2a* promoter and examine whether induction of invadopodia promotes PG exit and motor axon outgrowth at ectopic locations.

In summary, I demonstrate that PG precursors specified in the middle of each hemisegment project dynamic invadopodia-like protrusions to the periphery, which are likely involved in the specification of MEP TZs and motor axon exit from the spinal cord. Future studies characterizing the nature of PG precursor protrusions and elucidating their functions will provide novel insights into spinal cord development.

CHAPTER IV

Phagocytosis of Cellular Debris by Neural Crest Cells

Abstract

During neural tube closure and subsequent spinal cord development, a vast number of cells undergo programmed cell death in both the central and peripheral nervous systems (CNS and PNS, respectively). However, myeloid-derived professional phagocytes have not yet colonized the trunk region during early neurogenesis. How apoptotic cells are removed from this region during early development remains largely unknown. Using live imaging in zebrafish, I demonstrate that multipotent neural crest cells (NCC) respond rapidly to dying cells and phagocytose cellular debris around the neural tube. Furthermore, migratory NCCs have the ability to enter the CNS through motor exit point transition zones and clear debris in the spinal cord. Surprisingly, NCC phagocytosis mechanistically resembles macrophage phagocytosis and their recruitment towards cellular debris is mediated by interleukin-1β signaling. Taken together, my results reveal an unexpected role of NCCs in phagocytosis of debris in the developing nervous system before the presence of professional phagocytes.

Introduction

Cell death is prevalent during development in multicellular organisms and is important for the removal of unnecessary cells and tissues as well as for the correction of developmental errors (Arya and White, 2015). During vertebrate embryogenesis, dying cells are present during neural tube closure and spinal cord development (Schlüter, 1973;

Weil, Jacobson and Raff, 1997; Buss, Sun and Oppenheim, 2006; Massa *et al.*, 2009). Therefore, a rapid and efficient phagocytic response is crucial for the clearance of this debris. In mouse, chicken and zebrafish, a group of primitive macrophages derived from the yolk sac migrate into the developing brain, differentiate into microglia, and contribute to ongoing neurogenesis by clearing apoptotic debris (Cuadros *et al.*, 1993; Herbomel, Thisse and Thisse, 1999; Bertrand *et al.*, 2013). Yolk-sac-derived macrophages, however, do not infiltrate the trunk of developing embryos until the formation of the circulatory system at embryonic day (E)10.5 in mice (McGrath *et al.*, 2003; Bertrand *et al.*, 2013; Stremmel *et al.*, 2018) and 35 hours post fertilization (hpf) in zebrafish (Herbomel, Thisse and Thisse, 1999, 2001). However, neural tube closure and motor axon pathfinding start at E9 and 16 hpf in mice and fish, respectively (Beattie, 2000; Wang *et al.*, 2014), prior to the colonization of macrophages in the trunk region. Although cell death during neural tube closure has been extensively studied, very little is known about the clearance of debris in the trunk during the earliest stages of neural development.

NCCs are a conserved cell lineage in vertebrate embryos that differentiate into a variety of cell types, including pigment cells and neurons and glia of the PNS (Roberto Mayor and Theveneau, 2013). After neural tube closure, a subset of trunk NCCs delaminate and migrate ventral-medially around the perimeter of the spinal cord in segmentally-organized streams (R. Mayor and Theveneau, 2013; Vega-Lopez, Cerrizuela and Aybar, 2017). When motor neurons in the CNS send their axons out of the spinal cord, NCCs reach motor exit points (MEP) and migrate ventrally along motor axons (R. Mayor and Theveneau, 2013; Vega-Lopez, Cerrizuela and Aybar, 2017). Previous studies in mice demonstrate a correlation between the presence of apoptotic debris and migratory

NCCs (Massa *et al.*, 2009; Yoshida *et al.*, 2013). Therefore, given the spatiotemporal correlations of NCC migration, the presence of dead cells, and the absence of macrophages at early developmental stages, I hypothesized that migratory NCCs may have the ability to clear cellular debris during early developmental stages.

Here, using live imaging in zebrafish, I demonstrate that NCCs are phagocytic during early development. I show that NCCs migrate away from their segmentally-restricted paths towards dead cells and phagocytose debris. They rapidly internalize this debris and form phosphatidylinositol 3-monophosphate (PI(3)P)-enriched engulfment vesicles that mature into lysosome-associated-membrane-protein-1-positive ($lamp1^{+}$) acidic phagolysosomes. Intriguingly, NCCs even migrate into the ventral spinal cord through MEP transition zones (TZ) and phagocytose debris in the CNS. Interestingly, both cell corpses and phagocytic NCCs express interleukin-1β (Il-1β), and blocking Il-1β signaling with an Il-1β receptor antagonist or a Caspase-1 inhibitor significantly impaired NCC recruitment to cellular debris after injury, demonstrating that activated Il-1β is required for NCC recruitment. Together, my findings reveal a role for migratory NCCs in phagocytosing debris in the CNS and PNS during early development.

Results

NCCs, but not macrophages, colonize the trunk region during early developmental stages

Although primitive macrophages are generated in the first wave of yolk sac hematopoiesis as early as 15 hours post fertilization (hpf) in zebrafish (Lieschke *et al.*, 2001), previous studies demonstrate that these early macrophages do not populate the

trunk until 35 hpf or later (Herbomel, Thisse and Thisse, 1999, 2001). To understand the temporal dynamics of macrophage colonization of the trunk, I crossed *Tg(mpeg1:GFP)* transgenic fish, where *mpeg1* regulatory sequences drive GFP expression in macrophages and microglia, with *Tg(olig2:DsRed)* transgenic fish, where *olig2* regulatory sequences label spinal cord neurons and glia, and counted the number of *mpeg1*$^{+}$ macrophages in the trunk of these embryos at 24, 36, and 48 hpf (Figure 4-1A). In these studies, I observed an increase macrophage number in both the yolk and trunk between 24 and 36 hpf, and then again from 36 to 48 hpf (Figure 4-1A & 1B). To better characterize macrophage distribution, I plotted their individual locations into 2D histograms and found that at 24 hpf, macrophages resided in the yolk extension (Figure 4-1C, n = 9 fish). By 36 hpf, most macrophages remained in and around the yolk extension, while a few of started to appear near the notochord and the ventral spinal cord, which is referred to as the dorsal trunk below (Figure 4-1C, n = 9 fish). Ultimately, by 48 hpf, macrophages fully colonized the trunk with an equal distribution in both the yolk extension and dorsal trunk (Figure 4-1C, n = 9 fish).

Because I did not observe any macrophages in the dorsal trunk in 24 hpf embryos, I sought to determine whether dead cells were present at this stage. To visualize apoptotic cells in live animals, I created a transgenic line, *Tg(bactin2:Gal4),* which has Gal4 factor the control of β-actin regulatory sequences and crossed it with *Tg(UAS:secA5-YFP)* zebrafish*,* to drive expression of secreted human Annexin V protein fused to YFP (secA5-YFP), which binds to the membrane of apoptotic cells (van Ham *et al.*, 2010). In *Tg(bactin2:Gal4);Tg(UAS:secA5-YFP)* embryos at 20 hpf, I observed *secA5*$^{+}$ cells in the yolk extension and intermediate cell mass (Figure 4-1D) (Sarvothaman *et al.*, 2015;

Stachura and Traver, 2016). Additionally, I also found *secA5*$^{+}$ cells in the dorsal trunk (Figure 4-1D) at both 20 and 36 hpf (Figure 4-1D). Quantification of the percentage of somites with *secA5*$^{+}$ cells in the dorsal trunk at 20 and 36 hpf (n = 65/56 somites in 6/9 embryos for 20/36 hpf) showed that the presence of dead cells was robust and consistent among embryos at these stages (Figure 4-1E). Using a newly created line, *Tg(sox10:TagRFP),* where TagRFP is expressed in NCCs under *sox10* regulatory sequences, I found that *sox10*$^{+}$ NCCs were spatially correlated with apoptotic cells near the spinal cord (Figure 4-1D), which is consistent with a previous study demonstrating the presence of apoptotic cells around the neural tube during NCC migration in mice (Massa *et al.*, 2009). These data demonstrate that migratory NCCs colonize the dorsal trunk in zebrafish when macrophages are absent but apoptotic debris is present.

The association of migratory NCCs with dead cells at early developmental stages (Figure 4-1D) prompted me to investigate whether NCCs expressed genes implicated in phagocytosis. To do this, I performed RNA-sequencing of *foxd3*$^{+}$/*sox10*$^{+}$ NCCs collected from the trunk of *Gt(foxd3:mCherry);Tg(sox10:mEGFP)* embryos at 36 and 72 hpf, which represent developmental stages before and after the full colonization of macrophages into the trunk (Figure 4-1C) (Simoes-Costa and Bronner, 2015). Using Gene Ontology (GO) enrichment analysis and KEGG pathway analysis (Ashburner *et al.*, 2000; Kanehisa and Goto, 2000; Yu *et al.*, 2012; The Gene Ontology Consortium, 2019), I found that 36 hpf NCCs were highly enriched in cellular components related to debris clearance such as the endoplasmic reticulum, lysosomes, endosomes and V-ATPase (Figure 4-2A & B). Lysosome and endosome pathways were also up-regulated (Figure 4-2C & D). Moreover, many genes required for phagocytosis were highly expressed in 36

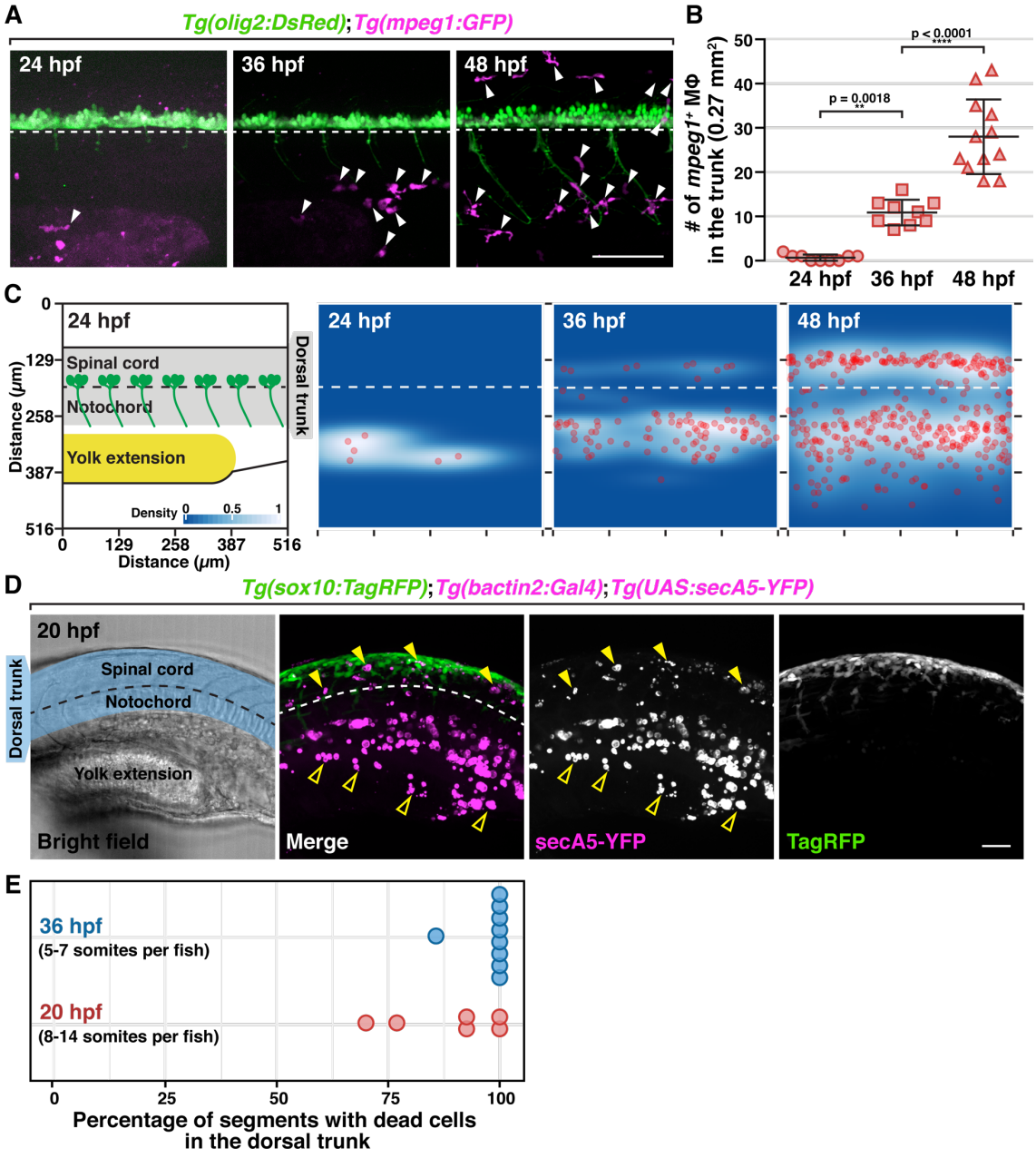

Figure 4-1. NCCs, but not macrophages, colonize the trunk region during early development. (A) Trunk lateral views of *Tg(olig2:DsRed);Tg(mpeg1:GFP)* embryos at 24, 36 and 48 hpf. Arrowheads denote *mpeg1*$^{+}$ macrophages. **(B)** Macrophage quantification in a 0.27 mm^2 region in the trunk of embryos at 24, 36 and 48 hpf (mean ± SD). **(C)** 2D distribution of macrophages in the trunk of embryos at 24, 36 and 48 hpf (n = 9 fish in each condition). Diagram on the left shows the region quantified. All images used for quantification are aligned based on the position of the

ventral edge of the spinal cord (dashed line). **(D)** Lateral view of a *Tg(sox10:TagRFP);Tg(bactin2:Gal4);Tg(UAS:secA5-YFP)* embryo at 20 hpf. Blue shading denotes dorsal trunk. Filled arrowheads denote dead cells in the dorsal trunk. Open arrowheads denote debris in the ventral trunk/yolk extension. **(E)** Quantification of the percentage of somites with *secA5*$^{+}$ cells in 20 and 36 hpf embryos (n = 6/9 fish for 20/36 hpf). Dashed lines mark the ventral edge of the spinal cord. Scale bars, 50 μm.

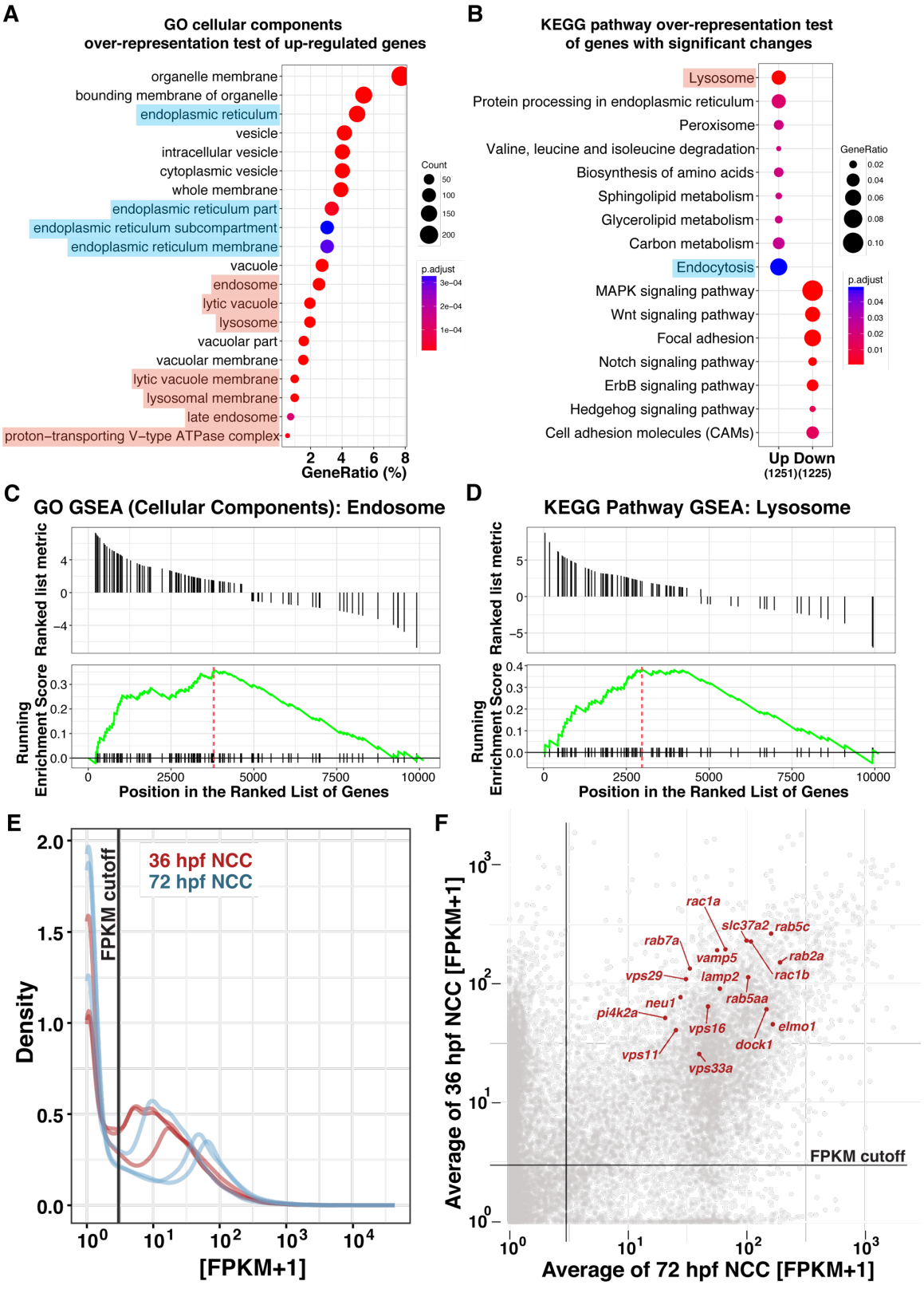
A
GO cellular components
over-representation test of up-regulated genes
organelle membrane
bounding membrane of organelle
endoplasmic reticulum
vesicle
intracellular vesicle
cytoplasmic vesicle
whole membrane
endoplasmic reticulum part
endoplasmic reticulum subcompartment
endoplasmic reticulum membrane
vacuole
endosome
lytic vacuole
lysosome
vacuolar part
vacuolar membrane
lytic vacuole membrane
lysosomal membrane
late endosome
proton−transporting V−type ATPase complex
2 4 6 8
GeneRatio (%)
Count
50
100
150
200
p.adjust
3e−04
2e−04
1e−04
B
KEGG pathway over-representation test
of genes with significant changes
Lysosome
Protein processing in endoplasmic reticulum
Peroxisome
Valine, leucine and isoleucine degradation
Biosynthesis of amino acids
Sphingolipid metabolism
Glycerolipid metabolism
Carbon metabolism
Endocytosis
MAPK signaling pathway
Wnt signaling pathway
Focal adhesion
Notch signaling pathway
ErbB signaling pathway
Hedgehog signaling pathway
Cell adhesion molecules (CAMs)
Up Down
(1251)(1225)
GeneRatio
0.02
0.04
0.06
0.08
0.10
p.adjust
0.04
0.03
0.02
0.01
C
GO GSEA (Cellular Components): Endosome
Ranked list metric
Running Enrichment Score
Position in the Ranked List of Genes
D
KEGG Pathway GSEA: Lysosome
Ranked list metric
Running Enrichment Score
Position in the Ranked List of Genes
E
36 hpf NCC
72 hpf NCC
FPKM cutoff
Density
[FPKM+1]
F
Average of 36 hpf NCC [FPKM+1]
Average of 72 hpf NCC [FPKM+1]
FPKM cutoff
rac1a
slc37a2
rab5c
rab7a
vamp5
rab2a
vps29
lamp2
rac1b
neu1
rab5aa
pi4k2a
vps16
elmo1
dock1
vps11
vps33a

Figure 4-2. Phagocytosis related genes are up-regulated in 36 hpf NCCs. (A) Gene Ontology over-representation test of up-regulated genes in 36 hpf NCCs shows enrichment in endoplasmic reticulum (shaded in blue) and lysosome (shaded in red) related cellular components. **(B)** KEGG pathway over-representation test of genes differentially expressed in 36 hpf v.s. 72 hpf NCCs shows that lysosome (shaded in red) and endocytosis (shaded in blue) pathways are upregulated. **(C & D)** Results of GSEA show that **(C)** endosome genes and **(D)** the lysosome pathway are up-regulated in 36 hpf NCCs. **(E)** Density plot of 36 (red) and 72 hpf (blue) NCC RNA-Seq dataset in FPKM. The vertical line shows the FPKM cutoff used in **F**. **(F)** X-Y dot plot of NCC RNA-Seq data set. Genes critical to phagocytosis are highlighted in red. GSEA, gene set enrichment analysis.

hpf NCCs (Figure 4-2E & F) (Ashburner *et al.*, 2000; Villani *et al.*, 2019). Taken together, I hypothesize that NCCs have the capacity to clear debris at developmental stages before the appearance of professional phagocytes.

NCCs migrate away from their segmental stream of origin to engulf cellular debris

To monitor the migration and behavior of NCCs and investigate whether they contribute to debris clearance during development, I performed *in vivo*, time-lapse imaging. To do this, I used *Tg(sox10:nls-Eos)* embryos which express nuclear-localized Eos to track the movement of individual NCCs and a *Tg(nkx2.2a:nls-mCherry)* transgene to label lateral floorplate cells as a reference for the location of the ventral spinal cord (Figure 4-3A & B) (Kucenas, Snell and Appel, 2008). In time-lapse movies of *Tg(sox10:nls-Eos);Tg(nkx2.2a:nls-mCherry)* embryos from 19 to 40 hpf, I observed that the majority of newly-delaminated trunk NCCs migrated ventrally around the neural tube, reaching MEP TZs in the middle of each hemi-segment, and then migrated along motor axons (Figure 4-3A & B), as previously described (Banerjee *et al.*, 2011; Vega-Lopez, Cerrizuela and Aybar, 2017). I also observed approximately 1 to 2 NCCs per hemi-segment undergo apoptosis during their migration (Figure 4-3B, Movie S1). When cell death occurred, individual NCCs migrated away from their innate streams and moved towards these dying cells, and NCCs that associated with dying cells were observed both dorsal and ventral to MEP TZs (Figure 4-3B & Movie S1; see also Figure 4-4A & Movie S2).

I next examined whether NCCs that migrated towards dying cells engulfed them. In order to better visualize NCC behavior, I used a *Tg(sox10:Eos)* line to label NCC

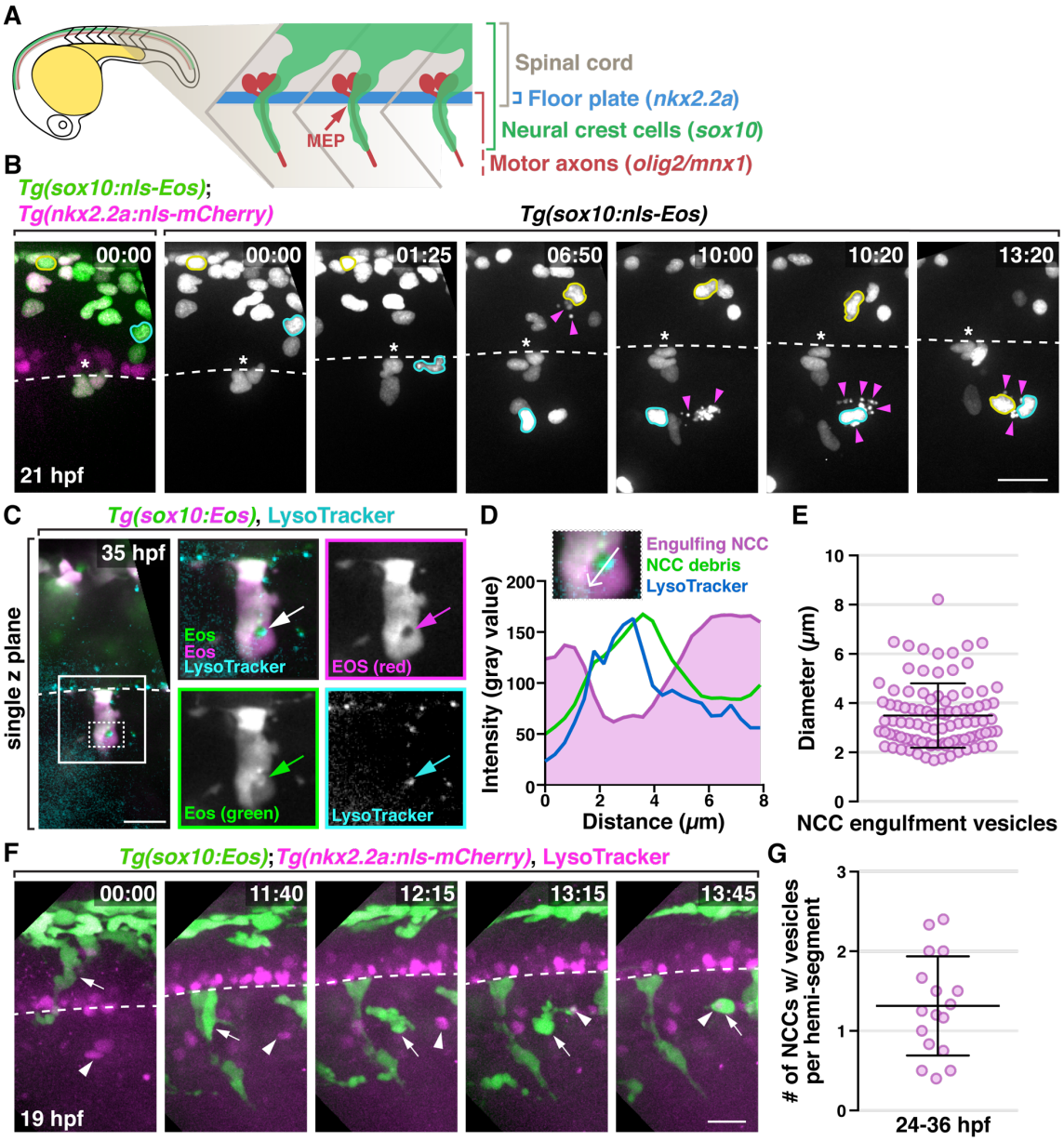

Figure 4-3. A subset of NCCs engulf cellular debris in the developing PNS.

(A) Schematic diagram showing NCC migration in a 22 hpf embryo. **(B)** Images from a 21 h time-lapse movie of a *Tg(sox10:nls-Eos);Tg(nkx2.2a:nls-mCherry)* embryo starting at 19 hpf. Asterisks denote the location of MEP TZs. Arrowheads denote dead NCCs. NCCs that migrated towards debris are outlined in yellow and cyan. **(C)** Images from a 35 hpf *Tg(sox10:Eos)* embryo treated with LysoTracker Deep Red. Boxed region is magnified on the right. Arrows denote an engulfment vesicle. Region outlined with dashed box is magnified in **D**. **(D)** Quantification of fluorescent intensity

across the engulfment vesicle shown in **C**. **(E)** Measurement of diameters of NCC engulfment vesicles (mean ± SD, n = 95 vesicles). **(F)** Images from a 21 h time-lapse movie starting at 19 hpf of a *Tg(sox10:nls-Eos);Tg(nkx2.2a:nls-mCherry)* embryo treated with LysoTracker Red DND-99. A NCC denoted (arrows) migrated towards and engulfs LysoTracker^{+} debris (arrowheads). Note that the white color of the engulfment vesicle indicates co-localization of that NCC and the corpse. Dashed line marks the ventral edge of the spinal cord. **(G)** Quantification of the number of engulfing NCCs per hemi-segment (mean ± SD, n = 17 fish, 3-6 somites per fish). Scale bars, 20 μm.

cytoplasm with Eos, a photoconvertible protein that when exposed to ultraviolet (UV) light, shifts its emission wavelength from a neutral state emitting green fluorescence (516 nm), to an anionic state emitting red fluorescence (581 nm) (Prendergast *et al.*, 2012). Recent studies demonstrate that the Eos protein settles in a pH-dependent equilibrium between these two states: the neutral form (green) favors lower pH (6-8), and the anionic state (red) favors physiological pH (8-10) (Berardozzi *et al.*, 2016; Turkowyd *et al.*, 2017). Considering the acidification that occurs during apoptosis and inside engulfment vesicles (Gottlieb, 1996; Levin, Grinstein and Canton, 2016), I hypothesized that healthy and apoptotic NCCs could be differentially labeled by the two forms of Eos protein. To verify this, I exposed *Tg(sox10:Eos)* embryos to UV light at 20 hpf, photoconverting existing Eos protein in NCCs to the anionic state (red), and performed time-lapse imaging. As expected, NCCs labeled with high levels of photoconverted (red) Eos switched to yellow upon apoptosis (Figure 4-4B & C). Yellow NCC corpses were then quickly engulfed by neighboring red NCCs which formed large engulfment vesicles with green debris inside (Figure 4-3C; see also Figure 4-4B & C). Moreover, these engulfment vesicles were positive for LysoTracker Deep Red (Figure 4-3C & D), a dye that labels acidic organelles (Fogel, Thein and Mariani, 2012), and measured approximately 2 to 8 μm in diameter (Figure 4-3E, n = 95 vesicles), similar to the size of phagosomes in professional phagocytes (Champion, Walker and Mitragotri, 2008). From these data, I conclude that migratory NCCs engulf apoptotic neighbors and form acidic engulfment vesicles.

I next asked whether these NCCs could engulf non-NCC debris. To do this, I treated *Tg(sox10:Eos);Tg(nkx2.2a:nls-mCherry)* embryos with 20 μM LysoTracker Red

DND-99, which stains both dying cells and acidic organelles (Fogel, Thein and Mariani, 2012), and time-lapse imaged from 19 to 40 hpf. In these movies, I observed NCCs migrate away from motor axons towards LysoTracker^{+} debris located between two spinal motor nerves in neighboring somites (Figure 4-3F; Movie S3). In one instance, I observed a NCC first send dynamic protrusions towards LysoTracker^{+} debris and then quickly engulf it (Figure 4-3F; Movie S3). When NCCs tried to engulf large debris, like dead muscle fibers, they exhibited a behavior similar to frustrated phagocytosis, where one or many NCCs circled around the dead cell for hours without successful engulfment (Figure 4-4D) (Cannon and Swanson, 1992). In spite of being highly active in response to cellular debris, NCCs do not engulf frequently in healthy embryos. Quantification of NCCs with engulfment vesicles showed that 1 to 2 cells per hemi-segment between 24 to 36 hpf had engulfment vesicles (Figure 4-3G, n = 17 fish), which is about 5% to 10% of all NCCs in a hemi-segment. Taken together, these data demonstrate that NCCs can migrate away from motor axons and engulf debris.

Engulfing NCCs have distinct migratory patterns but are not lineage restricted

Previous studies show that trunk NCCs migrate in segmentally-organized streams along motor axons in each somite (Figure 4-3A for schematic diagram) (Banerjee *et al.*, 2011; Vega-Lopez, Cerrizuela and Aybar, 2017). my data, however, demonstrate that individual NCCs can migrate away from motor axons towards dead cells (Figure 4-3B & F; see also Figure 4-4A). To better understand these unique migratory patterns, I tracked the migration of individual NCCs with or without engulfment vesicles for 10 hours after they reached MEP TZs and observed that NCCs with vesicles did not migrate along axons

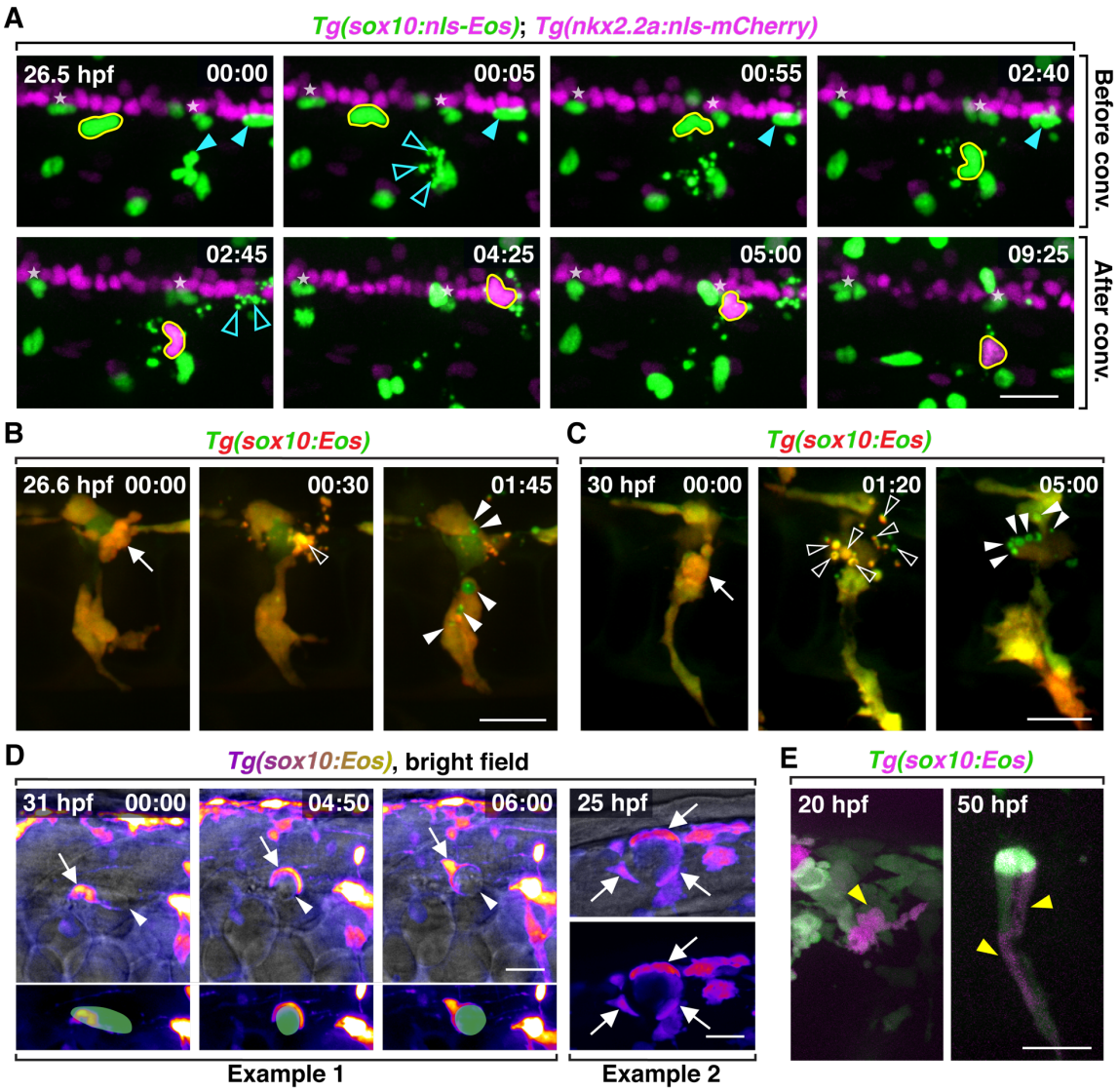

Figure 4-4. NCC migration and engulfment of PNS debris. (A) Images from a time-lapse movie of a *Tg(sox10:nls-Eos);Tg(nkx2.2a:nls-mCherry)* embryo. Starts denote estimated locations of MEP TZs. Filled arrowheads denote NCCs that are going to die. A NCC (outlined in yellow) migrated towards NCC debris (open arrowheads) on the neighboring nerve and was then photoconverted from green to magenta. **(B & C)** Color change of NCC Eos protein after cell death and engulfment. Images from two time-lapse movies of photoconverted NCCs in *Tg(sox10:Eos)* embryos. Arrows denote red NCCs before death. Open arrowheads denote yellow/green NCC debris after cell death. Filled arrowheads denote green NCC debris

inside neighboring NCCs. **(D)** Two examples of NCCs performing behaviors similar to frustrated phagocytosis in two time-lapse movies of *Tg(sox10:Eos)* embryos. Arrows denote NCCs circling large muscle corpses (shaded in green in the first example). **(E)** Lineage tracing of engulfing NCCs in *Tg(sox10:Eos)* embryos that were photoconverted at 20 hpf (arrowheads). Scale bars, 20 μm.

(5/5) as most trunk NCCs did (5/5) (Figure 4-5A). Occasionally, I also observed them cross somite boundaries and interact with axons and debris in neighboring somites (2/5) (Figure 4-5A; See also Figure 4-4A). Plotting the migration data from these movies into a directional histogram showed that 90% of the NCCs without vesicles were located 60-90˚ below the edge of the ventral spinal cord, along axonal bundles (Figure 4-5B, n = 10). In contrast, the majority of NCCs that contained engulfment vesicles were distributed in a 30˚-150˚ angle below the ventral spinal cord with only 20% of them following axonal bundles (Figure 4-5B, n = 10). Similarly, when I traced these NCCs 5 hours prior to when they reached MEP TZs, I found that 92% NCCs without engulfment vesicles came from a 30-60˚ angle dorsal to the spinal cord (Figure 4-5B, n = 13), as previously described (Honjo and Eisen, 2005). In contrast, those with engulfment vesicles reached MEP TZs from various directions, ranging from 30-150˚ (Figure 4-5B, n = 10). Interestingly, I never observed NCCs migrate dorsally after reaching the MEP TZ.

I next asked whether these NCCs were lineage restricted. To answer this question, I photoconverted engulfing NCCs in *Tg(sox10:Eos)* embryos at 20 hpf and tracked them using *in vivo* imaging. At 50 hpf, I found these NCCs had differentiated into pigment cells (Figure 4-5C & D) and motor nerve-associated glia (Figure 4-5D; see also Figure 4-4E). Among all the NCCs I were able to track (49/56 cells), 79.5% migrated laterally to the skin and had a pigment cell morphology, 16.3% migrated medially and associated with motor nerves where Schwann cells and dorsal root ganglion (DRG) neurons and glia reside, and 4.1% died during my imaging (Figure 4-5E). These data indicate that engulfing NCCs are not lineage restricted.

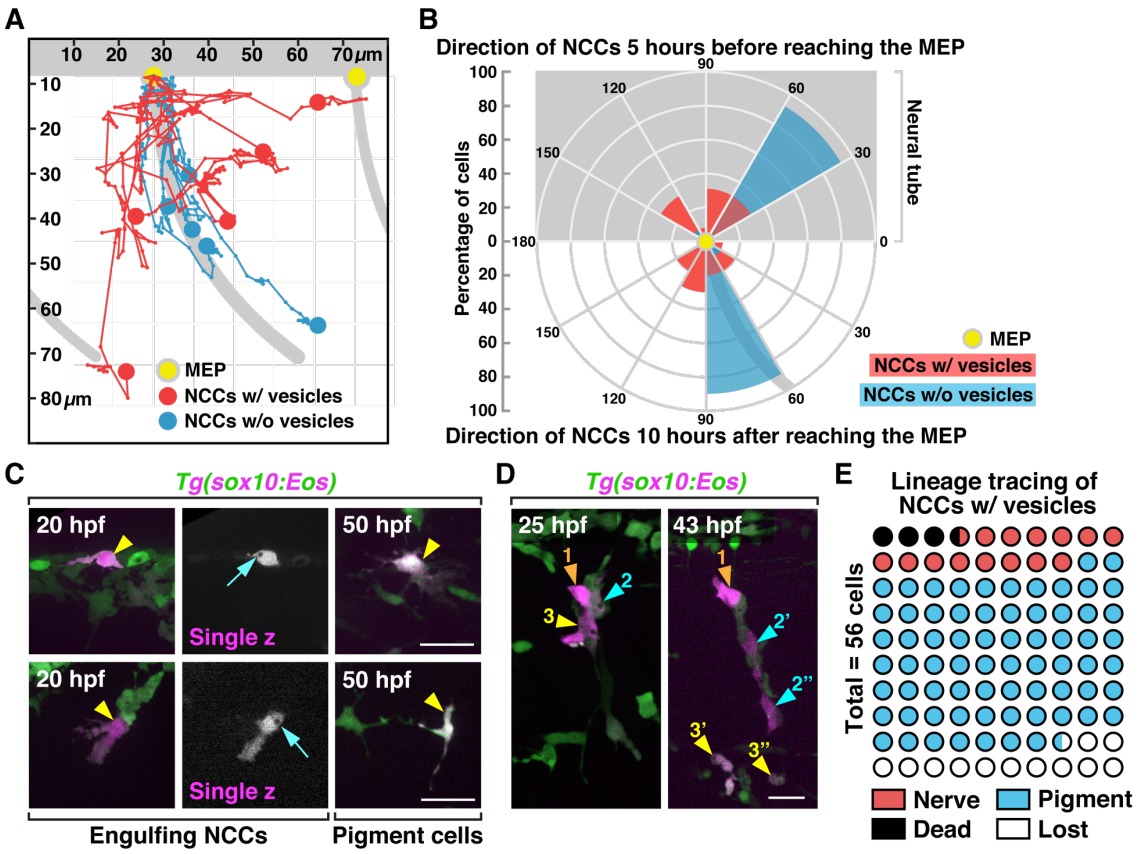

Figure 4-5. Migratory patterns and lineage tracing of engulfing NCCs.

(A) Trajectories of NCCs with (red, n = 5 cells) or without (blue, n = 5 cells) engulfment vesicles during a 10 h period after they reached MEP TZs (yellow dots). **(B)** Circular histogram showing directions of NCCs 5 h before (top, n = 13 cells for each group) or 10 hours after (bottom, n = 10 cells for each group) they reached MEP TZs (yellow dot). **(C&D)** Lineage tracing of engulfing NCCs that were photoconverted at 20 hpf (arrowheads). Arrows in **C** denote engulfment vesicles. Color-coded arrowheads in **D** denote daughter cells derived from individual photoconverted NCCs. **(E)** Quantification of the lineage of engulfing NCCs photoconverted at 20 hpf (n = 56 cells). Grey background shows location of the neural tube and motor axons in **A & B**. MEP, motor exit point. Scale bars, 20 μm.

NCCs form PI(3)P$^+$ and Lamp1$^+$ phagosomes after engulfment

Because NCCs engulf cellular debris in a manner similar to macrophages, I sought to determine whether NCC engulfment was mechanistically similar to phagocytosis. To investigate this, I determined whether NCC engulfment vesicles acidified progressively, which is required for the degradation of internalized debris (Kinchen and Ravichandran, 2008). To visualize the acidification process of NCC vesicles, I treated *Tg(sox10:Eos)* embryos with neutral red, a pH-sensitive dye that stains acidic lysosomes (Herbomel, Thisse and Thisse, 2001). In these embryos, I observed NCCs form phagocytic cups that then developed into circular vacuoles (Figure 4-6A; Movie S4). Approximately 40 minutes after the formation of engulfment vesicles, neutral red staining gradually appeared inside the newly formed compartments (Figure 4-6A; Movie S4). A similar acidification process was also observed using LysoTracker (Figure 4-6B). Therefore, I conclude that NCC engulfment vesicles are progressively acidified in a manner similar to phagosome maturation in professional phagocytes.

Next, I asked whether these vesicles acidify similarly to that of phagosomes in professional phagocytes. To investigate this, I first determined if NCC engulfment vesicles were PI(3)P$^+$, which is the characteristic phosphoinositide transferred to the membrane of newly formed phagosomes via fusion with early endosomes, and is crucial during early phagosome progression (Fratti *et al.*, 2001; Vieira *et al.*, 2001). To visualize PI(3)P activity in NCCs, I crossed *Tg(sox10:Gal4)* adults to a PI(3)P reporter line, *Tg(UAS:GFP-FYVE)* (Rasmussen *et al.*, 2015). Time-lapse imaging of these embryos from 20 to 40 hpf revealed labeling of dynamic PI(3)P$^+$ signals resembling early endosomes in NCCs (Figure 4-7A). When NCCs formed phagocytic cups and engulfed

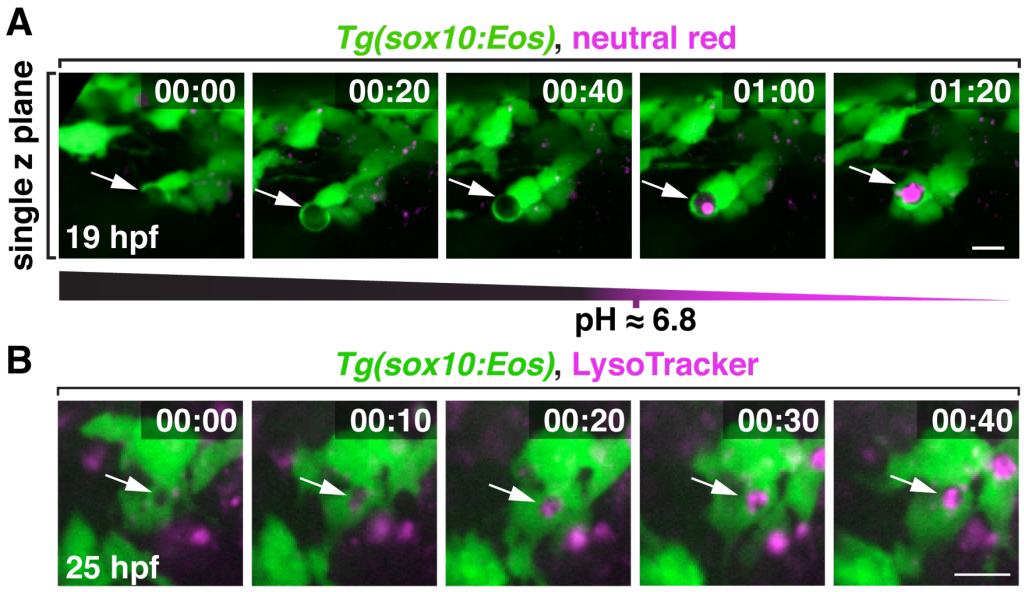

Figure 4-6. Progressive acidification of NCC engulfment vesicles. (A) Images from a time-lapse movie starting at 19 hpf in a *Tg(sox10:nls-Eos)* embryo treated with neutral red at 16 hpf. Arrows denote a NCC engulfment vesicle that was gradually stained by neural red. **(B)** Images from a time-lapse movie of a *Tg(sox10:Eos)* embryo after LysoTracker Red DND-99 treatment. Arrows denote a NCC engulfment vesicle gradually stained by LysoTracker. (B) Orthogonal views of NCC phagosomes in *Tg(sox10:TagRFP);Tg(sox10:lamp1-GFP)* embryos at 27 hpf. Scale bars, 10 µm.

debris, PI(3)P signals fused with engulfment vesicles within 2 minutes after the sealing of NCC vesicles, resulting in the formation of bright PI(3)P^+ spherical structures reminiscent of early phagosomes (Figure 4-7A) (Levin, Grinstein and Canton, 2016). After 4 to 12 minutes, PI(3)P signals quickly defused from engulfment vesicles and turned back into small spherical structures (Figure 4-7A). In addition to trunk NCCs, I also observed the formation of PI(3)P^+ engulfment vesicles in cranial NCCs (Figure 4-7B). This rapid and transient accumulation of PI(3)P to NCC engulfment vesicles closely resembles PI(3)P dynamics during phagosome maturation in cultured macrophages (Kamen *et al.*, 2008).

During phagosome maturation in macrophages, PI(3)P depletion is accompanied by the fusion of early phagosomes with late endosomes, which have a more acidic luminal pH (Levin, Grinstein and Canton, 2016). To determine whether NCC phagosomes have similar temporal regulation of PI(3)P activity and acidification, I treated *Tg(sox10:Gal4)*;*Tg(UAS:GFP-FYVE)* embryos with neutral red to visualize acidic organelles and imaged from 20 to 40 hpf. In these movies, I observed large PI(3)P^+ vesicles become neutral-red$^+$ upon the loss of the PI(3)P signal (Figure 4-7C and Movie S5). Quantification of PI(3)P^+ vacuole formation and neutral red fluorescent intensity over time showed that neutral red accumulation began during the depletion of PI(3)P on the NCC engulfment vesicle membrane (Figure 4-7D, n = 6 vesicles), which is similar to the transition from early to late phagosomes in macrophages (Levin, Grinstein and Canton, 2016). Moreover, acidification of NCC engulfment vesicles occurred within 10 minutes after the initial recruitment of PI(3)P (Figure 4-7D, n = 6 vesicles). This rapid

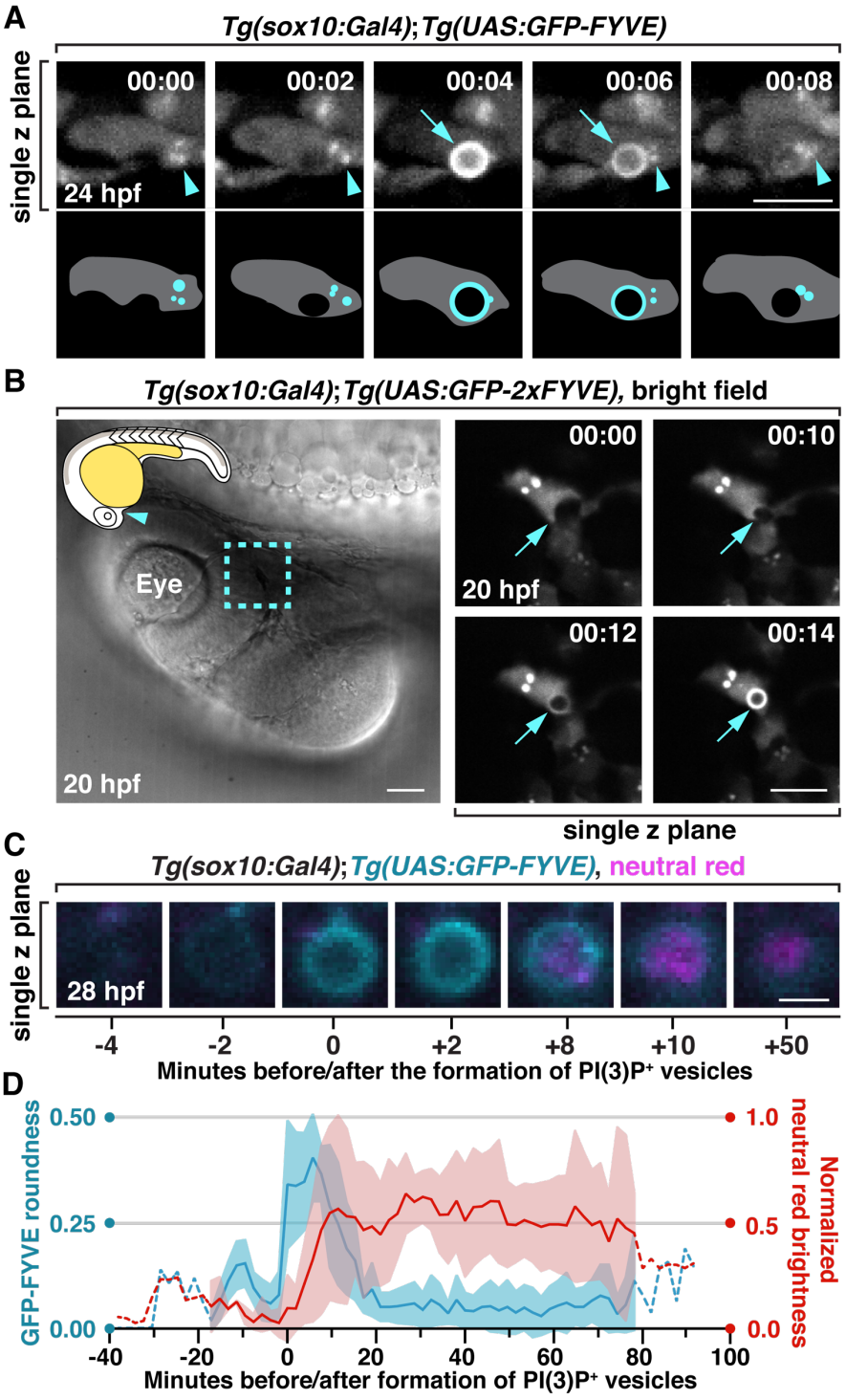

Figure 4-7. The formation of PI(3)P$^+$ phagosomes after NCC engulfment. (A) Images from a time-lapse movie of a 24 hpf *Tg(sox10:Gal4);Tg(UAS:GFP-FYVE)* embryo showing the fusion of scattered PI(3)P signals (arrowheads) with an engulfment vesicle (arrows). Schematic diagrams are shown below. **(B)** Left: bright

field image of the head of a *Tg(sox10:Gal4);Tg(UAS:GFP-FYVE)* embryo at 20 hpf with a schematic diagram. Boxed region denotes magnified views on the right. Right: images from a time-lapse movie starting at 20 hpf. Arrows denote a cranial NCC formed a PI(3)P^{+} engulfment vesicle. **(C)** Images of an engulfment vesicle from a time-lapse movie of a 28 hpf *Tg(sox10:Gal4);Tg(UAS:GFP-FYVE)* embryo treated with neutral red. **(D)** Quantification of PI(3)P^{+} vesicle formation and normalized neutral red brightness over time (mean ± SD, n = 6 vesicles). Dashed line indicates time points with a small sample size. Scale bars, 10 µm in **A**; 20 µm in **B**; 2 µm in **C**.

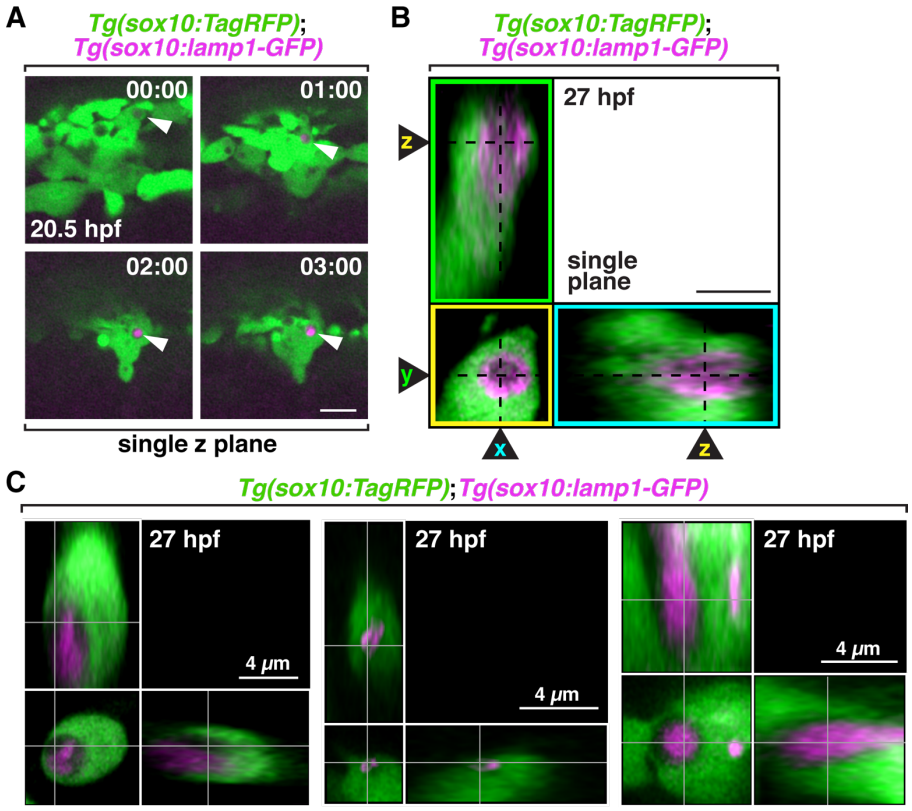

Figure 4-8. NCC engulfment vesicles are Lamp1^{+}. (A) Images from a time-lapse movie of a *Tg(sox10:TagRFP);Tg(sox10:lamp1-GFP)* embryo starting at 20 hpf. Arrowheads denote gradual enrichment of Lamp1-GFP in a NCC engulfment vesicle. **(B)** Orthogonal views of a Lamp1-GFP^{+} vesicle in a NCC. **(C)** Orthogonal views of NCC phagosomes in *Tg(sox10:TagRFP);Tg(sox10:lamp1-GFP)* embryos at 27 hpf. Scale bars: 10 µm in **A**; 4 µm in **B** & **C**.

acidification resembles phagosome pH regulation in alternatively activated M2 macrophages (Galli, Borregaard and Wynn, 2011; Canton *et al.*, 2014).

Finally, to determine if NCC phagosomes fuse with lysosomes and ultimately mature into phagolysosomes similar to those described in macrophages (Levin, Grinstein and Canton, 2016), I investigated whether these vesicles were enriched in Lamp1, an integral membrane protein crucial for phagolysosome maturation (Binker *et al.*, 2007; Huynh *et al.*, 2007; Levin, Grinstein and Canton, 2016). To do this, I created a transgenic line, *Tg(sox10:lamp1-GFP),* which expresses an established Lamp1-GFP fusion protein in NCCs (Rasmussen *et al.*, 2015). Time-lapse imaging of these embryos from 20 to 40 hpf showed that Lamp1-GFP was gradually enriched in NCC engulfment vesicles (Figure 4-8A), indicating a fusion process with lysosomes similar to phagolysosome biogenesis in macrophages (Binker *et al.*, 2007; Huynh *et al.*, 2007). Interestingly, I found that Lamp1-GFP formed a variety of ultrastructures within NCC phagocytic vesicles cells (Figure 4-8B & C), suggesting complex membrane topologies, consistent with published results showing multiple layers of $Lamp1^+$ membrane inside lysosomes of cultured cells (System and Klumperman, 2015). Taken together, I conclude that NCCs can migrate towards dying cells and phagocytose debris, which results in the formation of $PI(3)P^+$ and $Lamp1^+$ phagosomes. I therefore call these cells phagocytic NCCs.

Cell ablation induces NCC phagocytosis

Our data demonstrate that NCCs phagocytose debris like professional phagocytes. Therefore, I next asked whether cell death triggers the NCC phagocytic response. To investigate this, I ablated single migratory NCCs in the dorsal trunk using a pulsed

nitrogen dye laser in *Tg(sox10:Gal4)*;*Tg(UAS:GFP-FYVE)* embryos at 24 hpf (Figure 4-9A; Movie S6). Time-lapse imaging showed that multiple NCCs around the ablation site formed $PI(3)P^+$ phagosomes starting approximately 10 minutes post ablation (mpa) (Figure 4-9A; Movie S6). The NCC vesicle number peaked at 30 to 40 mpa and reduced to baseline levels by 50 to 60 mpa (Figure 4-9B; Movie S6). Notably, not every NCC responded to laser-induced damage and sometimes a single NCC formed multiple $PI(3)P^+$ vesicles (Figure 4-9A). Quantification of NCC phagocytosis within a 100 μm^2 region around the ablation site showed that in 100 mpa, 52.9% of the NCCs formed $PI(3)P^+$ phagosomes and 4.6% of them engulfed at least 4 times (Figure 4-9C, n = 5 fish).

To confirm that the induction of phagosome formation in NCCs was directly correlated to ablation, I quantified the number of $PI(3)P^+$ vesicles in each time frame for 100 minutes, before and after the ablation within the same 100 μm^2 region around the ablation site (Figure 4-9D). I found that more phagosomes formed post-ablation as compared to pre-ablation (Figure 4-9D). Similarly, the majority of NCC phagosomes formed in a 100 μm^2 region proximal to the ablation site (Figure 4-9E). Therefore, I conclude that NCCs phagocytose debris after cell ablation.

NCCs and macrophages clear debris during distinct developmental stages

NCCs phagocytose dead cells before macrophage colonization of the trunk. Therefore, I wanted to investigate the temporal dynamics of NCC and macrophage-mediated debris clearance during development. To do this, I time-lapse imaged *Tg(sox10:Eos)* and *Tg(mpeg1:GFP)* embryos and quantified phagocytic events between 22 and 44 hpf. my results showed that before 36 hpf, the majority of debris in the trunk was cleared by

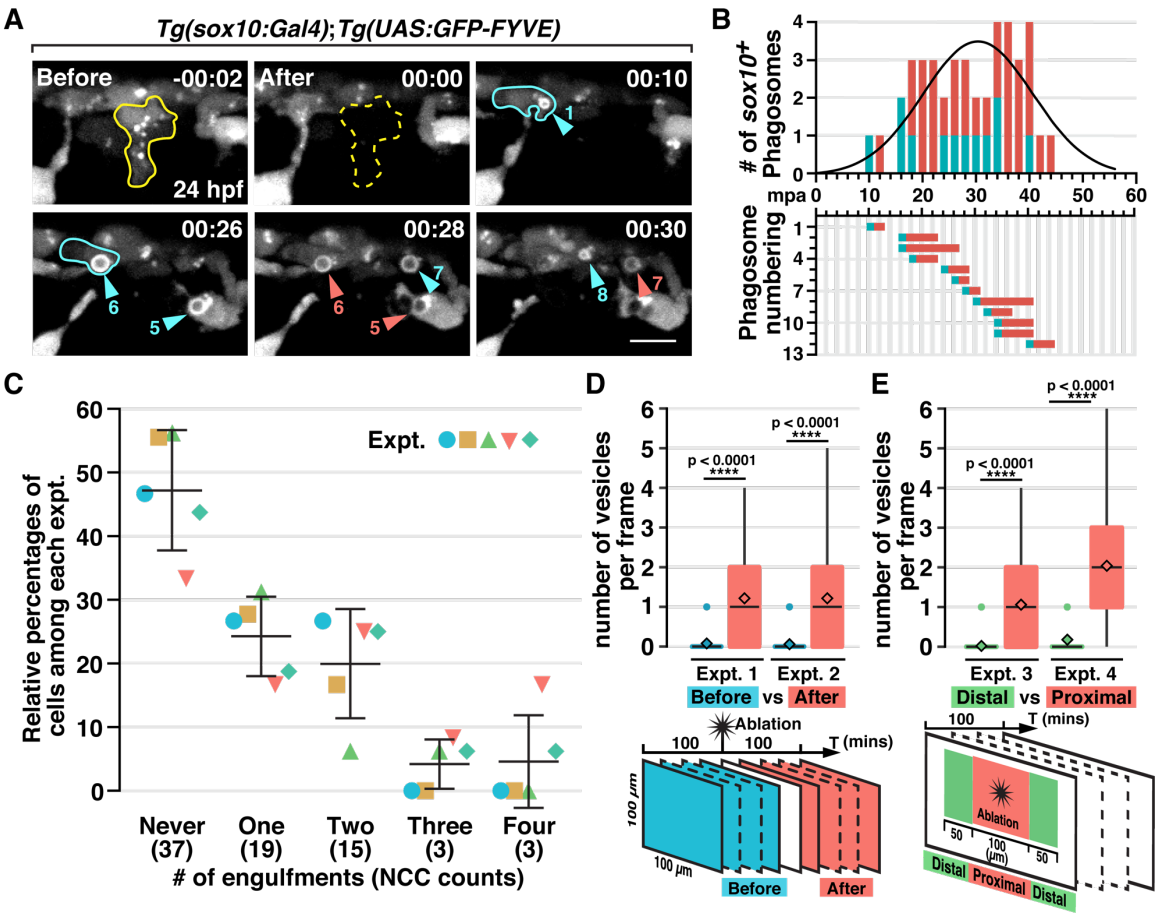

Figure 4-9. Laser ablation-induced NCC phagocytosis. (A) Images from a time-lapse movie of a *Tg(sox10:Gal4);Tg(UAS:GFP-FYVE)* embryo after ablation of a NCC (outlined in yellow) at 24 hpf. Arrowheads denote NCC engulfment vesicles. Cyan and red arrowheads denote newly-formed and pre-existing vesicles, respectively, in each frame, correlating with the quantification in **B**. A NCC that engulfed twice is outlined in cyan. **(B)** Quantification of phagosome formation in panel A. Top panel shows phagosome count per frame fitted with a Gaussian curve (R square = 0.7075). Bottom panel shows the duration of each $PI(3)P^+$ vesicle. **(C)** Quantification of the number of times NCCs phagocytose in a 100 μm^2 region around the ablation site in 100 mpa (mean ± SD, n = 5 fish). **(D & E)** Quantification of the number of NCC phagosomes per frame before and after cell ablation **(D)**, or distal and proximal to ablation sites **(E)** (n = 50 frames). mpa, minutes post ablation. Scale bar, 10 µm.

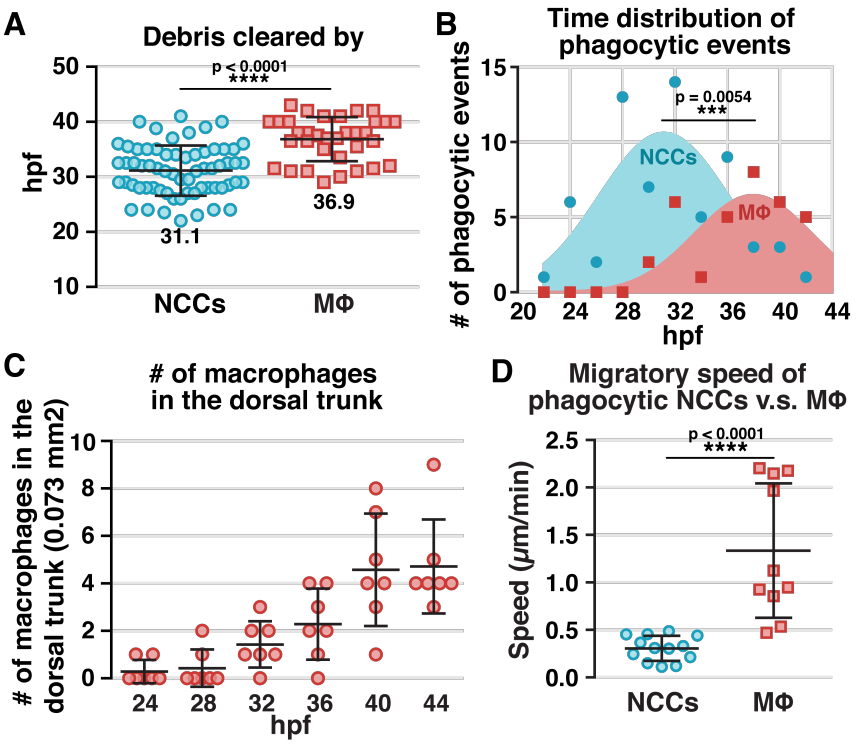

Figure 4-10. Characterization of NCCs and macrophages phagocytosis. (A) Quantification of phagocytic events performed by NCCs and macrophages between 22 and 44 hpf (mean ± SD). **(B)** Histogram of data in A fitted with Gaussian distribution (R^2 = 0.7573/0.6164 for NCCs/Macrophages). **(C)** Quantification of the number of macrophages in a 0.073 mm^2 region in the dorsal trunk of *Tg(mpeg1:GFP)* embryos over time (mean ± SD, n = 7 fish). **(D)** Quantification of the average velocity of phagocytic NCCs (n = 13 cells) and macrophages (mean ± SD, n = 10 cells). For NCCs, only their migration before reaching debris were calculated. 65-400 min of time-lapse movies of each cell were used for quantification.

NCCs, whereas macrophages phagocytosed more actively at later stages (Figure 4-10A & S4B). This time difference correlated with the presence of active trunk NCC migration between 16 to 36 hpf and increased abundance of macrophages in the dorsal trunk after 36 hpf (Figure 4-10C, n = 7 fish).

In these movies, I also noticed a difference in the migratory speed between NCCs and macrophages. Quantification of the average velocity of phagocytic NCCs and macrophages showed that phagocytic NCCs migrated 0.3 μm/min (Figure 4-10D, n = 13 cells), while macrophages migrated much more rapidly, with an average velocity of 1.3 μm/min (Figure 4-10D, n = 10 cells), identical to the macrophage migratory speed reported in previous studies (Grabher *et al.*, 2006). This difference in cell motility indicates that the phagocytic NCCs identified in my study are not macrophages.

NCCs migrate into the spinal cord and clear CNS debris

Our findings demonstrate that NCCs phagocytose cellular debris around the spinal cord. However, during these developmental stages, there is also a significant amount of debris inside the spinal cord (van Ham *et al.*, 2010; Shklover, Levy-Adam and Kurant, 2015) and how this debris is cleared, is not well understood. A previous finding from the lab showed that NCCs can migrate into the ventral spinal cord after reaching motor axons (Smith *et al.*, 2016). This led me to hypothesize that cell death in the spinal cord recruits NCCs into the CNS to phagocytose debris. To investigate this, I imaged MEP TZs in *Tg(sox10:nls-Eos)*;*Tg(nkx2.2a:nls-mCherry)* embryos from 22 to 40 hpf and captured NCCs migrating into the spinal cord (Figure 4-11A; see also Movie S7). Once inside the

CNS, these cells migrated both around and underneath floorplate cells (Figure 4-11A; see also Movie S7).

I then asked whether inducing cell death in the spinal cord would increase NCC migration into the CNS. To do this, I generated *Tg(sox10:nls-Eos);Tg(nkx2.2a:nls-mCherry);Tg(mnx1:mCerulean)* embryos and laser ablated two *nkx2.2a*$^{+}$ floorplate cells at 20 hpf. I then imaged these embryos for 20 hours post ablation (hpa) and found more NCCs in the spinal cord when compared to control embryos (Figure 4-11B & C; see also Movie S7). Interestingly, these CNS-located NCCs always migrated underneath motor neuron cell bodies (Figure 4-11A & C; Movie S7). These findings demonstrate that cell death in the CNS induces NCC migration into the spinal cord.

Considering that laser ablation might cause damage and lead to increased NCC entry, I examined the effect of drug-induced CNS cell death. I made use of *Tg(gfap:NTR-mCherry)* embryos, which when treated with a pro-drug, Metronidazole (MTZ), results in the specific loss of radial glial cells (Johnson *et al.*, 2016a; Smith *et al.*, 2016). In *Tg(sox10:nls-Eos);Tg(gfap:NTR-mCherry)* embryos treated with 15 mM MTZ in 1% DMSO starting from 10 hpf, I observed more NCCs in the spinal cord between 20 to 40 hpf when compared to DMSO-treated controls (Figure 4-11D & E, n = 6/5 fish for mock/drug). This increase in the number of CNS-located NCCs was attributed to cell migration because the total number of NCCs and their proliferation rate remained unchanged (Figure 4-11F & G, n = 6/5 fish for mock/drug). However, when I delayed MTZ treatment to 30 hpf and imaged from 40 to 60 hpf, I rarely observed NCCs entering the CNS (Figure 4-11E, n = 6/7 fish for mock/drug), suggesting that NCCs can only migrate into the spinal cord before 40 hpf, corresponding with the time frame when they

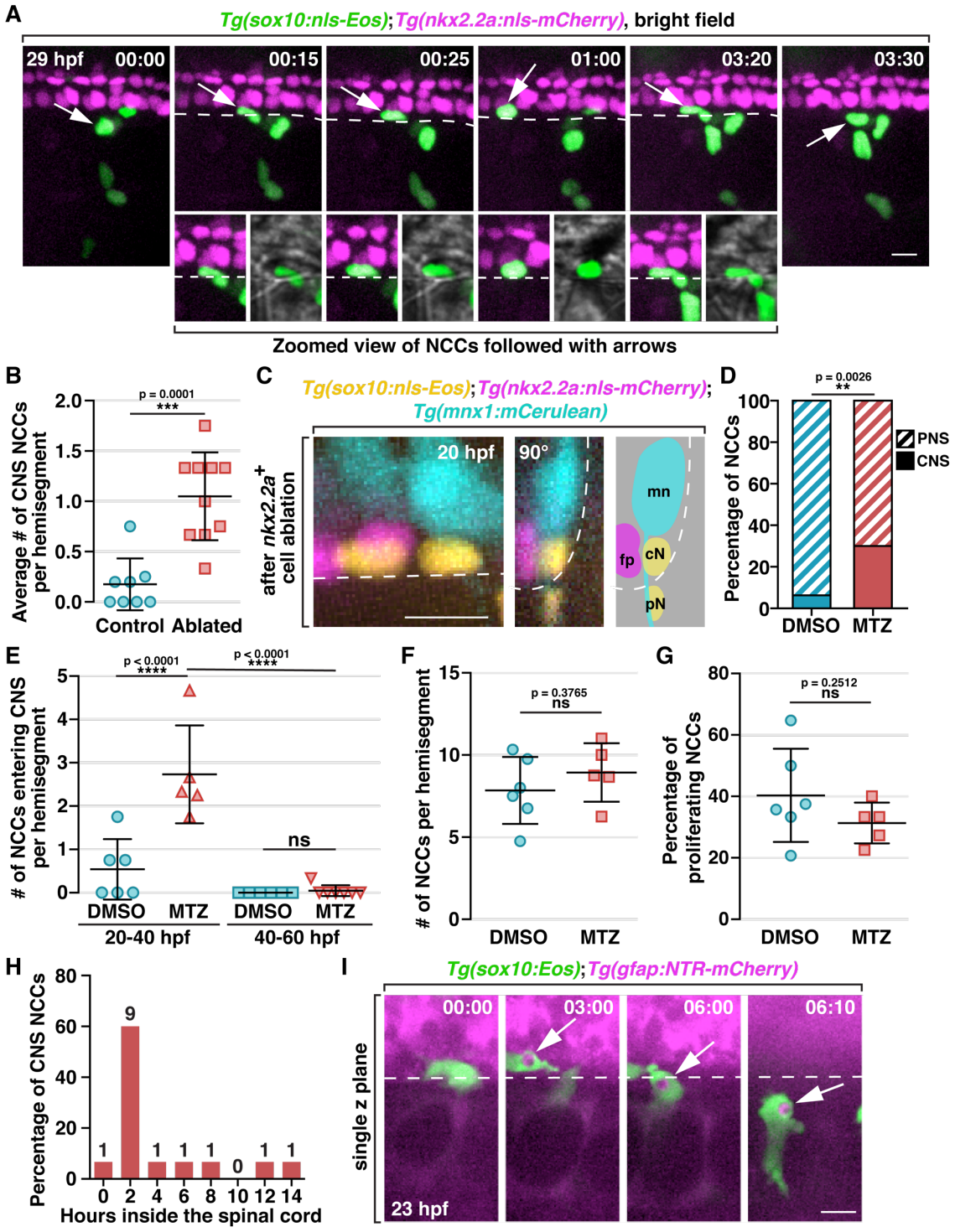
A
Tg(sox10:nls-Eos);Tg(nkx2.2a:nls-mCherry), bright field
29 hpf
00:00
00:15
00:25
01:00
03:20
03:30
Zoomed view of NCCs followed with arrows
B
Average # of CNS NCCs per hemisegment
p = 0.0001
***
Control
Ablated
C
Tg(sox10:nls-Eos);Tg(nkx2.2a:nls-mCherry);
Tg(mnx1:mCerulean)
after nkx2.2a+ cell ablation
20 hpf
90°
mn
fp
cN
pN
D
Percentage of NCCs
p = 0.0026
**
PNS
CNS
DMSO
MTZ
E
# of NCCs entering CNS per hemisegment
p < 0.0001
****
p < 0.0001
****
ns
DMSO
MTZ
DMSO
MTZ
20-40 hpf
40-60 hpf
F
# of NCCs per hemisegment
p = 0.3765
ns
DMSO
MTZ
G
Percentage of proliferating NCCs
p = 0.2512
ns
DMSO
MTZ
H
Percentage of CNS NCCs
1
9
1
1
1
0
1
1
Hours inside the spinal cord
I
Tg(sox10:Eos);Tg(gfap:NTR-mCherry)
single z plane
00:00
03:00
06:00
06:10
23 hpf

Figure 4-11. NCCs migrate into the spinal cord and phagocytose CNS debris. **(A)** Images from a time-lapse movie of a *Tg(sox10:nls-Eos);Tg(nkx2.2a:nls-mCherry)* embryo starting at 20 hpf. Arrows denote a NCC nuclei crossing into the CNS, which is magnified below. **(B)** Quantification of the ratio of CNS-located NCCs per hemi-segment after ablation of 2 floorplate cells (mean ± SD, n = 8/10 fish for control/ablated). **(C)** Images of a *Tg(sox10:nls-Eos);Tg(nkx2.2a:nls-mCherry);Tg(mnx1:mCerulean)* embryo at 20 hpf after ablation of 2 *nkx2.2a*$^{+}$ floorplate cells. Left: z projection; middle: 90-degree rotated image; right: schematic view of the rotated image, illustrating the locations of floorplate cells (fp), motor neurons (mn) and NCCs in the CNS (cN) and PNS (pN). **(D)** Quantification of the ratio of CNS-located NCCs in embryos with radial glial ablation (n = 5 fish) or DMSO-treated controls (n = 6 fish). The data includes NCCs in 3 hemi-segments per fish. **(E)** Quantification of the number of NCCs entering the CNS per hemi-segment in DMSO and MTZ-treated embryos within a 20 h time window (mean ± SD). **(F & G)** Quantification of the number of NCCs per hemi-segment **(F)** and the ratio of proliferating NCCs **(G)** in DMSO and MTZ-treated embryos between 20 to 40 hpf (mean ± SD). **(H)** Distribution of the length of time NCCs spent in the CNS (n = 15 cells). **(I)** Images from a time-lapse movie of a *Tg(sox10:Eos);Tg(gfap:NTR-mCherry)* embryo. Arrows denote a NCC engulfment vesicle filled with radial glia debris. Dashed lines mark the ventral edge of the spinal cord. Scale bars, 10 μm.

are highly phagocytic (Figure 4-10A & B). Based on these results, I conclude that NCCs can be recruited into the spinal cord by inducing cell death in the CNS.

To understand the behavior of these CNS-located NCCs, I traced 15 individual NCCs after they entered the CNS and found that 60% of them spent approximately 2 hours in the ventral spinal cord before exiting back into the periphery, while 13.3% NCCs stayed inside for more than 10 hours (Figure 4-11H). When I traced all the CNS-located NCCs until the end of my movies, I found that 75.0% of them ultimately returned to the periphery (n = 52 cells).

Lastly, to examine whether CNS-located NCCs also phagocytosed cellular debris, I treated *Tg(sox10:Eos);Tg(gfap:NTR-mCherry)* embryos with MTZ starting at 10 hpf and imaged from 20 to 40 hpf. In these movies, I observed single NCCs migrate into the spinal cord through the MEP TZ, form engulfment vesicles filled with $mCherry^{+}$ debris, and bring them back into the periphery (Figure 4-11I). Taken together, I conclude that NCCs can migrate into the spinal cord in response to CNS cell death, phagocytose debris.

Inhibition of Il-1β signaling impairs NCCs recruitment to debris

Interleukin-1β (Il-1β) is a proinflammatory cytokine secreted by macrophages and CNS neurons and glia after injury and infection and is crucial for the recruitment of professional phagocytes (Srinivasan, 2004; Lopez-Castejon and Brough, 2011; van der Vaart *et al.*, 2014; Tsarouchas *et al.*, 2018). Therefore, I asked whether Il-1β signaling was involved in NCC recruitment.

Il-1β is cleaved from pro-Il-1β by activated Caspase-1 (or zebrafish homolog Caspase A) before it can be secreted as a pro-inflammatory cytokine (Masumoto *et al.*,

2003; Lopez-Castejon and Brough, 2011; Vojtech *et al.*, 2012). To investigate the role of Il-1β signaling in NCC recruitment, I treated *Tg(sox10:nls-Eos);Tg(olig2:DsRed)* embryos at 12 hpf with 75 μM Ac-YVAD-cmk, a Caspase-1 inhibitor (Masumoto *et al.*, 2003; Tsarouchas *et al.*, 2018), to block the secretion of Il-1β, then laser ablated two *olig2*$^{+}$ motor neurons at 20 hpf, and performed time-lapse imaging (Figure 4-12A & C). In DMSO-treated controls, I observed NCC recruitment to a 50 μm x 50 μm region surrounding the MEP TZs where motor neurons were ablated within 4 to 8 hpa (Figure 4-12C & D). In contrast, fewer NCCs were recruited after ablation in YVAD-treated embryos (Figure 4-12D). It is important to note that YVAD treatment alone did not influence migration of NCCs (Figure 4-12D). Because YVAD inhibits the cleavage of pro-Il-1β (Mathiak *et al.*, 2000), I conclude that bioactive Il-1β is required for NCC recruitment during phagocytosis.

To further validate the function of Il-1β in NCC recruitment, I treated *Tg(sox10:nls-Eos);Tg(olig2:DsRed)* embryos with an IL-1 receptor antagonist (IL-1Ra) to block the detection of Il-1β by NCCs (Vojtech *et al.*, 2012), and performed the laser ablation experiment described above (Figure 4-12B). Strikingly, I found that NCC recruitment was abolished with IL-1Ra treatment, while their normal migration remained intact in embryos without ablation (Figure 4-12E). Based on these results, I conclude that Il-1β signaling is critical for the recruitment of NCCs towards debris.

Il-1β can be produced by both NCCs and debris

Next, I wanted to determine the source of Il-1β used by NCCs during phagocytosis. To do that, I labeled 20 hpf *Tg(sox10:TagRFP*) embryos with an antibody specific to Il-1β

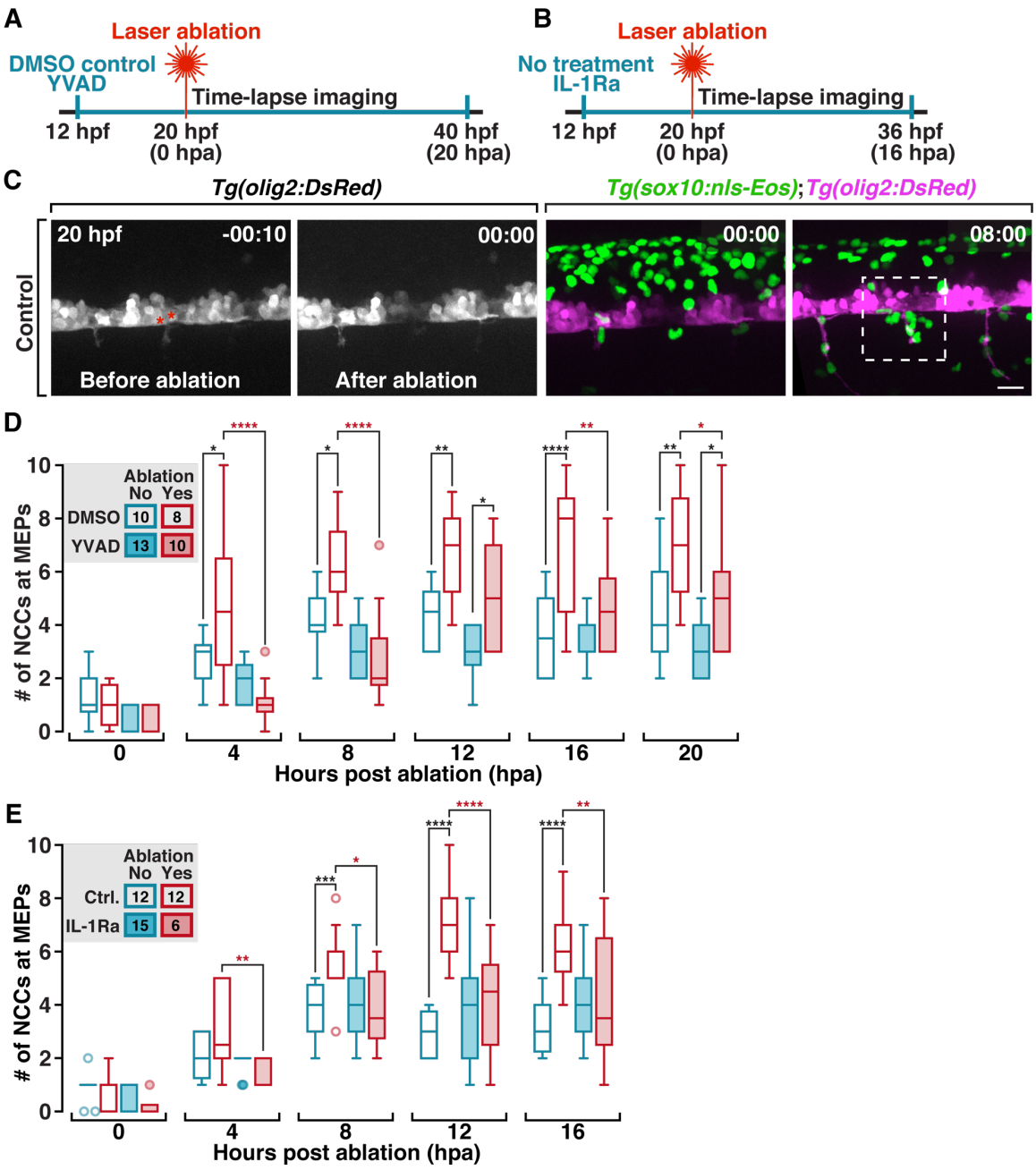

Figure 4-12. NCC recruitment towards damage is mediated by Il-1β signaling. **(A & B)** Illustrations of experimental design in D and E, respectively. **(C)** Images from a time-lapse movie of a *Tg(sox10:nls-Eos);Tg(olig2:DsRed)* embryo before and after ablation of two motor neurons (asterisks). Dashed box indicates the region where the numbers of NCCs are counted in D and E. **(D & E)** Quantification of the number of NCCs after ablation in embryos treated with YVAD **(D)** or IL-1Ra **(E)** (Numbers in the legends denote the number of embryos quantified). Scale bars, 20 μm.

and found Il-1β^{+} puncta on the tip of NCC extensions (Figure 4-13A, arrows), suggesting that NCCs may either express Il-1β or associate with Il-1β^{+} debris. To clarify this, I ablated 2 to 3 NCCs in each hemi-segment of *Tg(sox10:TagRFP*) embryos and then labeled for Il-1β. Interestingly, I observed co-localization between Il-1β labeling and a variety of NCC structures, including NCC corpses (Figure 4-13A, open arrowheads), engulfment protrusions (filled arrowheads), and debris engulfed by NCCs (open arrows). These results demonstrate that dying cells and their debris contain high levels of Il-1β.

Professional phagocytes secrete Il-1β in response to injury or infection to recruit more phagocytes (Madej *et al.*, 2017). Therefore, I next examined whether NCCs also express Il-1β. I genetically labeled the membrane of cells expressing Il-1β by transiently injecting an established *il1b:GFP-F* construct into *Tg(sox10:TagRFP)* embryos (Nguyen-Chi *et al.*, 2014). Under physiological conditions at 20 hpf, I observed that a subset of NCCs with engulfment vesicles were GFP-F^{+} (Figure 4-13B, arrowheads). I also detected robust GFP-F signal inside NCC engulfment vesicles, supporting my observations that NCCs phagocytose Il-1β^{+} cellular debris (Figure 4-13B, open arrows). Based on these results, I conclude that Il-1β is expressed by both dying cells and NCCs.

Because Il-1β maturation requires activated Caspase-1, I wanted to determine whether NCCs and/or dying cells express apoptosis-associated speck-like protein containing a caspase recruitment domain (Asc), which is required for the activation of Caspase-1 (Lopez-Castejon and Brough, 2011). To do that, I used an established line, *Tg(asc:asc-EGFP),* where endogenous Asc is fused with EGFP (Kuri *et al.*, 2017), to detect Asc and crossed it to *Tg(sox10:TagRFP)*. Live imaging of these embryos showed that macrophages were Asc^{+} (Figure 4-13C, dashed arrows), which has been described in

previous studies (Lopez-Castejon and Brough, 2011; Stehlik *et al.*, 2019; Verkhratsky *et al.*, 2019). Excitingly, I also detected colocalization of Asc with a variety of NCC structures (Figure 4-13C), including NCC corpses (open arrowheads), NCC cell bodies (filled arrowheads) and NCC vesicles (open arrows).

Discussion

During development, dead cells must be removed via phagocytosis (Arya and White, 2015). Because myeloid-derived professional phagocytes are not always present or sufficient for clearing developmental debris, previous studies show that many non-professional phagocytes contribute to debris clearance during embryogenesis, including glia in the embryonic *Drosophila* CNS, zebrafish skin epithelial cells, satellite glial precursors and neural progenitor cells in mice, as well as retinal cells in the developing human retina (Kurant *et al.*, 2008; Wu *et al.*, 2009; Lu *et al.*, 2011; Francisco-Morcillo *et al.*, 2014; Rasmussen *et al.*, 2015). In this study, I demonstrate that NCCs also phagocytose debris in the developing PNS and CNS using a mechanism similar to macrophage phagocytosis.

NCCs as a distinct type of phagocyte

Other non-professional phagocytes are mostly stationary and have limited phagocytic ability (Shklover, Levy-Adam and Kurant, 2015). However, my results show that NCCs are highly motile and respond to cell death and injury more that 100 μm away from their innate paths, which also enables them to phagocytose many types of debris, including other NCCs, CNS neurons and glia, and muscle cells.

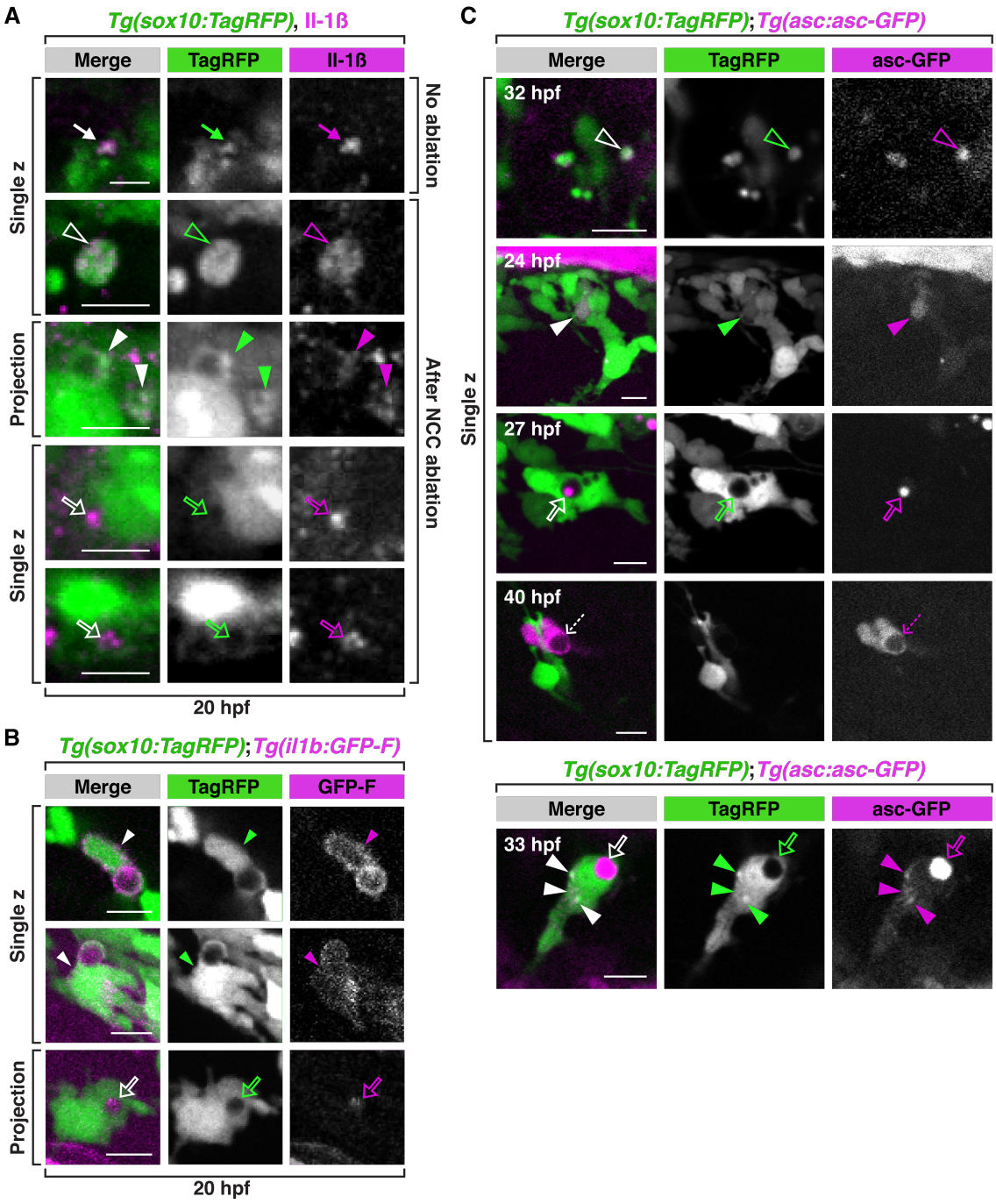
A
Tg(sox10:TagRFP), Il-1ß
Merge
TagRFP
Il-1ß
Single z
Projection
Single z
No ablation
After NCC ablation
20 hpf
B
Tg(sox10:TagRFP);Tg(il1b:GFP-F)
Merge
TagRFP
GFP-F
Single z
Projection
20 hpf
C
Tg(sox10:TagRFP);Tg(asc:asc-GFP)
Merge
TagRFP
asc-GFP
Single z
32 hpf
24 hpf
27 hpf
40 hpf
Tg(sox10:TagRFP);Tg(asc:asc-GFP)
Merge
TagRFP
asc-GFP
33 hpf

Figure 4-13. Il-1β and Asc are colocalized with both phagocytic NCCs and dead cells. (A) Images from 20 hpf *Tg(sox10:TagRFP)* embryos labeled with an Il-1β antibody. NCC protrusions (filled arrows), NCC debris (open arrowheads), NCC engulfment vesicles (filled arrowheads), and debris engulfed by NCC (open arrows) are colocalized with Il-1β staining. **(B)** Images from *Tg(sox10:TagRFP);il1b:GFP-F* embryos at 20 hpf. Open arrowheads denote phagocytic NCCs that are *il-1β*$^{+}$. Filled arrowheads denote *il-1β*$^{+}$ debris inside a NCC vesicle. **(C)** Images from *Tg(sox10:TagRFP);Tg(asc:asc-EGFP)* embryos showing a variety of NCC structures colocalized with Asc, including NCC debris (open arrowheads), NCC cytoplasm (filled arrowheads), and debris engulfed by NCC (open arrows). Dashed arrows denote a macrophage labeled by Asc-EGFP. Scale bars: 10 μm.

In my movies, I noted another difference between NCCs and other non-professional phagocytes: the nearest NCC was not always the first cell to respond to cell death. In contrast, studies demonstrate that other non-professional phagocytes show less heterogeneity and mostly phagocytose adjacent debris (Shklover, Levy-Adam and Kurant, 2015). This finding raises an interesting possibility: only a subgroup of NCCs respond to cell death and phagocytose debris, which is also supported by the distinct migratory pattern of these NCCs. However, results from my cell ablation assay provide evidence that the phagocytic population can be drastically increased by inducing damage, suggesting that a large proportion of NCCs are capable of phagocytosis. Additionally, my lineage tracing results demonstrate that phagocytic NCCs become a variety of NCC derivatives. Taken together, I propose an alternative explanation to the heterogeneity in NCC phagocytic response: early NCCs have variations in their sensitivities to phagocytic signals and under physiological conditions, only the most sensitive cells respond to debris during development, while under injury or disease conditions, other NCCs with low sensitives can be activated aid in clearance.

Developmental role of NCC phagocytosis

Although cell death during neural tube closure has been studied extensively (Schlüter, 1973; Mirkes, 2002; Massa *et al.*, 2009; Yamaguchi *et al.*, 2011), the mechanism of debris clearance remains unknown. My study demonstrates that migratory NCCs clear cellular corpses in the trunk of developing embryos. In addition to trunk NCCs, I also observed cranial NCCs phagocytosing debris (Figure 4-7B). Interestingly, live imaging in mice showed that apoptotic cells are cleared both during and after closure of the cranial

neural tube, prior to the maturation of professional phagocytes (Yamaguchi *et al.*, 2011). Given that massive migration of cranial NCCs in mice occurs during neurulation (Theveneau and Mayor, 2012), I hypothesize that NCCs also remove dead cells during neural tube closure in mice.

Our study raises another intriguing question: whether inhibition of NCC phagocytosis causes developmental defects? Unfortunately, many targetable components in the phagocytosis pathway are also required for cell migration, which limits me from blocking NCC phagocytosis without impairing their motility and development. Given that the level of NCC phagocytosis can be significantly increased after damage, I hypothesize that it is important for correcting developmental errors. Recently, a study in zebrafish *bubblebrain (blb)* mutants demonstrated that Slc37a2, a solute carrier transporter, is required for phagosomal shrinkage in professional phagocytes and maintenance of their phagocytic ability (Villani *et al.*, 2019). Since *slc37a2* is highly expressed in NCCs (Figure 4-2F) and I observed phagosomal shrinkage in NCC phagocytosis (data not shown), manipulation of Slc37a2 could be a potential future approach to block NCC phagocytosis and examine its developmental role.

Our results also demonstrate that NCCs are capable of entering the spinal cord and phagocytosing CNS debris. In certain disease conditions, Schwann cells are observed inside the spinal cord (BLAKEMORE, 1976; Duncan, Hammang and Gilmore, 1988; Duncan and Hoffman, 1997). Given that Schwann cells de-differentiate and phagocytose axonal debris after nerve injury (Jessen and Mirsky, 2016), I hypothesize that, in certain neurodegenerative diseases or after injury, Schwann cells may behave like NCCs, reactivate phagocytic pathways, and migrate into the spinal cord to clear debris.

The role of Il-1β in NCC phagocytosis

The function of Il-1β as a pro-inflammatory cytokine has been widely studied, with most studies focusing on its secretion and regulation within the innate immune system (Lopez-Castejon and Brough, 2011). My data demonstrate that Il-1β signaling is critical for NCC recruitment during development. However, I note that the level of Il-1β expression in NCCs after cell ablation is significantly lower than that which has been shown in professional phagocytes after bacterial infection (Bernut *et al.*, 2014; Nguyen-Chi *et al.*, 2014). Given that my cell ablation is precise compared to whole body bacterial infection, the low level of Il-1β release I observe supports the hypothesis that Il-1β secretion is dependent upon the strength of the inflammatory stimulus (Lopez-Castejon and Brough, 2011). In addition, I observe NCCs phagocytosing Il-1β^{+} debris, suggesting that Il-1β can be released by both phagocytic NCCs and dead cells. Similarly, a recent study showed that zebrafish epidermal cells also express Il-1β after fin fold amputation (Hasegawa *et al.*, 2017). These findings suggest that regulated Il-1β secretion might be a universal mechanism to initiate immune responses.

CHAPTER V

Discussions and Future Directions

Summary

In this dissertation, I provide a detailed description of the origin of perineurial glia (PG) and demonstrate novel functions of PG precursors and neural crest cells (NCC) in directing motor axon pathfinding out of the spinal cord and phagocytosis of cellular debris in the developing nervous system, respectively.

In Chapter III, I demonstrated that two primary PG precursors in each hemisegment are specified in the lateral floorplate (LFP) during early spinal cord patterning. PG precursors are located dorsal to motor exit point (MEP) transition zones (TZ) in the middle of each somite. Each primary PG precursor divides into one secondary PG precursor and one sister cell at approximately 35 hours post fertilization (hpf). At about 50 hpf, two secondary PG precursors derived from the two primary precursors in each hemisegment migrate out of the central nerves system (CNS) through the MEP TZ and ultimately differentiate into PG on motor nerves. Moreover, ablation of the two secondary precursors results in the absence of PG on motor nerves, indicating that other LFP cells do not compensate for the loss of PG precursors. This study provides the first description of the precise origin of PG and also allows further investigation of the cellular behavior of PG precursors during neural development. Using mosaic labeling and chemical inhibition, I showed that PG precursors at MEP TZs send dynamic actin-based protrusions resembling invadopodia towards the periphery and require MMP to leave the spinal cord. Moreover, the presence of these invadopodia-like protrusions correlates

spatiotemporally with the outgrowth of motor axons from the neural tube, suggesting that PG precursors are likely involved in the early determination of MEP TZs and motor axon pathfinding. These findings not only elucidate the development of PG but also provide novel insights into early spinal cord patterning and motor axon pathfinding.

In Chapter IV, I switched my focus to another type of glial precursor, NCCs, which have been extensively studied in the context of neural development. Here, taking advantage of the imaging capability in zebrafish embryos, I demonstrate novel roles of NCCs in debris clearance before the colonization of professional phagocytes. With the presence of dead cells, a subgroup of NCCs can migrate away from their innate pathways, towards dead cells and phagocytose cellular debris. NCCs can also enter the ventral spinal through MEP TZs and phagocytose CNS debris. Phagocytic NCCs use a mechanism similar to professional phagocytes to engulf and digest debris and can give rise to a variety of NCC derivatives. Moreover, using immunohistochemistry, live imaging and chemical inhibition, I showed that recruitment of NCCs towards dead cells is mediated by the interleukin-1β (Il1b) signaling pathway. Taken together, my data demonstrate an unexpected role of NCCs in phagocytosis of dead cells. This work fills the gap in our knowledge regarding the mechanism of debris clearance during early developmental stages.

The specification of MEP TZs

Developmental biologists and neuroscientists have been fascinated by the differentiation, morphology, and functions of spinal motor neurons for more than 100 years (Sherrington, 1906; Burke, 2006). Spinal motor nerves have been extensively studied and widely used

as experimental model systems (Arber, 2012; Griffin *et al.*, 2013; Geuna, 2015; Namgung, 2015). One of the most compelling characteristics of spinal motor neurons is that axons from distinct populations of motor neurons converge at segmentally organized MEP TZs and exit the spinal cord (Bravo-Ambrosio and Kaprielian, 2011). However, to date, little is known about how motor axons decide where to exit the spinal cord.

To answer this question, we first need to discuss the nature of MEP TZs. MEP TZs are defined as specialized positions on the margin of the CNS where motor axons exit the spinal cord. According to this definition, MEP TZs seem to be determined by motor neurons and their axons. However, motor axons do not protrude through boundaries closest to their cell bodies, instead, they somehow decide to exit from the same specialized position in the middle of each hemisegment in zebrafish, or in the anterior part of each somite in mice and amniotes (axons of mice spinal accessory motor neurons exit through lateral exit points, will be discussed later) (J. S. Eisen, 1991; Bonanomi and Samuel L Pfaff, 2010; Bravo-Ambrosio and Kaprielian, 2011; Bravo-Ambrosio, Mastick and Kaprielian, 2012). Many studies demonstrate that extrinsic signals or mechanisms directing motor axon exit must exist. Therefore, these specialized positions on the boundaries of the ventral spinal cord are likely determined through other mechanisms or by other types of cells. When motor axons exit through these locations, they are defined as MEP TZs.

What mechanisms determine the positions of MEP TZs? Because the segmental outgrowth of motor axons shows a preference for a certain part of the somite (J. S. Eisen, 1991; Kelly Kuan *et al.*, 2004; Bonanomi and Samuel L Pfaff, 2010; Bravo-Ambrosio and Kaprielian, 2011; Bravo-Ambrosio, Mastick and Kaprielian, 2012), one possible

answer is that segmental cues from sclerotomes or muscle cells determine the precise location of MEP TZs. Previous studies in amniote embryos showed that 180-degree rotation of a portion of somites in the anterior-posterior (A-P) axis led to motor axon outgrowth from the original anterior half-sclerotomes and A-P rotation of a portion of neural tube did not alter the outgrowth location of the majority of axons (Keynes and Stern, 1984). However, in neural-tube-rotated embryos, some axons did exit from the posterior half of the sclerotome and grew horizontally along the neural tube into the anterior half of the somite (Keynes and Stern, 1984). These pioneer studies indicate that somite cues guide axon pathfinding in the periphery (many attractive and repulsive signaling pathways have been revealed by later works), but are not essential to determine their initial outgrowth from the neural tube. Because of the imaging capability of zebrafish embryos, later studies in zebrafish have identified many muscle-derived cues directing motor axon outgrowth (Beattie, 2000). For example, Schweitzer et al. demonstrate that, Tenascin-C, a component of the extracellular matrix, is expressed in adaxial cells in the center of each hemisegment and is required for proper motor axon extension in the PNS (Schweitzer *et al.*, 2005). Unfortunately, removal of these somite-derived cues did not impair segmental patterning of MEP TZs but only affected motor axon pathfinding in the periphery. Therefore, the positions of MEP TZs are likely determined by mechanisms other than somite-derived cues.

Recently mice spinal accessory motor neurons (SACMNs) have been used as a model system to study motor axon exit from the spinal cord (Bravo-Ambrosio, Mastick and Kaprielian, 2012). SACMNs are a homogeneous population of spinal motor neurons with axons that leave the CNS through a discrete lateral exit point (LEP). In this study,

Bravo-Ambrosio et al. demonstrate that SACMNs express Robo2 under the control of Nkx2.9 and Robo2 directs axon pathfinding to LEP associated cells expressing Slit1/2 (Bravo-Ambrosio, Mastick and Kaprielian, 2012). This was the first identification of a gene required for motor axon exit from the vertebrate spinal cord (Bonanomi and Samuel L Pfaff, 2010; Bravo-Ambrosio, Mastick and Kaprielian, 2012). However, compared with SACMNs, ventral motor neurons derive from a different population of cells and they do not rely on Nkx2.9 to exit the spinal cord (Pabst *et al.*, 2003; Dillon *et al.*, 2005). Nevertheless, this study suggests that cells associated with exit points may be involved in the specification of MEP TZs.

In mice, during motor axon exit from the ventral spinal cord, a group of cells derived from the neural crest called boundary cap cells stay at MEP TZs (Altman *et al.*, 1982). However, boundary cap cells are located at the outer margin of the spinal cord, meaning that motor axons have to find the correct positions and cross the basal lamina before contact with these cells. Moreover, many studies have demonstrated that ablation of boundary cap cells leads to ectopic exit of motor neuron cell bodies from the spinal cord but do not cause MEP specification defects (Hjerling-Leffler *et al.*, 2005; Bron *et al.*, 2007).

Although boundary cap cells are not involved in the specification of MEP TZs in mice, Sepp et al. demonstrate that a type of CNS-derived PNS glia in *Drosophila*, called peripheral glia or exit glia, guide motor axon pathfinding through the CNS/PNS TZ (Sepp, Schulte and Auld, 2001). Similar to vertebrates, during *Drosophila* embryonic development, motor neurons in the CNS extend their exons towards the CNS/PNS boundary and exit the CNS in a segmentally organized pattern (Sepp, Schulte and Auld,

2001). In their study, Sepp et al. found that before motor axon exit from the CNS, their growth cones first approach peripheral glia at the CNS/PNS border; peripheral glia at the TZ then form a cone-shaped array to facilitate the exit of motor axons. Moreover, in the absence of peripheral glia, motor axons initially exit the CNS in abnormal patterns, indicating that peripheral glia at the TZ direct motor axon exit from the CNS (Sepp, Schulte and Auld, 2001). Together, these studies support the hypothesis that cells at the inner margin of the vertebrate spinal cord may play a role in the specification of MEP TZs.

Previous studies from our lab found that, similar to *Drosophila* peripheral glia, vertebrate PG derive from the CNS and migrate to the PNS through MEP TZs (Kucenas *et al.*, 2008; Clark *et al.*, 2014). In Chapter III, I demonstrate that PG derive from precursors located at MEP TZs in the lateral floorplate. Moreover, during motor axon outgrowth from the spinal cord, *nkx2.2a*$^{+}$ PG precursors project dynamic protrusions resembling invadopodia at MEP TZs. Therefore, I propose that PG precursors specified at the middle of each hemisegment are responsible for directing motor axons exit through the CNS/PNS boundary during early developmental stages.

Why are MEP TZs determined by floorplate cells? An answer to this question may related to their location in the spinal cord on the dorsal-ventral (D-V) axis. LFP cells belong to the p3 domain right underneath the pMN where motor neurons arise (Figure 1-2). After motor neuron specification, their cell bodies migrate dorsally while projecting axons towards the ventral spinal cord, and, ultimately, motor axons exit the spinal cord at the boundary of p3 and pMN domain (J. S. Eisen, 1991; Beattie, 2000; Bonanomi and Samuel L Pfaff, 2010; Ravanelli and Appel, 2015).

Moreover, given that floor plate cells are the earliest group of cells specified during folding of the neural tube (Catala *et al.*, 1996), it is likely that they are able to receive segmental information during early spinal cord patterning, which allows them to govern MEP specification in a segmentally organized pattern at later stages. This hypothesis also provides a possible explanation for the early specification of PG precursors in the middle of each hemisegment, which will be further discussed in the next section.

In summary, although how MEP TZs are specified in the middle of each hemisegment during early spinal cord patterning remains unclear, my work presented in this dissertation provides new insights into the mechanism of motor axon pathfinding through the CNS/PNS boundary.

Segmentation, spinal cord patterning, and PG specification

How various types of neurons and glia are specified in the nervous system is a fundamental question in neural development. Because of the complexity of the brain, a significant amount of our knowledge of neurogenesis and gliogenesis comes from the spinal cord. The spinal cord is also an ideal model to study nervous system patterning because considerable amount of cross sections can be acquired from one sample. Thus, the specification of neurons and glia in different domains across the D-V axis of the spinal cord has been studied extensively (Poh *et al.*, 2002). However, these studies mostly ignore the variations in domain patterning along the A-P axis within each segment and studies of the spinal cord A-P patterning mostly focus on the segmentation across the whole animal (Keynes and Stern, 1984; Hubaud and Pourquié, 2014). Therefore, very

little is known about how neurons and glia arise from different regions along the A-P axis of the spinal cord.

A few researchers have pioneered the study of spinal cord A-P patterning. For example, Schäfer et al. showed that, in the zebrafish LFP, different progenitor cells labeled by distinct transcription factors are discontinuously organized along the A-P axis (Schäfer, Kinzel and Winkler, 2007). They found that such alternating appearance of different progenitors in the LFP require Delta-Notch signaling and different levels of Hedgehog (Hh) activity (Schäfer, Kinzel and Winkler, 2007). Similarly, Huang et al. demonstrated that zebrafish LFP progenitors require Notch signaling to maintain Hh activity and induce fate identity, and the differentiation of these progenitors rely on the attenuation of Notch and Hh signaling (Huang *et al.*, 2012). To investigate the origin and cell lineage of Kolmer-Agduh" (KA") interneurons in the LFP, they performed a novel photoconvertible reporter of signaling history (PHRESH) assay and found that KA" cells derive from both symmetric and asymmetric divisions of LFP progenitors but daughter cells generated by these divisions are initially equivalent, suggesting that extrinsic cues determine the sites of KA" differentiation (Huang *et al.*, 2012). However, how these daughter cells acquired different Hh responsiveness and differentiate into KA" cells remain unknown.

Excitingly, a recent study from Hadjivasiliou et al. proposed a possible mechanism for the segmental patterning of neuron specification along the A-P axis of the spinal cord (Hadjivasiliou *et al.*, 2019). Using *in vivo* imaging in zebrafish embryos, they demonstrated that differentiating neurons transiently project two long protrusions along the A-P axis of the spinal cord; these protrusions express high levels of Delta and extend

the range of lateral inhibition, which regulates the spatiotemporal patterns of neuronal differentiation along the A-P axis (Hadjivasiliou *et al.*, 2019). This study not only provides new insights into the mechanisms of Notch-mediated lateral inhibition, but also shows that live imaging in zebrafish embryos is a powerful tool to understand the 3-D patterning of the spinal cord.

Although these studies demonstrate that neural progenitors in the spinal cord are distributed in a discontinuous pattern along the A-P axis, they did not map the A-P patterning of the spinal cord progenitor cells onto the somite segmentation. In contrast, the specification and organization of spinal motor neurons have been extensively studied in the context of segmentation.

During the development of vertebrate animals, pMN derived spinal motor neurons acquire specialized “pool” identities across both the D-V and A-P axis of the spinal cord, which determines their ability to form selective connections with their targets in the periphery (Dasen *et al.*, 2005; Stifani, 2014). Motor neurons specification and migration along the D-V axis have been extensively studied (Lewis and Eisen, 2003; Stifani, 2014; Ravanelli and Appel, 2015). Regarding the A-P axis, it is known that a combination of intrinsic signaling, including Nkx6.1 and Hox transcriptional regulatory network regulated by graded FGF signaling, and extrinsic cues, such as muscle derived GDNF signaling, specifies segmental identities of motor neuron pools (Dasen *et al.*, 2005; Stifani, 2014). However, compared with the segmental organization of spinal motor neurons, their intra-segmental specification and migration along the A-P axis is poorly understood.

In Chapter III, using time-lapse imaging in transgenic zebrafish embryos, I demonstrate that *hb9*$^{+}$ primary motor neurons are specified along the A-P axis in the spinal cord. At the earliest stage of their specification, primary motor neurons migrate along the A-P axis, towards the potential MEP TZ, and project their axons to the periphery (Figure 3-8A). In contrast to pMN derived motor neurons, *nkx2.2a*$^{+}$ LFP cells are relatively static and do not migrate during these stages, favoring a hypothesis that extrinsic cues from the LFP direct the migration of primary motor neurons and contribute to the formation of motor neuron pools. If this is true, a group of specialized LFP cells must be present at potential MEP TZs located in the middle of each hemisegment, which matches with my finding of PG precursors at MEP TZs. Taken together, I hypothesize that a subpopulation of LFP cells located in the middle of each hemisegment recruit motor neurons towards the potential MEP TZ and direct motor axon exit from the spinal cord; at later developmental stages, these cells become PG precursors and migrate into the periphery.

Do such LFP population exist? Excitingly, several studies indicate the existence of these specialized LFP cells in their study. In a study by Schäfer et al., they found that *nkx2.2b* labels the LFP robustly in a continuous pattern in wild type zebrafish embryos, while in homozygous *dtr*$^{-/-}$ (*gli1*) mutants, the pMN domain expands into the LFP and *nkx2.2b* staining is missing (Schäfer, Kinzel and Winkler, 2007). Interestingly, in heterozygous *dtr*$^{+/-}$ mutants, although *nkx2.2b* expression in most of the LFP cells is abolished, a small population of LFP cells in the middle of each somite remains *nkx2.2b*$^{+}$. Given that Gli1 is an immediate downstream activator of the Sonic hedgehog (Shh) signaling, these results indicate that a group of LFP cells in the middle of each

hemisegment exhibit a distinct responsiveness to Shh. These specialized LFP cells are likely the PG precursors I demonstrated above. To test if this is true, one can perform *in situ* hybridization against *nkx2.2* in *dtr*$^{+/-}$ mutants at 60 hpf and look for PG in the periphery. Alternatively, transgenic *dtr*$^{+/-}$ zebrafish expressing membrane tethered fluorescent protein in *nkx2.2b*$^{+}$ cells can be used to investigate whether LFP protrusions are present in these embryos.

Moreover, a recent work from the Huang lab demonstrate that LFP cells in the middle of each hemisegment express *pax9* (Ma *et al.*, 2018), which is a transcription factor downstream of segmental signaling and required for sclerotome development. These results support the hypothesis that LFP cells receive segmental signaling during early spinal cord development and contribute to further spinal cord patterning at later stages.

Taken together, my work presented in this dissertation sheds new light on roles of LFP cells in segmental organization and early patterning of spinal cord neurons and glia.

To eat, or not to eat?

In Chapter IV, I demonstrated that a subgroup of NCCs can phagocytose cellular debris in the developing CNS and PNS. However, I did not address any specific markers for phagocytic NCCs. To test whether phagocytic NCCs express specific genes, a direct approach is to identify markers specific to phagocytic NCCs. Hence, I went through our RNA-Sequencing data set and screened for genes that are both highly expressed in NCCs at 36 hpf and enriched in macrophages (Gautier *et al.*, 2012). Next, I checked the available expression information of these genes on ZFIN to confirm that they are

expressed in NCCs and performed *in situ* hybridization. Staining results of two candidate genes, *scarb1* and *csf1ra*, showed that both of them are only expressed in NCCs migrating dorsal-laterally, indicating that NCCs give rise to pigment cells are positive for *scarb1* and *csf1ra*. However, based on my lineage tracing results, phagocytic NCCs can differentiate into a variety of NCC derivatives, not just limited to pigment cells. Therefore, although *scarb1* and *csf1ra* are highly enriched in NCCs and are important for normal functions of macrophages, they do not label the phagocytic subset of NCCs. A possible explanation to this disappointing result is that phagocytic NCCs only compose 10% of the whole population under physiological conditions (Figure 4-3G). Moreover, NCCs used for RNA-Sequencing were collected at 36 hpf when their phagocytic ability started to decrease (Figure 4-10B). Therefore, our RNA-Sequencing may be unable to pull out genes specific to phagocytic NCCs because of their low expression levels. An improved method is to perform RNA-Sequencing of 24 hpf NCCs collected from embryos with/without laser injury and then analyze differentially expressed genes to identify upregulated genes in the injury group. An alternative method to selectively label phagocytic NCCs is to stain for components that are known to play a role in NCC phagocytosis, for instance, interleukin-1 receptor (Il-1r).

Because I showed that phagocytic NCCs are present in most NCC territories and can give rise to a variety of NCC derivatives, a greater possibility is that all NCCs can phagocytose debris, which has been discussed in Chapter IV. This is also supported by their slow digestion speed (Figure 4-7D), which indicates that they are not specialized to perform phagocytosis like professional phagocytes. Nevertheless, I did notice that NCCs in certain regions phagocytose more actively. In general, I observed more phagocytic

vesicles in NCCs close to the dorsal neural tube and on the dorsal-lateral migratory pathway. An explanation to this phenomenon is that these NCCs have more “freedom of migration”. NCCs close to the dorsal neural tube are the newly delaminated ones and those migrate dorsal-laterally are not constrained by axonal cues (Christiansen, Coles and Wilkinson, 2000; Roberto Mayor and Theveneau, 2013). Moreover, I demonstrated that NCC phagocytic abilities can be induce after injury (Figure 4-9), suggesting that all NCCs may have the potential to phagocytose. However, in those experiments, most of the ablations were executed in a region dorsal to the MEP TZs. I noticed that when ablation was performed on or between motor nerves, NCCs ventral to the spinal cord did not exhibit the same responsiveness. These results also support the hypothesis that NCCs with greater “freedom of migration” are more active in phagocytosis.

Although I did not identify specific markers for phagocytic NCCs, I demonstrated that their recruitment towards dead cells is mediated by Il-1β signaling. Such cues released from dead cells to recruit phagocytes are called “find me” signals with nucleotides being the most common one (Elliott *et al.*, 2009; Shklover, Levy-Adam and Kurant, 2015). Previous studies demonstrate that professional phagocytes sense ATP and ADP released from apoptotic cells using purinergic receptors (Elliott *et al.*, 2009). To test whether nucleotide signal is involved in NCC recruitment, I performed the same ablation assay presented in Figure 4-12 and treated embryos with a purinergic receptor inhibitor, suramin. Quantification of the number of NCCs recruited to the ablation site demonstrate that NCC recruitment was impaired in suramin treated embryos. However, compared with the inhibition of Il-1β signaling pathway, the reduction of NCC recruitment after blocking purinergic receptors was not as significant. Future studies may elucidate the

exact purinergic receptor expressed in NCCs using receptor-specific inhibitors and genetic manipulation.

After reaching dead cells, professional phagocytes can identify their food to eat by recognizing the "eat me" signal, such as phosphatidylserine, on the surface of dead cells (Shklover, Levy-Adam and Kurant, 2015). To investigate whether phosphatidylserine can be recognized by NCCs, I treated *Tg(sox10:EOS)* embryos with 500 μM of O-phospho-L-serine (L-SOP), a molecule that mimics the phosphatidylserine head group that can partially block macrophage phagocytosis of apoptotic cells (Witting *et al.*, 2000), from 14 to 22 hpf, and performed time-lapse imaging immediately afterwards. In all three treated embryos, I observed NCCs phagocytose dead neighbors. However, because L-SOP works as an agonist and I did not quantify colocalization of apoptotic cells with NCCs, these preliminary results cannot rule out the possibility that phosphatidylserine can be recognized by NCCs. Interestingly, in these embryos, I found significantly more macrophages colonizing the trunk region starting from 25 hpf. It is possible that elevated phosphatidylserine or L-SOP concentration induces macrophage proliferation and maturation. Future studies to understand how NCCs recognize dead cells may also examine roles of known phagocytic receptors, such as TIM-4, BAI1, Pear1 and Megf10, using genetic manipulation and chemical inhibition (Scheib, Sullivan and Carter, 2012; Mazaheri *et al.*, 2014; Shklover, Levy-Adam and Kurant, 2015).

Il-1β as a novel "find me" signal

Il-1β is traditionally viewed as a pro-inflammatory cytokine crucial for defence responses to infection and injury. In this dissertation, I demonstrate a novel role of Il-1β in

recruiting NCCs towards dead cells. I found that Il-1β is expressed by both dead cells and NCCs (Figure 4-13). Using chemical inhibition, I demonstrate that the Il-1β signaling in NCC recruitment requires activation Caspase-1 activity. Because the activation of Caspase-1 requires the recruitment of an apoptosis-associated speck-like protein containing a caspase recruitment domain (Asc) (Lopez-Castejon and Brough, 2011), I examined the Asc activity and found that both both dead cells and phagocytic NCCs express Asc, suggesting that they have the ability to activate Caspase-1 and release Il-1β (Figure 4-13).

In macrophages, Caspase-1 activation ususally leads to a rapid cell death called pyroptosis and the secretion of significant amount of Il-1β (Lopez-Castejon and Brough, 2011). A hallmark of pyroptosis is assembly of the inflammasome adaptor Asc into specks (Kuri *et al.*, 2017). However, during my imaiging of *Tg(asc:asc-EGFP)* embryos, I have never observed the formation of Asc specks before or after laser ablation, indicating that the secretion of Il-1β is not a result of pyroptosis. One possible explanation is that the damage generated by laser ablation was not intense enough to activate pyroptosis or pro-inflammatory responses. How Il-1β is secreted from dead cells and phagocytic NCCs remains unknown.

Unlike macrophages, which express high levels of pro-Il-1β and Asc under physiological conditions (Figure 4-13) (Lopez-Castejon and Brough, 2011), only a small portion of NCCs were *il-1β*$^{+}$ or *asc*$^{+}$ (Figure 4-13). However, the number of NCCs labeled by Il-1β or Asc significantly increased in response to injury, suggesting that NCC secretion of Il-1β is influenced by cell death. Excitingly, previous studies demonstrated that ATP stimulation of the P2X7 receptor induces the release of IL-1β in macrophages

(Solle *et al.*, 2001; Le Feuvre *et al.*, 2002). In addition, my suramin treatment results mentioned above indicate that NCCs can respond to extracellular ATP. Therefore, I hypothesize that ATP released from dying cells activates the expression of Asc in NCCs, and thus induces Caspase-1 dependent release of Il-1β. To test this hypothesis, futures studies may treat *Tg(il1b:GFP-F)* or *Tg(asc:asc:EGFP)* embryos with puerinergic receptor inhibitor, induce injury with laser ablation, and quantify the number of NCCs activating the expression of *il-1β* or *asc*.

Taken together, my results indicate that Il-1β released from dead cells after injury recruits NCC migration towards debris and induces the processing and secretion of Il-1β from phagocytic NCCs, which in turn, may recruit more NCCs to the injury site to facilite debris clearance. My findings highlights novel roles of NCCs in neural development and sheds light on the potential mechanism of regulated Il-1β secretion.

The novel behavior of PG precursors and NCCs I demonstrated in this dissertation advances our understanding of fundamental processes in neural development, including spinal cord patterning, segmentation, motor axon pathfinding, neural crest migration, and developmental debris clearance. My work also provides new insights into unexpected but crucial contributions of neural progenitors to the development of the nervous system. Future studies of progenitor cells in zebrafish and other model organisms may change the way we think about roles of progenitor cells in neural development.

Appendix: Abbreviations

Abbreviations are listed in alphabetical order. See Table 2-2 for abbreviations of transgenes.

A-P	anterior-posterior
Asc	apoptosis-associated speck-like protein containing a caspase recruitment domain
BMP	bone morphogenetic protein
CaP	caudal primary
CNS	central nervous system
CRISPR	clustered regularly interspaced short palindromic repeats
csf1ra	colony stimulating factor 1 receptor a
CXCL12	chemokine (C-X-C motif) ligand 12
CXCR4	chemokine (C-X-C motif) receptor 4
D-V	dorsal-ventral
DBX1	developing brain homeobox 1
DBX2	developing brain homeobox 2
DMSO	dimethyl sulfoxide
dpf	days post fertilization
DRG	dorsal root ganglion
ECM	extracellular matrix
EFNB1	ephrin-B1

EGFP	enhanced green fluorescent protein
Fgf	fibroblast growth factor
foxd3	forkhead box D3
FP	floorplate
hb9	motor neuron and pancreas homeobox 1
Hox	homebox
hpf	hours post fertilization
Il-1r	interleukin-1 receptor
Il-1β	interleukin-1β
IRZ3	iroquois homeobox protein 3
KA"	Kolmer-Agduh"
krox20	early growth response 2a
L-SOP	O-phospho-L-serine
Lamp1	lysosome-associated-membrane-protein-1
LEP	lateral exit point
lh3	procollagen-lysine, 2-oxoglutarate 5-dioxygenase 3
Lhx3	LIM homeobox 3
MEP	motor exit point
MiP	middle primary
MMP	matrix metalloproteases
NCC	neural crest cell
Ngn2	neurogenin 2
NKX2.2	NK2 homeobox 2

Nkx2.*9*	NK2 homeobox 9
NKX6.1	NK6 homeobox 1
Npn	neuropilin
OL	oligodendrocyte
Olig1	oligodendrocyte transcription factor 2
OLIG2	oligodendrocyte transcription factor 2
PAX6	paired box 6
Pdgf	platelet-derived growth factor
PG	perineurial glia
PI(3)P	phosphatidylinositol 3-monophosphate
PNS	peripheral nervous system
Rac	Rac family small GTPase
RFP	red fluorescent protein
RhoA	Ras homolog gene family, member A
Robo2	roundabout homolog 2
RoP	rostral primary
SACMN	spinal accessory motor neurons
SC	Schwann cell
scarb1	scavenger receptor class B member 1
SecA5	secreted annexin V
SEMA6A	semaphorin 6A
Shh	Sonic hedgehog
SLIT1	Slit Homolog 1

SLIT2	Slit Homolog 2
Sox10	SRY-box transcription factor 10
TZ	transition zone
UV	ultraviolet
VaP	variable primary
vMN	ventral motor neuron
YFP	yellow fluorescent protein
zfh1	Zn finger homeodomain 1

References

Akert, K *et al.* (1976) 'The fine structure of the perineural endothelium.', *Cell and tissue research*, 165(3), pp. 281–95. doi: 10.1007/bf00222433.

Akert, K. *et al.* (1976) 'The fine structure of the perineural endothelium', *Cell and Tissue Research*, 165(3), pp. 281–295. Available at: http://www.ncbi.nlm.nih.gov/pubmed/1082372.

Alaynick, W. A., Jessell, T. M. and Pfaff, S. L. (2011) 'Olig2 pMN SnapShot: Spinal Cord Development', *Cell*, 146. doi: 10.1016/j.cell.2011.06.038.

Altman, J. *et al.* (1982) *Development of the cranial nerve ganglia and related nuclei in the rat*. Springer-Verlag. Available at: http://agris.fao.org/agris-search/search.do?recordID=US201300342874 (Accessed: 11 August 2019).

Appel, B, Givan, L. A. and Eisen, J. S. (2001) 'Delta-Notch signaling and lateral inhibition in zebrafish spinal cord development.', *BMC developmental biology*. BioMed Central, 1, p. 13. doi: 10.1186/1471-213X-1-13.

Appel, Bruce, Givan, L. A. and Eisen, J. S. (2001) 'Delta-Notch signaling and lateral inhibition in zebrafish spinal cord development.', *BMC developmental biology*, 1, p. 13. doi: 10.1186/1471-213X-1-13.

Arber, S. (2012) 'Motor Circuits in Action: Specification, Connectivity, and Function', *Neuron*, 74(6), pp. 975–989. doi: 10.1016/j.neuron.2012.05.011.

Arya, R. and White, K. (2015) 'Cell death in development: Signaling pathways and core mechanisms', *Seminars in Cell & Developmental Biology*. Academic Press, 39, pp. 12–19. doi: 10.1016/J.SEMCDB.2015.02.001.

Ashburner, M. *et al.* (2000) 'Gene Ontology: tool for the unification of biology', *Nature Genetics*, 25(1), pp. 25–29. doi: 10.1038/75556.

Avilés, E. C., Wilson, N. H. and Stoeckli, E. T. (2013) 'Sonic hedgehog and Wnt: antagonists in morphogenesis but collaborators in axon guidance', *Frontiers in Cellular Neuroscience*. Frontiers, 7, p. 86. doi: 10.3389/fncel.2013.00086.

Banerjee, S. *et al.* (2011) 'A novel role for MuSK and non-canonical Wnt signaling during segmental neural crest cell migration', *Development*, 138(15), pp. 3287–3296. doi: 10.1242/jcs.96677.

Barres, B. A., Lazar, M. A. and Raff, M. C. (1994) 'A novel role for thyroid hormone, glucocorticoids and retinoic acid in timing oligodendrocyte development.', *Development (Cambridge, England)*, 120(5), pp. 1097–108. Available at: http://www.ncbi.nlm.nih.gov/pubmed/8026323 (Accessed: 19 July 2019).

Beattie, C. E. (2000) 'Control of motor axon guidance in the zebrafish embryo.', *Brain research bulletin*, 53(5), pp. 489–500. doi: 10.1016/S0361-9230(00)00382-8.

Berardozzi, R. *et al.* (2016) 'Arginine 66 Controls Dark-State Formation in Green-to-Red Photoconvertible Fluorescent Proteins', *Journal of the American Chemical Society*, 138(2), pp. 558–565. doi: 10.1021/jacs.5b09923.

Bernut, A. *et al.* (2014) 'Mycobacterium abscessus cording prevents phagocytosis and promotes abscess formation.', *Proceedings of the National Academy of Sciences of the United States of America*. National Academy of Sciences, 111(10), pp. E943-52. doi: 10.1073/pnas.1321390111.

Bertrand, J. Y. *et al.* (2013) 'Three pathways to mature macrophages in the early mouse yolk sac Three pathways to mature macrophages in the early mouse yolk sac', *Blood*,

106(9), pp. 3004–3011. doi: 10.1182/blood-2005-02-0461.

Binari, L. A., Lewis, G. M. and Kucenas, S. (2013) 'Perineurial glia require Notch signaling during motor nerve development but not regeneration', *The Journal of neuroscience: the official journal of the Society for Neuroscience*, 33(10), pp. 4241–4252. doi: 10.1523/JNEUROSCI.4893-12.2013.

Binker, M. G. *et al.* (2007) 'Arrested maturation of Neisseria -containing phagosomes in the absence of the lysosome-associated membrane proteins, LAMP-1 and LAMP-2', *Cellular Microbiology*, 9(9), pp. 2153–2166. doi: 10.1111/j.1462-5822.2007.00946.x.

BLAKEMORE, W. F. (1976) 'Invasion of Schwann Cells Into the Spinal Cord of the Rat Following Local Injections of Lysolecithin', *Neuropathology and Applied Neurobiology*, 2(1), pp. 21–39. doi: 10.1111/j.1365-2990.1976.tb00559.x.

Bonanomi, D. and Pfaff, Samuel L (2010) 'Motor axon pathfinding.', *Cold Spring Harbor perspectives in biology*. Cold Spring Harbor Laboratory Press, 2(3), p. a001735. doi: 10.1101/cshperspect.a001735.

Bonanomi, D. and Pfaff, Samuel L. (2010) 'Motor axon pathfinding.', *Cold Spring Harbor perspectives in biology*, 2(3), p. a001735. doi: 10.1101/cshperspect.a001735.

Bravo-Ambrosio, A. and Kaprielian, Z. (2011) 'Crossing the border: molecular control of motor axon exit.', *International journal of molecular sciences*. Multidisciplinary Digital Publishing Institute (MDPI), 12(12), pp. 8539–61. doi: 10.3390/ijms12128539.

Bravo-Ambrosio, A., Mastick, G. and Kaprielian, Z. (2012) 'Motor axon exit from the mammalian spinal cord is controlled by the homeodomain protein Nkx2.9 via Robo-Slit signaling', *Development*, 139(8), pp. 1435–1446. doi: 10.1242/dev.072256.

Briscoe, J. *et al.* (2000) 'A homeodomain protein code specifies progenitor cell identity and neuronal fate in the ventral neural tube.', *Cell*, 101(4), pp. 435–45. doi: 10.1016/s0092-8674(00)80853-3.

Briscoe, J. and Ericson, J. (2001) 'Specification of neuronal fates in the ventral neural tube', *Current Opinion in Neurobiology*. Elsevier Current Trends, 11(1), pp. 43–49. doi: 10.1016/S0959-4388(00)00172-0.

Bron, R. *et al.* (2007) 'Boundary cap cells constrain spinal motor neuron somal migration at motor exit points by a semaphorin-plexin mechanism', *Neural Development*, 2(1), p. 21. doi: 10.1186/1749-8104-2-21.

Bronner, M. E. and Simões-Costa, M. (2016) 'The Neural Crest Migrating into the Twenty-First Century', *Current Topics in Developmental Biology*, 116, pp. 115–134. doi: 10.1016/bs.ctdb.2015.12.003.

Burke, R. E. (2006) 'Sir Charles Sherrington's The integrative action of the nervous system: a centenary appreciation', *Brain*, 130(4), pp. 887–894. doi: 10.1093/brain/awm022.

Burkel, W. E. (1967) 'The histological fine structure of perineurium.', *The Anatomical record*, 158(2), pp. 177–89. doi: 10.1002/ar.1091580207.

Buschman, M. D. *et al.* (2009) 'The novel adaptor protein Tks4 (SH3PXD2B) is required for functional podosome formation.', *Molecular biology of the cell*. American Society for Cell Biology, 20(5), pp. 1302–11. doi: 10.1091/mbc.e08-09-0949.

Buss, R. R., Sun, W. and Oppenheim, R. W. (2006) 'ADAPTIVE ROLES OF PROGRAMMED CELL DEATH DURING NERVOUS SYSTEM DEVELOPMENT', *Annual Review of Neuroscience*. Annual Reviews, 29(1), pp. 1–

35. doi: 10.1146/annurev.neuro.29.051605.112800.

Cannon, G. J. and Swanson, J. A. (1992) 'The macrophage capacity for phagocytosis.', *Journal of cell science*, 101 (Pt 4, pp. 907–13. Available at: http://www.ncbi.nlm.nih.gov/pubmed/1527185.

Canton, J. *et al.* (2014) 'Contrasting phagosome pH regulation and maturation in human M1 and M2 macrophages.', *Molecular biology of the cell*. American Society for Cell Biology, 25(21), pp. 3330–41. doi: 10.1091/mbc.E14-05-0967.

Carney, T. J. *et al.* (2006) 'A direct role for Sox10 in specification of neural crest-derived sensory neurons.', *Development (Cambridge, England)*, 133(23), pp. 4619–30. doi: 10.1242/dev.02668.

Casano, A. M., Albert, M. and Peri, F. (2016) 'Developmental Apoptosis Mediates Entry and Positioning of Microglia in the Zebrafish Brain', *Cell Reports*. The Authors, 16(4), pp. 897–906. doi: 10.1016/j.celrep.2016.06.033.

Catala, M. *et al.* (1996) 'A spinal cord fate map in the avian embryo: While regressing, Hensen's node lays down the notochord and floor plate thus joining the spinal cord lateral walls', *Development*, 122(9), pp. 2599–2610.

Chambers, C. B. (2001) *Notch signals and telencephalic fate*. Available at: https://dev.biologists.org/content/develop/128/5/689.full.pdf (Accessed: 19 July 2019).

Champion, J. A., Walker, A. and Mitragotri, S. (2008) 'Role of Particle Size in Phagocytosis of Polymeric Microspheres', *Pharmaceutical Research*. Springer US, 25(8), pp. 1815–1821. doi: 10.1007/s11095-008-9562-y.

Chan, D. W. and Yager, T. D. (2002) 'Preparation and imaging of nuclear spreads from

cells of the zebrafish embryo', *Chromosoma*, 107(1), pp. 39–60. doi: 10.1007/s004120050280.

Christiansen, J. H., Coles, E. G. and Wilkinson, D. G. (2000) 'Molecular control of neural crest formation, migration and differentiation', *Current Opinion in Cell Biology*, 12(6), pp. 719–724. doi: 10.1016/S0955-0674(00)00158-7.

Clark, B. S. *et al.* (2011) 'Generation of Rab-based transgenic lines for in vivo studies of endosome biology in zebrafish', *Developmental Dynamics*. Wiley-Liss, Inc., 240(11), pp. 2452–2465. doi: 10.1002/dvdy.22758.

Clark, J. K. *et al.* (2014) 'Mammalian Nkx2.2+ perineurial glia are essential for motor nerve development', *Developmental Dynamics*, 243(9), pp. 1116–1129. doi: 10.1002/dvdy.24158.

Clay, M. R. and Halloran, M. C. (2014) 'Cadherin 6 promotes neural crest cell detachment via F-actin regulation and influences active Rho distribution during epithelial-to-mesenchymal transition.', *Development (Cambridge, England)*, 141(12), pp. 2506–15. doi: 10.1242/dev.105551.

Cong, L. *et al.* (2013) 'Multiplex genome engineering using CRISPR/Cas systems.', *Science (New York, N.Y.)*. NIH Public Access, 339(6121), pp. 819–23. doi: 10.1126/science.1231143.

Cuadros, M. A. *et al.* (1993) 'First appearance, distribution, and origin of macrophages in the early development of the avian central nervous system.', *The Journal of comparative neurology*, 330(1), pp. 113–29. doi: 10.1002/cne.903300110.

Dasen, J. S. *et al.* (2005) 'A Hox Regulatory Network Establishes Motor Neuron Pool Identity and Target-Muscle Connectivity', *Cell*. Cell Press, 123(3), pp. 477–491. doi:

10.1016/J.CELL.2005.09.009.

Davis-Dusenbery, B. N. *et al.* (2014) 'How to make spinal motor neurons', *Development*. The Company of Biologists, 141(3), pp. 491–501. doi: 10.1242/dev.097410.

Dewitz, C. *et al.* (2018) 'Nuclear Organization in the Spinal Cord Depends on Motor Neuron Lamination Orchestrated by Catenin and Afadin Function', *CellReports*, 22, pp. 1681–1694. doi: 10.1016/j.celrep.2018.01.059.

Dillon, A. K. *et al.* (2005) 'Molecular Control of Spinal Accessory Motor Neuron/Axon Development in the Mouse Spinal Cord', *The Journal of Neuroscience*, 25(44), pp. 10119–10130. doi: 10.1523/JNEUROSCI.3455-05.2005.

Don, E. K. *et al.* (2017) 'A Tol2 Gateway-Compatible Toolbox for the Study of the Nervous System and Neurodegenerative Disease', *Zebrafish*, 14(1), pp. 69–72. doi: 10.1089/zeb.2016.1321.

Duncan, I. D., Hammang, J. P. and Gilmore, S. A. (1988) 'Schwann cell myelination of the myelin deficient rat spinal cord following X-irradiation', *Glia*. John Wiley & Sons, Ltd, 1(3), pp. 233–239. doi: 10.1002/glia.440010309.

Duncan, I. D. and Hoffman, R. L. (1997) 'Schwann cell invasion of the central nervous system of the myelin mutants.', *Journal of anatomy*. Wiley-Blackwell, 190 (Pt 1)(Pt 1), pp. 35–49. doi: 10.1046/J.1469-7580.1997.19010035.X.

Eisen, J S (1991) 'Motoneuronal development in the embryonic zebrafish.', *Development (Cambridge, England)*, Suppl 2(9), pp. 141–147. Available at: http://www.jneurosci.org/content/15/9/5956 (Accessed: 17 January 2015).

Eisen, J. S. (1991) 'Motoneuronal development in the embryonic zebrafish', *Development (Cambridge, England)*, Suppl 2, pp. 141–147. Available at:

http://www.ncbi.nlm.nih.gov/pubmed/1842352.

Ellett, Felix *et al.* (2011) 'mpeg1 promoter transgenes direct macrophage-lineage expression in zebrafish.', *Blood*. American Society of Hematology, 117(4), pp. e49-56. doi: 10.1182/blood-2010-10-314120.

Ellett, F. *et al.* (2011) 'mpeg1 promoter transgenes direct macrophage-lineage expression in zebrafish', *Blood*, 117(4), pp. e49–e56. doi: 10.1182/blood-2010-10-314120.

Elliott, M. R. *et al.* (2009) 'Nucleotides released by apoptotic cells act as a find-me signal to promote phagocytic clearance', *Nature*. Nature Publishing Group, 461(7261), pp. 282–286. doi: 10.1038/nature08296.

Le Feuvre, R. A. *et al.* (2002) 'Priming of Macrophages with Lipopolysaccharide Potentiates P2X7-mediated Cell Death via a Caspase-1-dependent Mechanism, Independently of Cytokine Production', *Journal of Biological Chemistry*, 277(5), pp. 3210–3218. doi: 10.1074/jbc.M104388200.

Flanagan-Steet, H. *et al.* (2005) 'Neuromuscular synapses can form in vivo by incorporation of initially aneural postsynaptic specializations.', *Development (Cambridge, England)*, 132(20), pp. 4471–81. doi: 10.1242/dev.02044.

Fogel, J. L., Thein, T. Z. T. and Mariani, F. V. (2012) 'Use of LysoTracker to Detect Programmed Cell Death in Embryos and Differentiating Embryonic Stem Cells', *Journal of Visualized Experiments*, (68). doi: 10.3791/4254.

Fontenas, L. and Kucenas, S. (2018) 'Motor Exit Point (MEP) Glia: Novel Myelinating Glia That Bridge CNS and PNS Myelin.', *Frontiers in cellular neuroscience*. Frontiers Media SA, 12, p. 333. doi: 10.3389/fncel.2018.00333.

Francisco-Morcillo, J. *et al.* (2014) 'Ontogenetic Cell Death and Phagocytosis in the

Visual System of Vertebrates', *Developmental Dynamics*. John Wiley & Sons, Ltd, 243(10), pp. 1203–1225. doi: 10.1002/dvdy.24174.

Fratti, R. A. *et al.* (2001) 'Role of phosphatidylinositol 3-kinase and Rab5 effectors in phagosomal biogenesis and mycobacterial phagosome maturation arrest.', *The Journal of cell biology*. Rockefeller University Press, 154(3), pp. 631–44. doi: 10.1083/jcb.200106049.

Furutani, M. *et al.* (2006) 'Application of phosphoinositide-binding domains for the detection and quantification of specific phosphoinositides', *Analytical Biochemistry*, 355(1), pp. 8–18. doi: 10.1016/j.ab.2006.05.014.

Gaiano, N., Nye, J. S. and Fishell, G. (2000) 'Radial glial identity is promoted by Notch1 signaling in the murine forebrain.', *Neuron*. Elsevier, 26(2), pp. 395–404. doi: 10.1016/S0896-6273(00)81172-1.

Galli, S. J., Borregaard, N. and Wynn, T. A. (2011) 'Phenotypic and functional plasticity of cells of innate immunity: macrophages, mast cells and neutrophils', *Nature Immunology*. Nature Publishing Group, 12(11), pp. 1035–1044. doi: 10.1038/ni.2109.

Gautier, E. L. *et al.* (2012) 'Gene-expression profiles and transcriptional regulatory pathways that underlie the identity and diversity of mouse tissue macrophages', *Nature Immunology*, 13(11), pp. 1118–1128. doi: 10.1038/ni.2419.

Gawden-Bone, C. *et al.* (2010) 'Dendritic cell podosomes are protrusive and invade the extracellular matrix using metalloproteinase MMP-14', *Journal of Cell Science*, 123(9), pp. 1427–1437. doi: 10.1242/jcs.056515.

Geuna, S. (2015) 'The sciatic nerve injury model in pre-clinical research', *Journal of Neuroscience Methods*, 243, pp. 39–46. doi: 10.1016/j.jneumeth.2015.01.021.

Ghislain, J. and Charnay, P. (2006) 'Control of myelination in Schwann cells: a Krox20 cis-regulatory element integrates Oct6, Brn2 and Sox10 activities.', *EMBO reports*. European Molecular Biology Organization, 7(1), pp. 52–8. doi: 10.1038/sj.embor.7400573.

Gottlieb, R. A. (1996) 'Cell acidification in apoptosis', *Apoptosis*. Kluwer Academic Publishers, 1(1), pp. 40–48. doi: 10.1007/BF00142077.

Grabher, C. *et al.* (2006) 'Birth and life of tissue macrophages and their migration in embryogenesis and inflammation in medaka', *Journal of Leukocyte Biology*, 81(1), pp. 263–271. doi: 10.1189/jlb.0806526.

Griffin, J. W. *et al.* (2013) 'Peripheral Nerve Repair and Reconstruction', *The Journal of Bone & Joint Surgery*, 95(23), pp. 2144–2151. doi: 10.2106/JBJS.L.00704.

Hadjivasiliou, Z. *et al.* (2019) 'Basal Protrusions Mediate Spatiotemporal Patterns of Spinal Neuron Differentiation', *Developmental Cell*. Elsevier Inc., 49(6), pp. 907-919.e10. doi: 10.1016/j.devcel.2019.05.035.

Hagedorn, E. J. and Sherwood, D. R. (2011) 'Cell invasion through basement membrane: the anchor cell breaches the barrier', *Current Opinion in Cell Biology*. (Cell-to-cell contact and extracellular matrix), 23(5), pp. 589–596. doi: 10.1016/j.ceb.2011.05.002.

van Ham, T. J. *et al.* (2010) 'Live imaging of apoptotic cells in zebrafish.', *The FASEB journal : official publication of the Federation of American Societies for Experimental Biology*, 24(11), pp. 4336–4342. doi: 10.1096/fj.10-161018.

Hasegawa, T. *et al.* (2017) 'Transient inflammatory response mediated by interleukin-1β is required for proper regeneration in zebrafish fin fold', *eLife*, 6, pp. 1–22. doi: 10.7554/eLife.22716.

Helker, C. S. M. *et al.* (2013) 'The zebrafish common cardinal veins develop by a novel mechanism: lumen ensheathment', *Development*, 140(13), pp. 2776–2786. doi: 10.1242/dev.091876.

Herbomel, P., Thisse, B. and Thisse, C. (1999) 'Ontogeny and behaviour of early macrophages in the zebrafish embryo.', *Development (Cambridge, England)*, 126(17), pp. 3735–45.

Herbomel, P., Thisse, B. and Thisse, C. (2001) 'Zebrafish early macrophages colonize cephalic mesenchyme and developing brain, retina, and epidermis through a M-CSF receptor-dependent invasive process.', *Developmental biology*, 238(2), pp. 274–88. doi: 10.1006/dbio.2001.0393.

Hjerling-Leffler, J. *et al.* (2005) 'The boundary cap: a source of neural crest stem cells that generate multiple sensory neuron subtypes', *Development (Cambridge, England)*, 132(11), pp. 2623–2632. doi: 10.1242/dev.01852.

Hochgreb-Hägele, T. and Bronner, M. E. (2013) 'A novel FoxD3 gene trap line reveals neural crest precursor movement and a role for FoxD3 in their specification.', *Developmental biology*. NIH Public Access, 374(1), pp. 1–11. doi: 10.1016/j.ydbio.2012.11.035.

Honjo, Y. and Eisen, J. S. (2005) 'Slow muscle regulates the pattern of trunk neural crest migration in zebrafish', *Development*, 132(20), pp. 4461–4470. doi: 10.1242/dev.02026.

Huang, P. *et al.* (2012) 'Attenuation of Notch and hedgehog signaling is required for fate specification in the spinal cord', *PLoS Genetics*, 8(6). doi: 10.1371/journal.pgen.1002762.

Hubaud, A. and Pourquié, O. (2014) 'Signalling dynamics in vertebrate segmentation', *Nature Reviews Molecular Cell Biology*. Nature Publishing Group, 15(11), pp. 709–721. doi: 10.1038/nrm3891.

Huynh, K. K. *et al.* (2007) 'LAMP proteins are required for fusion of lysosomes with phagosomes', *The EMBO Journal*, 26(2), pp. 313–324. doi: 10.1038/sj.emboj.7601511.

Hwang, W. Y. *et al.* (2013) 'Efficient genome editing in zebrafish using a CRISPR-Cas system', *Nature biotechnology*, 31(3), pp. 227–229. doi: 10.1038/nbt.2501.

Jao, L.-E., Appel, B. and Wente, S. R. (2012) 'A zebrafish model of lethal congenital contracture syndrome 1 reveals Gle1 function in spinal neural precursor survival and motor axon arborization', *Development*, 139(7), pp. 1316–1326. doi: 10.1242/dev.074344.

Jessell, T. M. (2000) 'Neuronal specification in the spinal cord: inductive signals and transcriptional codes', *Nature Reviews Genetics*, 1(1), pp. 20–29. doi: 10.1038/35049541.

Jessen, K. R. and Mirsky, R. (2005) 'The origin and development of glial cells in peripheral nerves', *Nature Reviews Neuroscience*. Nature Publishing Group, 6(9), pp. 671–682. doi: 10.1038/nrn1746.

Jessen, K. R. and Mirsky, R. (2016) 'The repair Schwann cell and its function in regenerating nerves', *The Journal of Physiology*. John Wiley & Sons, Ltd (10.1111), 594(13), pp. 3521–3531. doi: 10.1113/JP270874.

Johnson, K. *et al.* (2016a) 'Gfap-positive radial glial cells are an essential progenitor population for later-born neurons and glia in the zebrafish spinal cord', *Glia*, 64(7),

pp. 1170–1189. doi: 10.1002/glia.22990.

Johnson, K. *et al.* (2016b) 'Gfap-positive radial glial cells are an essential progenitor population for later-born neurons and glia in the zebrafish spinal cord', *Glia*, 64(7), pp. 1170–1189. doi: 10.1002/glia.22990.

Johnsson, A.-K. E. *et al.* (2014) 'The Rac-FRET Mouse Reveals Tight Spatiotemporal Control of Rac Activity in Primary Cells and Tissues', *Cell Reports*. Cell Press, 6(6), pp. 1153–1164. doi: 10.1016/J.CELREP.2014.02.024.

Kamen, L. A. *et al.* (2008) 'SHIP-1 increases early oxidative burst and regulates phagosome maturation in macrophages.', *Journal of immunology (Baltimore, Md. : 1950)*. American Association of Immunologists, 180(11), pp. 7497–505. doi: 10.4049/JIMMUNOL.180.11.7497.

Kanehisa, M. and Goto, S. (2000) 'KEGG: kyoto encyclopedia of genes and genomes.', *Nucleic acids research*, 28(1), pp. 27–30. Available at: http://www.ncbi.nlm.nih.gov/pubmed/10592173 (Accessed: 22 March 2019).

Kania, A. (2014) 'Spinal Motor Neuron Migration and the Significance of Topographic Organization in the Nervous System', in. Springer, Dordrecht, pp. 133–148. doi: 10.1007/978-94-007-7687-6_8.

Kawahara, A. (2017) 'CRISPR/Cas9-Mediated Targeted Knockin of Exogenous Reporter Genes in Zebrafish', in *Methods in molecular biology (Clifton, N.J.)*, pp. 165–173. doi: 10.1007/978-1-4939-7128-2_14.

Kawakami, K. (2004) 'Transgenesis and Gene Trap Methods in Zebrafish by Using the Tol2 Transposable Element', *Methods in Cell Biology*. Academic Press, 77, pp. 201–222. doi: 10.1016/S0091-679X(04)77011-9.

Kelly Kuan, C.-Y. *et al.* (2004) 'Somite polarity and segmental patterning of the peripheral nervous system', *Mechanisms of Development*. Elsevier, 121(9), pp. 1055–1068. doi: 10.1016/J.MOD.2004.05.001.

Keynes, R. J. and Stern, C. D. (1984) 'Segmentation in the vertebrate nervous system', *Nature*. Nature Publishing Group, 310(5980), pp. 786–789. doi: 10.1038/310786a0.

Kim, M., Bjorke, B. and Mastick, G. S. (2019) 'Motor neuron migration and positioning mechanisms: New roles for guidance cues', *Seminars in Cell & Developmental Biology*. Academic Press, 85, pp. 78–83. doi: 10.1016/J.SEMCDB.2017.11.016.

Kimmel, C. B. *et al.* (1995) 'Stages of embryonic development of the zebrafish', *Developmental dynamics: an official publication of the American Association of Anatomists*, 203(3), pp. 253–310. doi: 10.1002/aja.1002030302.

Kinchen, J. M. and Ravichandran, K. S. (2008) 'Phagosome maturation: going through the acid test.', *Nature reviews. Molecular cell biology*. NIH Public Access, 9(10), pp. 781–95. doi: 10.1038/nrm2515.

Kirby, B. B. *et al.* (2006) 'In vivo time-lapse imaging shows dynamic oligodendrocyte progenitor behavior during zebrafish development', *Nature neuroscience*, 9(12), pp. 1506–1511. doi: 10.1038/nn1803.

Kristensson, K. and Olsson, Y. (1971) 'The perineurium as a diffusion barrier to protein tracers. Differences between mature and immature animals.', *Acta neuropathologica*, 17(2), pp. 127–38. Available at: http://www.ncbi.nlm.nih.gov/pubmed/5101596 (Accessed: 22 July 2019).

Kucenas, S. *et al.* (2008) 'CNS-derived glia ensheath peripheral nerves and mediate motor root development', *Nature neuroscience*, 11(2), pp. 143–151. doi:

10.1038/nn2025.

Kucenas, S. *et al.* (2009) ‘A selective glial barrier at motor axon exit points prevents oligodendrocyte migration from the spinal cord.’, *The Journal of neuroscience : the official journal of the Society for Neuroscience*, 29(48), pp. 15187–94. doi: 10.1523/JNEUROSCI.4193-09.2009.

Kucenas, S. (2015) ‘Perineurial glia.’, *Cold Spring Harbor perspectives in biology*. Cold Spring Harbor Laboratory Press, 7(6). doi: 10.1101/cshperspect.a020511.

Kucenas, S., Snell, H. and Appel, B. (2008) ‘nkx2.2a promotes specification and differentiation of a myelinating subset of oligodendrocyte lineage cells in zebrafish.’, *Neuron glia biology*. NIH Public Access, 4(2), pp. 71–81. doi: 10.1017/S1740925X09990123.

Kurant, E. *et al.* (2008) ‘Six-Microns-Under Acts Upstream of Draper in the Glial Phagocytosis of Apoptotic Neurons’, *Cell*. Cell Press, 133(3), pp. 498–509. doi: 10.1016/J.CELL.2008.02.052.

Kuri, P. *et al.* (2017) ‘Dynamics of in vivo ASC speck formation.’, *The Journal of cell biology*. Rockefeller University Press, 216(9), pp. 2891–2909. doi: 10.1083/jcb.201703103.

Kwan, Kristen M *et al.* (2007) ‘The Tol2kit: a multisite gateway-based construction kit for Tol2 transposon transgenesis constructs.’, *Developmental dynamics : an official publication of the American Association of Anatomists*, 236(11), pp. 3088–99. doi: 10.1002/dvdy.21343.

Kwan, Kristen M. *et al.* (2007) ‘The Tol2kit: A multisite gateway-based construction kit forTol2 transposon transgenesis constructs’, *Developmental Dynamics*, 236(11), pp.

3088–3099. doi: 10.1002/dvdy.21343.

Lam, P. *et al.* (2015) 'In Vivo Imaging and Characterization of Actin Microridges', *PLoS ONE*, 10(1), p. e0115639. doi: 10.1371/journal.pone.0115639.

Le, N. *et al.* (2005) 'Analysis of congenital hypomyelinating Egr2Lo/Lo nerves identifies Sox2 as an inhibitor of Schwann cell differentiation and myelination', *Proceedings of the National Academy of Sciences*, 102(7), pp. 2596–2601. doi: 10.1073/pnas.0407836102.

Lee, R. T. H. *et al.* (2013) 'An exclusively mesodermal origin of fin mesenchyme demonstrates that zebrafish trunk neural crest does not generate ectomesenchyme', *Development*, 140(14), pp. 2923–2932. doi: 10.1242/dev.093534.

Lee, S.-K. *et al.* (2005) 'Olig2 and Ngn2 function in opposition to modulate gene expression in motor neuron progenitor cells', *Genes & Development*. Cold Spring Harbor Laboratory Press, 19(2), p. 282. doi: 10.1101/GAD.1257105.

Leung, L. C., Wang, G. X. and Mourrain, P. (2013) 'Imaging zebrafish neural circuitry from whole brain to synapse', *Frontiers in Neural Circuits*. Frontiers, 7, p. 76. doi: 10.3389/fncir.2013.00076.

Levin, R., Grinstein, S. and Canton, J. (2016) 'The life cycle of phagosomes: formation, maturation, and resolution', *Immunological Reviews*, 273(1), pp. 156–179. doi: 10.1111/imr.12439.

Lewis, G. M. and Kucenas, S. (2014) 'Perineurial Glia Are Essential for Motor Axon Regrowth following Nerve Injury', *Journal of Neuroscience*, 34(38), pp. 12762–12777. doi: 10.1523/JNEUROSCI.1906-14.2014.

Lewis, K. E. and Eisen, J. S. (2003) 'From cells to circuits: development of the zebrafish

spinal cord', *Progress in neurobiology*, 69(6), pp. 419–449. Available at: http://www.ncbi.nlm.nih.gov/pubmed/12880634.

Lieberam, I. *et al.* (2005) 'A Cxcl12-Cxcr4 Chemokine Signaling Pathway Defines the Initial Trajectory of Mammalian Motor Axons', *Neuron*, 47(5), pp. 667–679. doi: 10.1016/j.neuron.2005.08.011.

Lieschke, G. J. *et al.* (2001) 'Morphologic and functional characterization of granulocytes and macrophages in embryonic and adult zebrafish', *Blood*, 98(10), pp. 3087–3096. doi: 10.1182/blood.V98.10.3087.

Lopez-Castejon, G. and Brough, D. (2011) 'Understanding the mechanism of IL-1β secretion', *Cytokine and Growth Factor Reviews*. Elsevier Ltd, 22(4), pp. 189–195. doi: 10.1016/j.cytogfr.2011.10.001.

Love, M. I., Huber, W. and Anders, S. (2014) 'Moderated estimation of fold change and dispersion for RNA-seq data with DESeq2', *Genome Biology*. BioMed Central, 15(12), p. 550. doi: 10.1186/s13059-014-0550-8.

Lu, Q. R. *et al.* (2002a) 'Common developmental requirement for Olig function indicates a motor neuron/oligodendrocyte connection.', *Cell*, 109(1), pp. 75–86. doi: 10.1016/s0092-8674(02)00678-5.

Lu, Q. R. *et al.* (2002b) 'Common developmental requirement for Olig function indicates a motor neuron/oligodendrocyte connection.', *Cell*, 109(1), pp. 75–86. doi: 10.1016/s0092-8674(02)00678-5.

Lu, Z. *et al.* (2011) 'Phagocytic activity of neuronal progenitors regulates adult neurogenesis', *Nature Cell Biology*. Nature Publishing Group, 13(9), pp. 1076–1083. doi: 10.1038/ncb2299.

Lyons, D. A. *et al.* (2005) 'erbb3 and erbb2 Are Essential for Schwann Cell Migration and Myelination in Zebrafish', *Current Biology*, 15(6), pp. 513–524. doi: 10.1016/j.cub.2005.02.030.

Ma, R. C. *et al.* (2018) 'Stereotypic generation of axial tenocytes from bipartite sclerotome domains in zebrafish', *PLOS Genetics*. Edited by C. Moens. Public Library of Science, 14(11), p. e1007775. doi: 10.1371/journal.pgen.1007775.

Madej, M. P. *et al.* (2017) 'Different regulation of interleukin-1 production and activity in monocytes and macrophages: Innate memory as an endogenous mechanism of IL-1 inhibition', *Frontiers in Pharmacology*, 8(JUN), pp. 1–12. doi: 10.3389/fphar.2017.00335.

Maden, M. (2007) 'Retinoic acid in the development, regeneration and maintenance of the nervous system', *Nature Reviews Neuroscience*, 8(10), pp. 755–765. doi: 10.1038/nrn2212.

Margiotta, A. (2019) 'Coordination between Rac1 and Rab Proteins ':, pp. 1–17.

Massa, V. *et al.* (2009) 'Apoptosis is not required for mammalian neural tube closure.', *Proceedings of the National Academy of Sciences of the United States of America*, 106(20), pp. 8233–8. doi: 10.1073/pnas.0900333106.

Masumoto, J. *et al.* (2003) 'Caspy, a zebrafish caspase, activated by ASC oligomerization is required for pharyngeal arch development', *Journal of Biological Chemistry*, 278(6), pp. 4268–4276. doi: 10.1074/jbc.M203944200.

Mathiak, G. *et al.* (2000) 'Caspase-1-inhibitor ac-YVAD-cmk reduces LPS-lethality in rats without affecting haematology or cytokine responses.', *British journal of pharmacology*. Wiley-Blackwell, 131(3), pp. 383–6. doi: 10.1038/sj.bjp.0703629.

Mauti, O. *et al.* (2007) 'Semaphorin6A acts as a gate keeper between the central and the peripheral nervous system.', *Neural development*. BioMed Central, 2(1), p. 28. doi: 10.1186/1749-8104-2-28.

Mayor, Roberto and Theveneau, E. (2013) 'The neural crest', *Development*, 140(11), pp. 2247–2251. doi: 10.1242/dev.091751.

Mayor, R. and Theveneau, E. (2013) 'The neural crest', *Development*, 140(11), pp. 2247–2251. doi: 10.1242/dev.091751.

Mazaheri, F. *et al.* (2014) 'Distinct roles for BAI1 and TIM-4 in the engulfment of dying neurons by microglia.', *Nature communications*. Nature Publishing Group, 5(May), p. 4046. doi: 10.1038/ncomms5046.

McGrath, K. E. *et al.* (2003) 'Circulation is established in a stepwise pattern in the mammalian embryo.', *Blood*. American Society of Hematology, 101(5), pp. 1669–76. doi: 10.1182/blood-2002-08-2531.

McGraw, H. *et al.* (2012) 'Postembryonic neuronal addition in Zebrafish dorsal root ganglia is regulated by Notch signaling', *Neural Development*, 7(1), p. 23. doi: 10.1186/1749-8104-7-23.

Mesureur, J. *et al.* (2017) 'Macrophages, but not neutrophils, are critical for proliferation of Burkholderia cenocepacia and ensuing host-damaging inflammation', *PLOS Pathogens*. Edited by D. M. Tobin. Public Library of Science, 13(6), p. e1006437. doi: 10.1371/journal.ppat.1006437.

Meyers, J. R. (2018) 'Zebrafish: Development of a Vertebrate Model Organism', *Current Protocols in Essential Laboratory Techniques*, 16(1), pp. 1–26. doi: 10.1002/cpet.19.

Mirkes, P. E. (2002) '2001 Warkany lecture: To die or not to die, the role of apoptosis in

normal and abnormal mammalian development', *Teratology*, 65(5), pp. 228–239. doi: 10.1002/tera.10049.

Mitew, S. *et al.* (2014) 'Mechanisms regulating the development of oligodendrocytes and central nervous system myelin', *Neuroscience*. (Secrets of the CNS White Matter), 276, pp. 29–47. doi: 10.1016/j.neuroscience.2013.11.029.

Monk, K. R. *et al.* (2009) 'A G protein-coupled receptor is essential for Schwann cells to initiate myelination.', *Science (New York, N.Y.)*. NIH Public Access, 325(5946), pp. 1402–5. doi: 10.1126/science.1173474.

Morrissey, M. A., Hagedorn, E. J. and Sherwood, D. R. (2013) 'Cell invasion through basement membrane', *Worm*, 2(3). doi: 10.4161/worm.26169.

Murphy, D. A. and Courtneidge, S. A. (2011) 'The "ins" and "outs" of podosomes and invadopodia: characteristics, formation and function', *Nature Reviews Molecular Cell Biology*, 12(7), pp. 413–426. doi: 10.1038/nrm3141.

Myers, P. Z., Eisen, J. S. and Westerfield, M. (1986) 'Development and axonal outgrowth of identified motoneurons in the zebrafish.', *The Journal of neuroscience : the official journal of the Society for Neuroscience*, 6(8), pp. 2278–89. Available at: http://www.jneurosci.org/content/6/8/2278 (Accessed: 15 January 2015).

Myers, Paul Z, Eisen, J. S. and Westerfield, M. (1986) *Development and Axonal Outgrowth of Identified Motoneurons in the Zebrafish*. Available at: https://www.jneurosci.org/content/jneuro/6/8/2278.full.pdf (Accessed: 17 July 2019).

Namgung, U. (2015) 'The Role of Schwann Cell-Axon Interaction in Peripheral Nerve Regeneration', *Cells Tissues Organs*, 200(1), pp. 6–12. doi: 10.1159/000370324.

Nguyen-Chi, M. *et al.* (2014) 'Transient infection of the zebrafish notochord with E. coli

induces chronic inflammation', *Disease Models & Mechanisms*, 7(7), pp. 871–882. doi: 10.1242/dmm.014498.

Nikolopoulou, E. *et al.* (2017) 'Neural tube closure: cellular, molecular and biomechanical mechanisms'. doi: 10.1242/dev.145904.

Noble, M. *et al.* (1988) 'Platelet-derived growth factor promotes division and motility and inhibits premature differentiation of the oligodendrocyte/type-2 astrocyte progenitor ceil', *Nature*, 333(6173), pp. 560–562. doi: 10.1038/333560a0.

Odenthal, J. *et al.* (2000) 'Two distinct cell populations in the floor plate of the zebrafish are induced by different pathways.', *Developmental biology*, 219, pp. 350–363. doi: 10.1006/dbio.1999.9589.

Oikawa, T., Itoh, T. and Takenawa, T. (2008) 'Sequential signals toward podosome formation in NIH-src cells.', *The Journal of cell biology*. The Rockefeller University Press, 182(1), pp. 157–69. doi: 10.1083/jcb.200801042.

Olson, M. F. and Sahai, E. (2009) 'The actin cytoskeleton in cancer cell motility', *Clinical & Experimental Metastasis*. Springer Netherlands, 26(4), pp. 273–287. doi: 10.1007/s10585-008-9174-2.

Pabst, O. *et al.* (2003) 'Targeted disruption of the homeobox gene Nkx2.9 reveals a role in development of the spinal accessory nerve', *Development*, 130(6), pp. 1193–1202. doi: 10.1242/dev.00346.

Pagès H, Carlson M, Falcon S, L. N. (2019) *AnnotationDbi: Manipulation of SQLite-based annotations in Bioconductor*, *R package version 1.46.0.* doi: 10.18129/B9.bioc.AnnotationDbi.

Palaisa, K. A. and Granato, M. (2007) 'Analysis of zebrafish sidetracked mutants reveals

a novel role for Plexin A3 in intraspinal motor axon guidance.', *Development (Cambridge, England)*. The Company of Biologists Ltd, 134(18), pp. 3251–7. doi: 10.1242/dev.007112.

Pauls, S. *et al.* (2007) 'Function and regulation of zebrafish nkx2.2a during development of pancreatic islet and ducts', *Developmental Biology*. Academic Press, 304(2), pp. 875–890. doi: 10.1016/J.YDBIO.2007.01.024.

Paulus, J. D. and Halloran, M. C. (2006) 'Zebrafish bashful/laminin-α1 mutants exhibit multiple axon guidance defects', *Developmental Dynamics*, 235(1), pp. 213–224. doi: 10.1002/dvdy.20604.

Pike, S. H. and Eisen, J. S. (1990) 'Identified primary motoneurons in embryonic zebrafish select appropriate pathways in the absence of other primary motoneurons', *The Journal of Neuroscience: The Official Journal of the Society for Neuroscience*, 10(1), pp. 44–49. Available at: http://www.ncbi.nlm.nih.gov/pubmed/2299400.

Poh, A. *et al.* (2002) 'Patterning of the vertebrate ventral spinal cord', *International Journal of Developmental Biology*, 46(4 SPEC.), pp. 597–608.

Prendergast, A. *et al.* (2012) 'The metalloproteinase inhibitor Reck is essential for zebrafish DRG development.', *Development (Cambridge, England)*. Company of Biologists, 139(6), pp. 1141–52. doi: 10.1242/dev.072439.

Qi, Y. *et al.* (2001) 'Control of oligodendrocyte differentiation by the Nkx2.2 homeodomain transcription factor.', *Development (Cambridge, England)*, 128(14), pp. 2723–33. Available at: http://www.ncbi.nlm.nih.gov/pubmed/11526078 (Accessed: 19 July 2019).

Rasmussen, J. P. *et al.* (2015) 'Vertebrate epidermal cells are broad-specificity

phagocytes that clear sensory axon debris.', *The Journal of neuroscience : the official journal of the Society for Neuroscience*. Society for Neuroscience, 35(2), pp. 559–70. doi: 10.1523/JNEUROSCI.3613-14.2015.

Ravanelli, A. M. and Appel, B. (2015) 'Motor neurons and oligodendrocytes arise from distinct cell lineages by progenitor recruitment.', *Genes & development*, 29(23), pp. 2504–2515. doi: 10.1101/gad.271312.115.

Riedl, J. *et al.* (2008) 'Lifeact: a versatile marker to visualize F-actin', *Nature Methods*, 5(7), pp. 605–607. doi: 10.1038/nmeth.1220.

Sainath, R. and Granato, M. (2013) 'Plexin A3 and Turnout Regulate Motor Axonal Branch Morphogenesis in Zebrafish', *PLoS ONE*, 8(1), p. e54071. doi: 10.1371/journal.pone.0054071.

Sarvothaman, S. *et al.* (2015) 'Apoptosis: Role in myeloid cell development', *Blood Research*, 50(2), pp. 73–79. doi: 10.5045/br.2015.50.2.73.

Scardigli, R. *et al.* (2001) 'Crossregulation between Neurogenin2 and pathways specifying neuronal identity in the spinal cord.', *Neuron*, 31(2), pp. 203–17. Available at: http://www.ncbi.nlm.nih.gov/pubmed/11502253 (Accessed: 17 July 2019).

Schäfer, M. *et al.* (2005) 'Hedgehog and retinoid signalling confines nkx2.2b expression to the lateral floor plate of the zebrafish trunk', *Mechanisms of development*, 122(1), pp. 43–56. doi: 10.1016/j.mod.2004.09.002.

Schäfer, M., Kinzel, D. and Winkler, C. (2007) 'Discontinuous organization and specification of the lateral floor plate in zebrafish', *Developmental biology*, 301(1), pp. 117–129. doi: 10.1016/j.ydbio.2006.09.018.

Scheib, J. L., Sullivan, C. S. and Carter, B. D. (2012) 'Jedi-1 and MEGF10 signal engulfment of apoptotic neurons through the tyrosine kinase Syk.', *The Journal of neuroscience : the official journal of the Society for Neuroscience*, 32(38), pp. 13022–31. doi: 10.1523/JNEUROSCI.6350-11.2012.

Schlüter, G. (1973) 'Ultrastructural observations on cell necrosis during formation of the neural tube in mouse embryos.', *Zeitschrift fur Anatomie und Entwicklungsgeschichte*, 141(3), pp. 251–64. Available at: http://www.ncbi.nlm.nih.gov/pubmed/4767584 (Accessed: 31 July 2018).

Schweitzer, J. *et al.* (2005) 'Tenascin-C is involved in motor axon outgrowth in the trunk of developing zebrafish', *Developmental Dynamics*, 234(3), pp. 550–566. doi: 10.1002/dvdy.20525.

Seiler, C. *et al.* (2012) 'Smooth muscle tension induces invasive remodeling of the zebrafish intestine.', *PLoS biology*, 10(9), p. e1001386. doi: 10.1371/journal.pbio.1001386.

Sepp, K. J., Schulte, J. and Auld, V. J. (2001) 'Peripheral glia direct axon guidance across the CNS/PNS transition zone', *Developmental biology*, 238(1), pp. 47–63. doi: 10.1006/dbio.2001.0411.

Sherrington, C. S. (1906) 'The integrative action of the nervous system', *CTYale University Press*.

Shin, J. *et al.* (2003) 'Neural cell fate analysis in zebrafish using olig2 BAC transgenics', *Methods in Cell Science*. Kluwer Academic Publishers, 25(1/2), pp. 7–14. doi: 10.1023/B:MICS.0000006847.09037.3a.

Shklover, J., Levy-Adam, F. and Kurant, E. (2015) *Apoptotic Cell Clearance in*

Development. 1st edn, *Current Topics in Developmental Biology*. 1st edn. Elsevier Inc. doi: 10.1016/bs.ctdb.2015.07.024.

Simoes-Costa, M. and Bronner, M. E. (2015) 'Establishing neural crest identity: a gene regulatory recipe', *Development*, 142(2), pp. 242–257. doi: 10.1242/dev.105445.

Smith, C. J. *et al.* (2014) 'Contact-Mediated Inhibition Between Oligodendrocyte Progenitor Cells and Motor Exit Point Glia Establishes the Spinal Cord Transition Zone', *PLoS Biology*. Edited by B. A. Barres, 12(9), p. e1001961. doi: 10.1371/journal.pbio.1001961.

Smith, C. J. *et al.* (2016) 'Radial glia inhibit peripheral glial infiltration into the spinal cord at motor exit point transition zones', *Glia*, 64(7), pp. 1138–1153. doi: 10.1002/glia.22987.

Solle, M. *et al.* (2001) 'Altered cytokine production in mice lacking P2X(7) receptors.', *The Journal of biological chemistry*, 276(1), pp. 125–32. doi: 10.1074/jbc.M006781200.

Soneson, C., Love, M. I. and Robinson, M. D. (2016) 'Differential analyses for RNA-seq: transcript-level estimates improve gene-level inferences', *F1000Research*, 4(2), p. 1521. doi: 10.12688/f1000research.7563.2.

Soula, C. *et al.* (2001) 'Distinct sites of origin of oligodendrocytes and somatic motoneurons in the chick spinal cord: oligodendrocytes arise from Nkx2.2-expressing progenitors by a Shh-dependent mechanism.', *Development (Cambridge, England)*, 128(8), pp. 1369–79. Available at: http://www.ncbi.nlm.nih.gov/pubmed/11262237 (Accessed: 19 July 2019).

Srinivasan, D. (2004) 'Cell Type-Specific Interleukin-1 Signaling in the CNS', *Journal*

of Neuroscience, 24(29), pp. 6482–6488. doi: 10.1523/jneurosci.5712-03.2004.

Stachura, D. L. and Traver, D. (2016) *Cellular dissection of zebrafish hematopoiesis*. Third Edit, *Methods in Cell Biology*. Third Edit. Elsevier Ltd. doi: 10.1016/bs.mcb.2016.03.022.

Stehlik, C. *et al.* (2019) 'Recruitment Domain Speck-Like Protein Containing a Caspase Intracellular Redistribution of the Apoptotic Activation of Inflammasomes Requires', *J Immunol References*, 182, pp. 3173–3182. doi: 10.4049/jimmunol.0802367.

Stifani, N. (2014) 'Motor neurons and the generation of spinal motor neuron diversity', *Frontiers in Cellular Neuroscience*. Frontiers, 8, p. 293. doi: 10.3389/fncel.2014.00293.

Stremmel, C. *et al.* (2018) 'Yolk sac macrophage progenitors traffic to the embryo during defined stages of development', *Nature Communications*. Nature Publishing Group, 9(1), p. 75. doi: 10.1038/s41467-017-02492-2.

System, E. and Klumperman, J. (2015) 'The Complex Ultrastructure of the Endolysosomal System', *Cold Spring Harbor Perspectives in Biology*, 6, pp. 1–22. doi: 10.1101/cshperspect.a016857.

TAKAHASHI, H. (1977) 'Juvenile Hermaphroditism in the Zebrafish, Brachydanio rerio', 北海道大學水産學部研究彙報, 28(2), pp. 57–65. Available at: https://eprints.lib.hokudai.ac.jp/dspace/bitstream/2115/23605/1/28(2)_P57-65.pdf (Accessed: 31 July 2019).

The Gene Ontology Consortium (2019) 'The Gene Ontology Resource: 20 years and still GOing strong', *Nucleic Acids Research*, 47(D1), pp. D330–D338. doi: 10.1093/nar/gky1055.

Theveneau, E. and Mayor, R. (2012) 'Neural crest delamination and migration: From epithelium-to-mesenchyme transition to collective cell migration', *Developmental Biology*. (Neural Crest), 366(1), pp. 34–54. doi: 10.1016/j.ydbio.2011.12.041.

Tsarouchas, T. M. *et al.* (2018) 'Dynamic control of proinflammatory cytokines Il-1β and Tnf-α by macrophages in zebrafish spinal cord regeneration', *Nature Communications*, 9(1). doi: 10.1038/s41467-018-07036-w.

Turkowyd, B. *et al.* (2017) 'A General Mechanism of Photoconversion of Green-to-Red Fluorescent Proteins Based on Blue and Infrared Light Reduces Phototoxicity in Live-Cell Single-Molecule Imaging', *Angewandte Chemie International Edition*. Wiley-Blackwell, 56(38), pp. 11634–11639. doi: 10.1002/anie.201702870.

van der Vaart, M. *et al.* (2014) 'Cellular Visualization of Macrophage Pyroptosis and Interleukin-1 Release in a Viral Hemorrhagic Infection in Zebrafish Larvae', *Journal of Virology*, 88(20), pp. 12026–12040. doi: 10.1128/jvi.02056-14.

Vega-Lopez, G. A., Cerrizuela, S. and Aybar, M. J. (2017) 'Trunk neural crest cells: formation, migration and beyond.', *The International journal of developmental biology*, 61(1–2), pp. 5–15. doi: 10.1387/ijdb.160408gv.

Verkhratsky, D. *et al.* (2019) 'NLRP3 during Macrophage Swelling Not Activate Caspase-1 in the Absence of Containing a CARD Forms Specks but Does Apoptosis-Associated Speck-like Protein'. doi: 10.4049/jimmunol.1301676.

Vieira, O. V. *et al.* (2001) 'Distinct roles of class I and class III phosphatidylinositol 3-kinases in phagosome formation and maturation', *Journal of Cell Biology*, 155(1), pp. 19–25. doi: 10.1083/jcb.200107069.

Villani, A. *et al.* (2019) 'Clearance by Microglia Depends on Packaging of Phagosomes

into a Unique Cellular Compartment', *Developmental Cell*. Elsevier Inc., pp. 1–12. doi: 10.1016/j.devcel.2019.02.014.

Vojtech, L. N. *et al.* (2012) 'Roles of inflammatory caspases during processing of zebrafish interleukin-1β in Francisella noatunensis infection.', *Infection and immunity*. American Society for Microbiology (ASM), 80(8), pp. 2878–85. doi: 10.1128/IAI.00543-12.

Wang, L. *et al.* (2014) 'A conserved axon type hierarchy governing peripheral nerve assembly.', *Development*, 141(9), pp. 1875–83. doi: 10.1242/dev.106211.

Wang, Y. *et al.* (2005) 'Visualizing the mechanical activation of Src', *Nature*, 434(7036), pp. 1040–1045. doi: 10.1038/nature03469.

Weil, M., Jacobson, M. D. and Raff, M. C. (1997) 'Is programmed cell death required for neural tube closure?', *Current biology : CB*, 7(4), pp. 281–4. Available at: http://www.ncbi.nlm.nih.gov/pubmed/9094312 (Accessed: 31 July 2018).

Witting, A. *et al.* (2000) 'Phagocytic clearance of apoptotic neurons by microglia/brain macrophages in vitro: Involvement of lectin-, integrin-, and phosphatidylserine-mediated recognition', *Journal of Neurochemistry*, 75(3), pp. 1060–1070. doi: 10.1046/j.1471-4159.2000.0751060.x.

Woodhoo, A. *et al.* (2009) 'Notch controls embryonic Schwann cell differentiation, postnatal myelination and adult plasticity', *Nature Neuroscience*, 12(7), pp. 839–847. doi: 10.1038/nn.2323.

Wu, H.-H. *et al.* (2009) 'Glial precursors clear sensory neuron corpses during development via Jedi-1, an engulfment receptor.', *Nature neuroscience*, 12(12), pp. 1534–41. doi: 10.1038/nn.2446.

Yamaguchi, H. and Condeelis, J. (2007) 'Regulation of the actin cytoskeleton in cancer cell migration and invasion', *Biochimica et Biophysica Acta - Molecular Cell Research*, 1773(5), pp. 642–652. doi: 10.1016/j.bbamcr.2006.07.001.

Yamaguchi, Y. *et al.* (2011) 'Live imaging of apoptosis in a novel transgenic mouse highlights its role in neural tube closure', *Journal of Cell Biology*, 195(6), pp. 1047–1060. doi: doi/10.1083/jcb.201104057.

Yang, L., Rastegar, S. and Strähle, U. (2010) 'Regulatory interactions specifying Kolmer-Agduhr interneurons', *Development (Cambridge, England)*, 137(16), pp. 2713–2722. doi: 10.1242/dev.048470.

Yoshida, H. *et al.* (2013) 'Local Apoptosis Modulates Early Mammalian Brain Development through the Elimination of Morphogen-Producing Cells', *Developmental Cell*. Elsevier Inc., 27(6), pp. 621–634. doi: 10.1016/j.devcel.2013.11.015.

Yu, G. *et al.* (2012) 'clusterProfiler: an R Package for Comparing Biological Themes Among Gene Clusters', *OMICS: A Journal of Integrative Biology*. Mary Ann Liebert, Inc. 140 Huguenot Street, 3rd Floor New Rochelle, NY 10801 USA , 16(5), pp. 284–287. doi: 10.1089/omi.2011.0118.